University of North Dakota
UND Scholarly Commons

Theses and Dissertations | Theses, Dissertations, and Senior Projects

January 2012

Single Layered Periodic Structure Loaded Textile Patch Antennas

Corey Bergsrud

Follow this and additional works at: https://commons.und.edu/theses

Recommended Citation
Bergsrud, Corey, "Single Layered Periodic Structure Loaded Textile Patch Antennas" (2012). *Theses and Dissertations*. 1226.
https://commons.und.edu/theses/1226

This Thesis is brought to you for free and open access by the Theses, Dissertations, and Senior Projects at UND Scholarly Commons. It has been accepted for inclusion in Theses and Dissertations by an authorized administrator of UND Scholarly Commons. For more information, please contact zeineb.yousif@library.und.edu.

SINGLE LAYERED PERIODIC STRUCTURE LOADED TEXTILE PATCH ANTENNAS

by

Corey A.M. Bergsrud

Bachelor of Science, University of North Dakota, 2009

A Thesis

Submitted to the Graduate Faculty

of the

University of North Dakota

in partial fulfillment of the requirements

for the degree of

Master of Science

Grand Forks, North Dakota

May

2012

This thesis, submitted by Corey A.M. Bergsrud in partial fulfillment of the requirements for the Degree of Master of Science from the University of North Dakota, has been read by the Faculty Advisory Committee under whom the work has been done and is hereby approved.

Sima Noghanian, Ph.D., Chairperson

Hossein Salehfar, Ph.D.

Graeme Dewar, Ph.D.

This thesis is being submitted by the appointed advisory committee as having met all of the requirements of the Graduate School at the University of North Dakota and is hereby approved.

Wayne E. Swisher, Ph.D.,
Dean of the Graduate School

5/1/2012

PERMISSION

Title Single Layered Periodic Structure Loaded Textile Patch Antennas

Department Electrical Engineering

Degree Master of Science

In presenting this thesis in partial fulfillment of the requirements for a graduate degree from the University of North Dakota, I agree that the library of this University shall make it freely available for inspection. I further agree that permission for extensive copying for scholarly purposes may be granted by the professor who supervised my thesis work or, in her absence, by the chairperson of the department or the dean of the Graduate School. It is understood that any copying or publication or other use of this thesis or part thereof for financial gain shall not be allowed without my written permission. It is also understood that due recognition shall be given to me and to the University of North Dakota in any scholarly use which may be made of any material in my thesis.

Corey Bergsrud

5/1/2012

TABLE OF CONTENTS

LIST OF FIGURES

LIST OF TABLES

ACKNOWLEDGMENTS

I would first like to thank my Advisor Dr. Sima Noghanian for all the opportunities and guidance she has given me. Also, Camerin Hahn (EE), for his help in the laboratory as well as other contributions, Tessa Haagenson (EE) for her contribution with wearable antennas, and Matt Anderson (IT) for his contributions in manufacturing of textile antennas, Dr. Abas Sabouni for his help on simulations, Dr. Isaac Chang for supervising Matt Anderson and helping in fabrication, and, to my Advisory committee. Finally, thanks to North Dakota EPSCoR and Space Grant for financial support.

DEDICATION PAGE

I dedicate this thesis to long lost friends, Kayla Rose Thompson, and Zac Moen. I will always remember. Also, to my family, and friends. Finally, to the University of North Dakota, and to the State of North Dakota.

ABSTRACT

This thesis provides an investigation of a Single Layered Periodic Structure Loaded Textile Patch Antenna with probe feed excitation. Specifically, this thesis is concentrated on the application of wearable antenna arrays with space suit, since this thesis has collaboration with the University of North Dakota (UND) Space Suit Laboratory in the Space Studies Department. Topics include; platform interaction and placement of the antenna system. The goal is to increase antenna gain by loading the antenna with periodic cells. First, an introduction to items contained within this thesis will be given. The second chapter introduces microstrip patch antennas, their basic characteristics, and their feeding excitation methods. Continuing with microstip patch antennas, and how they are viewed with their fringing field effects. Then the theoretical designs of the physical dimensions of a patch antenna relative to its electrical length are included. This part then ends with a basic introduction to periodic structures, namely Electromagnetic Band Gap (EBG) structures.

The third chapter covers wearable antennas, with and without periodic structures, and their applications. A review of surface waves and wave modes is given. This review produces a picture of how this once un-utilized energy (*i.e.* surface waves) can be recycled and reused to benefit positively increased gain. This can be accomplished by use of periodic structures loaded with the antenna. The fourth chapter covers the material, manufacturing, assembling, and measuring processes of textile antennas. This range of

processes is journeyed as a joint collaboration between UNDs Electrical Engineering Department's Applied Electromagnetics Laboratory, and the Technology Department's Machine Shop.

Lastly, simulation and design of a periodic loaded patch antenna are analyzed. This begins by first designing and simulating a free standing periodic cell coined "C-mirror". The simulation results for reflection and dispersion characteristics are given. A 1 GHz antenna with specifications of textile material was designed. Once this antenna was realized, it was then loaded uni-planar with periodic cells with no vias. Experiments included varying the orientation, number of rows, and the placement of the cells with respect to the antenna. It was found that the Up-Down (UD) orientation with 2 rows and $\lambda_o/12$ placement demonstrated the greatest increase in gain. Furthermore, surface currents were seen to interact with the periodic cells. It could be seen that the arrangement of the cells adapted a network internally with the current flowing through the cells obtaining an inductive behavior and the capacitive behavior occurred between the cells stubs as well as between the cells defined by the Periodic Boundary Conditions (PBC). This surface current behavior, with the orientation of the periodic array with no vias became known as a "Uni-Planar Parasitic Loaded Patch Antenna".

1 INTRODUCTION

1.1 Preface

The concept of microstrip antennas was first brought into recorded history in 1953 by Deschamps [1]. However, the first practical microstrip antennas were not developed until the early 1970's by Howell [2] and Munson [3]. Since then, because of the practicality of microstrip antennas, extensive research and development has been done on this topic.

Some advantages of microstrip antennas include: low profile, conformable to planar and non-planar surfaces, simple and inexpensive to manufacture using modern printed-circuit technology, mechanically robust when mounted on rigid surfaces, [4]. These advantages make microstrip antennas desirable for many applications, such as; satellite communications, aerospace, radars, biomedical radiators, etc. Some disadvantages of microstrip antennas include; spurious feed radiation, surface wave excitation [4, 5]. These disadvantages have put a limit on their applications, particularly in the communication field.

In order to make better use of microstrip antennas many engineering efforts have been made to reduce their disadvantages. For example, Bhalla, Shafai, and Lee have achieved very wide bandwidths by designing microstrip patch antennas with various slot shapes [6, 7]. Other methods, such as using stacked patch antennas [8] or using

impedance matching techniques [9, 10], have also been found useful in enhancing microstrip antenna performance.

In recent years, Electromagnetic Band Gap (EBG) structures have attracted increasing interest in the antenna and electromagnetics community because of their desirable electromagnetic properties which cannot be obtained with natural materials. Note here that EBG structures are patterns of periodic structures that are mainly designed to produce a band gap feature from either stopping or assisting the propagation of electromagnetic waves for all incident angles and all polarization states [11]. Other methods, as presented in this thesis, show that periodic structures with no band gap behave as a parasitic element. This can improve the antenna gain.

These desirable properties of periodic structures presented a new solution to overcoming the disadvantages of microstrip antennas by allowing more degrees of control over traveling electromagnetic waves. With diverse research activities on periodic structures being on the rise, a wide range of applications have been reported, and will be briefly covered in this thesis. Antennas loaded with periodic structures have shown to enhance antenna's properties by:

- Suppressing surface waves
- Increasing antenna gain
- Reducing side and back lobe levels

However, achieving bandwidth in the periodic structure realm is still an ongoing challenge as more advanced geometries of cells need to be discovered, arranged in the configurations such as: uni-planar, and/or multi-planar, with or without via, and to set

periodicity. Once a good choice of the above is achieved the cells need to be fine-tuned according to their individual characteristics with respect to the antenna.

1.2 Motivation for this Thesis

The motivation for this thesis is to study the properties of periodic structures and their effects on the performance of microstrip textile patch antennas. This thesis is motivated towards engineering an antenna system from textile materials for future application in space suits. The effect of periodic structure on the resonant frequency, return loss, bandwidth, gain, and half-powered beam width of a probe fed microstrip patch antenna is of interest. Mainly, this thesis focuses on antenna gain enhancement.

Microstrip antennas have low power efficiency; hence, the antenna gain is low. This means, in terms of a specific application, that the distance a transmitted signal can travel through a medium from the space explorer to the base station is reduced. This limited range of exploration can increase the cost of the mission due to the time needed to explore an area. This, in-turn, will slow and can reduce or terminate the outcome of the mission altogether. Another potential problem due to low gain is that the base station has a greater chance of receiving distorted signals that are vital for space explorer's survival due to extreme environmental conditions. Biomedical and other vital information needs to be constantly monitored via telemetry between the space explorer and the base station. If the received signals at the base station are distorted (*e.g.* lost to the void) this presents safety problems for the space explorer as the intended information cannot be completely interpreted.

The properties of a uni-planar antenna system loaded with periodic structures around an antenna backed by a grounded dielectric are investigated in this thesis. This investigation shows a decrease in back lobe radiation which amounts to an increase in antenna gain.

1.3 Parasitic Loaded Antennas

Antennas loaded with periodic structures have allowed for gain enhancements as was mentioned in Section 1.1, and will be mentioned throughout this thesis. Generally speaking, a periodic loaded antenna is an antenna loaded with artificial periodic structures either on the same plane (uni-planar) and/or on a separate plane (multi-planar). The purpose of this loading specifically for this thesis is to increase the gain, thus eliminating the two main problems mentioned in Section 1.2 for space exploration missions. Electromagnetic Band Gap (EBG) structures have been used frequently for gain increase because of their interaction with surface waves. Periodic parasitic elements added to the antenna structure may also be used to increase the radiating aperture at minimum cost.

This thesis takes a glimpse at an ongoing process at the University of North Dakota (UND) relative to manufacturing and fabrication of textile antenna systems. This is important because it is projected that there will be a variety of consumer electronics that are going to be built into the garments of future clothing. This might include:

- Transmitter/receiver systems
- Central Processing Unit (CPU)
- Liquid Crystal Display (LCD)

- Wireless communication links
- Tracking, and positioning systems
- Batteries

Strictly speaking all of these wearable electronic systems have a common entity, the antenna. Without a well-designed antenna that adapts enhanced properties like an increase in gain and bandwidth, most wearable systems will not be efficient enough for marketability. Therefore, the interest in this thesis is to understand the textile antenna behavior while it is loaded with periodic structures, as well as the process for manufacturing and fabricating textile antennas for later integration in a spacesuit application.

1.4 Scope of this Thesis

To understand the antenna behavior of textile and loaded with periodic structures, computer aided design (CAD) is used. Various parameters were investigated such as; 1) a left to right (LR) cell orientation, 2) up to down (UD) cell orientation, 3) all around cells, 4) number of rows of cells (1, 2, or 3), and 5) the distance of the cells from the antenna in terms of wavelength. These were done by first gaining familiarity with the theoretical models and design requirements for microstrip antennas as well as periodic structures. Next a rectangular microstrip textile patch antenna with probe feed were designed using a CAD software given the initial conditions of relative permittivity $\left(\varepsilon_r = 1.2\ F/m\right)$, height (thickness) of the substrate (h_s = 1.6 mm), and resonant frequency (f_o = 1 GHz). The simulation results for resonant frequency, return loss, bandwidth, E-plane and H-plane radiation patterns, half powered beam width, and gain, are presented.

Simultaneously, a cell for periodic structure was designed with CAD software to determine the dispersive characteristics which give information about the cell's operating band. Once the antenna and the cell are matched to their displayed results, they were integrated together on a single substrate. The cells have user defined periodic boundary conditions (PBC) of 2mm and the cells were placed in the various periodic structures, as mentioned above, around the antenna to increase the gain of the antenna.

Manufacturing, fabricating, and testing of textile antennas are briefly covered in Chapter 4. Chapter 5 shows the results of the simulations, and finally, Chapter 0 includes conclusions, plans, and goals for future research.

2 MICROSTRIP ANTENNAS AND PERIODIC STRUCTURES

This chapter begins by introducing what a microstrip "Patch" antenna is, and reviewing some operational advantages and disadvantages of the patch. Section 2.2 gives the basic characteristics of the patch antenna followed by feeding methods discussed in Section 2.3. Next, Section 2.4 gives a theoretical description of fringing field effects and why understanding their behavior is so important in helping more precisely design a rectangular patch antenna in Section 2.5. Finally, this chapter ends with information about Electomagnetic Band Gap structures given in Section 2.6, and conclusion in Section 2.7.

2.1 Introduction to Microstrip Antennas

A microstrip line is an electrical transmission line which can be fabricated using Printed Circuit Board (PCB) technology, and is used to convey microwave-frequency signals. Therefore, the basic microstrip antenna is a resonant patch of metal on the surface of a grounded dielectric slab. For this reason it is called a "Patch" antenna. It radiates power in a beam broadside to the plane of the antenna and displays input impedance similar to a parallel resonant circuit near its operating frequency. The operating frequency range of interest is an alternating current in the *microwave* spectrum between 300 MHz (3×10^8 Hz) and 300 GHz (3×10^{11} Hz), and with a corresponding electrical free-space wavelength between $\lambda_o = c/f_o = 1m$ and $\lambda_o = 1mm$, respectively. In

free space, λ_o is the operating wavelength, f_o is the operating frequency, and c is the speed of light.

Operational advantages of patch antennas include; low profile, conformable to planar and non-planar surfaces, simple and inexpensive to manufacture using modern printed-circuit technology, mechanically robust when mounted on rigid surfaces, and when the particular patch shape and mode are selected, they are very versatile in terms of resonant frequency, polarization, pattern, and impedance. In addition, by adding loads between the patch and the ground plane, such as pins or varactor diodes, adaptive elements with variable resonant frequency, impedance, polarization, and pattern can be designed [4].

Operational disadvantages are their low efficiency, low power, high Q factor, poor polarization purity, poor scan performance, spurious feed radiation and very narrow frequency bandwidth, which is typically only a fraction of a percent or at most a few percent [4]. However there are methods, as mentioned above, such as increasing the height (thickness) of the substrate that can be used to enhance the efficiency and bandwidth [4]. Although, as the height increases, surface waves are introduced which usually are not desirable because they extract power from the total available as they do not radiate normal to the patch but rather they travel transverse, which decreases the main lobe. In Chapter 3, we will see that EBGs have shown to alleviate the problem of surface waves.

2.2 Basic Characteristics of Microstrip Antennas

Starting in the 1970s, microstrip antennas received a lot of attention, although the idea of a microstrip antenna can be traced to 1953 [1] and a patent in 1955 [12]. An example of a microstrip antenna is shown in Figure 2.1 and Figure 2.2. Generally, microstrip antennas consist of a very thin ($t \ll \lambda_o$, where λ_o is the free-space wavelength) metallic strip (patch) placed a small fraction of a wavelength ($d \ll \lambda_o$, usually $0.003\ \lambda_o \leq d \leq 0.05\ \lambda_o$) above a ground plane. The microstrip patch is designed so that's its radiation pattern maximum is normal to the patch (broadside radiator). The patch and the ground plane are separated by a dielectric sheet (substrate).

There are numerous substrates that can be used for the design of microstrip antennas, and according to [4] their dielectric constants are usually in the range of $2.2 \leq \varepsilon_r \leq 12$. Most desirable antenna performance comes from thick substrates whose ε_r is in the lower end of the range. For one thing, higher ε_r means smaller size antenna, but they are more expensive if they have low loss. These thicker substrates with lower ε_r can provide better bandwidth, with loosely bound fields for radiation into space, but at the expense of larger element size [13]. Thin substrates with higher dielectric constants are desirable for microwave circuitry because they require tightly bound fields to minimize undesired radiation and coupling, and lead to smaller element sizes [13]. Since microstrip antennas are often integrated with other microwave circuitry, a balance has to be reached between cost, good antenna performance, and circuit design.

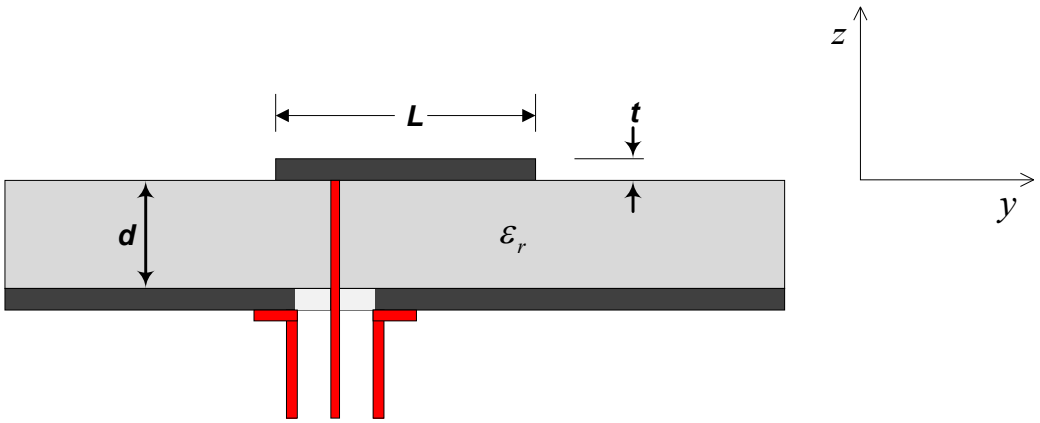

Figure 2.1 Side view of a microstrip patch antenna with coaxial probe feed.

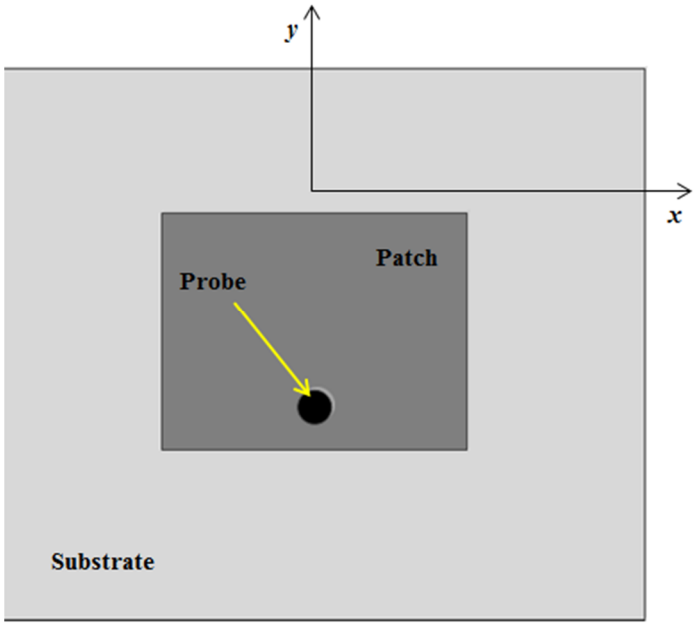

Figure 2.2 Top view of a microstrip (patch) antenna.

Patch antennas are a subset of microstrip antennas. The radiating elements and the feed lines are usually photo-etched on the dielectric substrate. The radiating patch may be square, rectangular, thin strip (dipole), circular, elliptical, triangular, or any other configuration. Several of these geometries are illustrated in Figure 2.3 where the most common shapes are square, rectangular, dipole (strip), and circular. These shapes have ease of analysis and fabrication and attractive radiation characteristics, especially low

cross-polarization radiation. Furthermore, both linear and circular polarizations can be achieved with either single elements or arrays of microstrip antennas. To achieve linear polarization is rather straight forward, whereas circular polarization takes some manipulating of the design and feed location in order to select this type of polarization.

The fundamental characteristics of an antenna, in-particular of a patch antenna, are its gain and half power beamwidth. The gain is a measure of how much of the input power is concentrated in a particular direction. It is expressed with respect to a hypothetical isotropic antenna, which radiates equally in all directions. Furthermore, an antenna can behave as a transmitter and a receiver, and interestingly enough according to the reciprocity theorem, the transmitting and receiving patterns of a passive antenna are identical at a given wavelength [14]. This theory is very helpful to the antenna designer since the power that is sent is the same that can be received. Half power beamwidth is covered in Chapter 3.

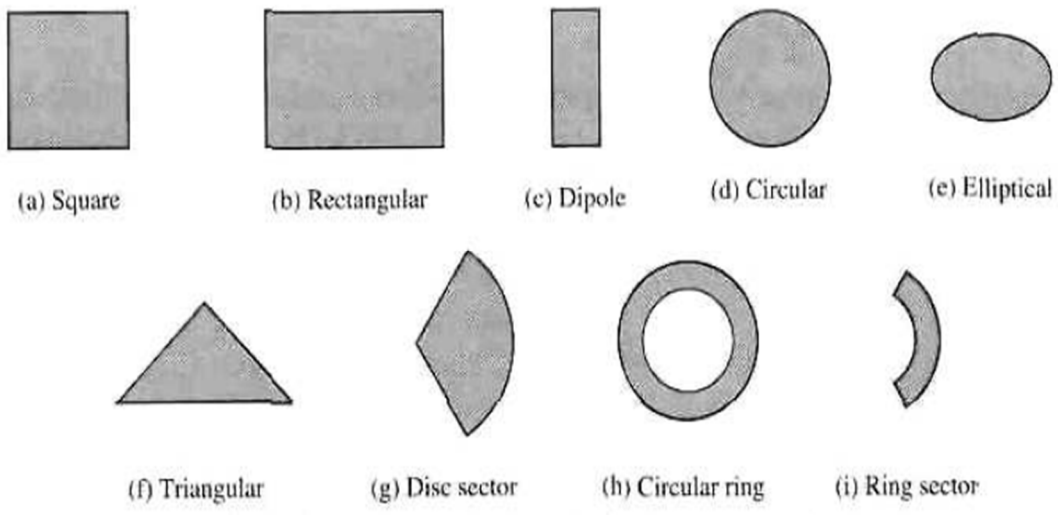

Figure 2.3 Representative geometries of microstrip patch elements [4]

2.3 Feeding Methods

Now that some basic characteristics of patch antennas have been covered methods of feeding power to the antenna will be covered. There are many ways to feed microstrip antennas. According to [4] the four most popular feeding methods are the microstrip line, coaxial probe, aperture coupling, and proximity coupling. These are illustrated in Figure 2.5 and Figure 2.5. One set of equivalent circuits for each of these methods is shown in Figure 2.6. This thesis is only concerned with coaxial-line feeds. Coaxial-line feeds have the inner conductor of the coax attached to the patch while the outer conductor is connected to the ground plane. The coaxial probe feed is easy to fabricate and network match. Additionally, the coax is preferred for traveling electromagnetic waves as it is designed to keep the electromagnetic fields contained between conducting surface and thus it has low spurious radiation.

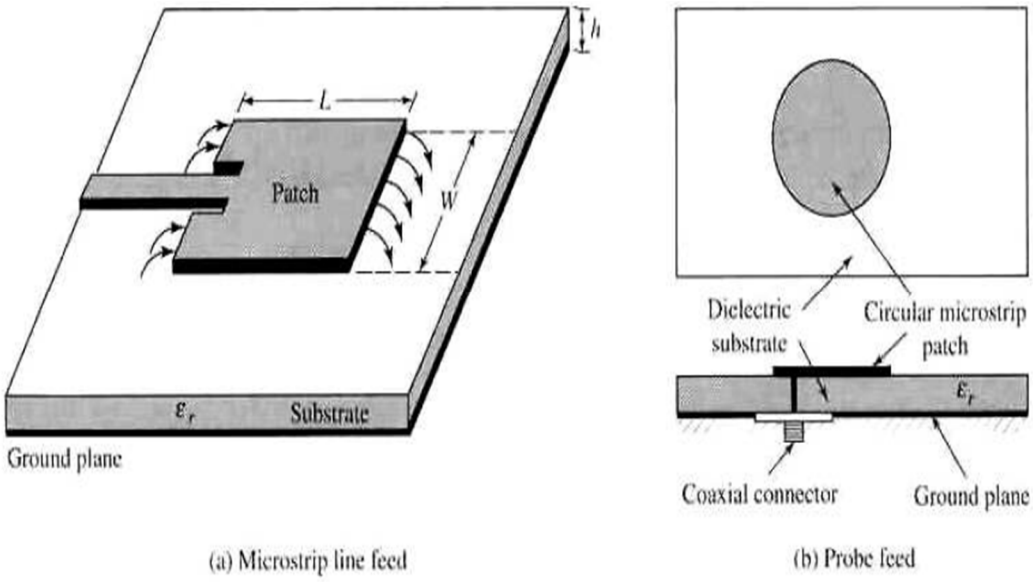

Figure 2.4 Typical feeds for microstrip antennas [4].

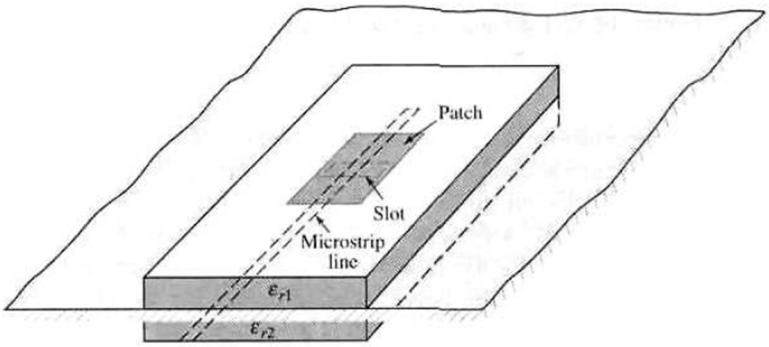

(c) Aperture-coupled feed

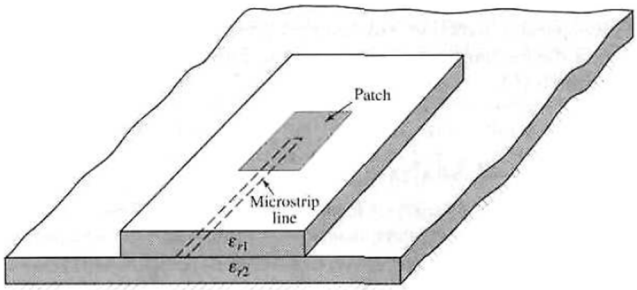

(d) Proximity-coupled feed

Figure 2.5 Typical feeds continued for microstrip antennas [4].

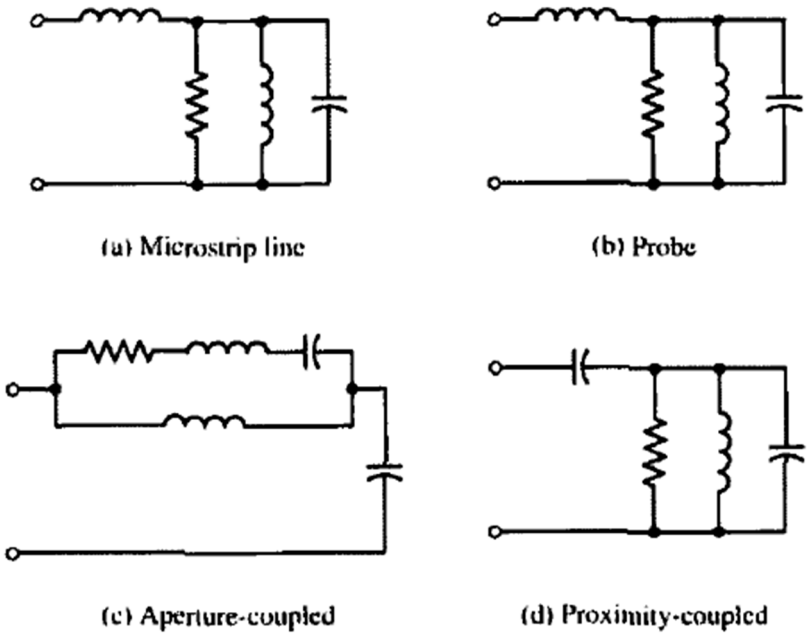

Figure 2.6 Equivalent circuits for typical feeds [4].

2.4 Fringing Field Effects

Because the dimensions of the patch are finite along the length and width, the fields at the edges of the patch undergo fringing, as shown in Figure 2.7. The amount of fringing is a function of the dimensions of the patch and the height of the substrate. For the principal *E*-plane (*zy* plane in this case) fringing is a function of the ratio of the length of the patch L to the height d of the substrate (L/d) and the dielectric constant ε_r of the substrate. Since for microstrip antennas $L/d \gg 1$, fringing is reduced; however, it must be taken into account because it influences the resonant frequency of the antenna (a.k.a. shift in resonant frequency) [4]. This shift is due to fringing fields around the antenna, which makes the patch seem longer (i.e. the electrical length as opposed to the physical length). The fringing fields around the antenna can help explain the radiation of the microstrip antenna [15].

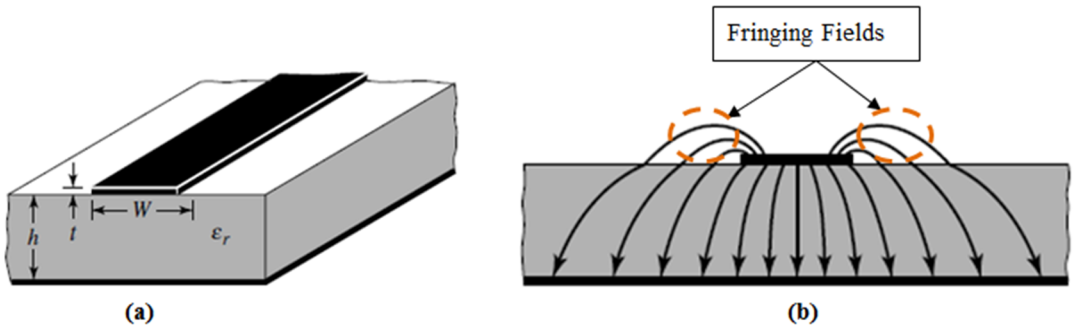

Figure 2.7 (a) Microstrip line, and (b) electric field lines [4].

Typical electric field lines for a microstrip line are also shown in Figure 2.7. This is a non-homogeneous situation as there are two dielectrics; usually the substrate and air. As can be seen from Figure 2.7, most of the electric field lines reside in the substrate with parts of some of the field lines existing in the air medium which is where the phenomena

of fringing field effects takes place. Balanis points out that as $W/h \gg 1$ and $\varepsilon_r \gg 1$, the electric field lines concentrate mostly in the substrate [4]. Fringing affects causes the microstrip line to appear larger. This is relative to a reference frame of electrical dimensions compared to a reference frame of its physical dimensions.

Since some of the waves travel in the substrate and some in air, an *effective dielectric constant* ε_{eff} is introduced to account for fringing and the wave propagation in the line [4]. The effective dielectric constant is defined *by "setting a reference dielectric constant out of the uniform dielectric material so that any situation with two dielectric constants has the identical electrical characteristics as the actual line"* [4]. For a line with air above the substrate, the effective dielectric constant has values in the range of $1 < \varepsilon_{eff} < \varepsilon_r$ [4]. For most applications where the dielectric constant of the substrate is much greater than unity ($\varepsilon_r \gg 1$), the value of ε_{eff} will be closer to the value of the actual dielectric constant ε_r of the substrate (*i.e.* $\varepsilon_{eff} \approx \varepsilon_r$)[4].

Pozar takes the previous analysis further by stating the exact fields of a microstrip line constitute a hybrid TM-TE wave, and require more advanced analysis techniques [16]. However, in most practical applications the dielectric substrate is electrically very thin ($d \ll \lambda$), and hence the near fields are quasi-TEM [16]. In other words, the fields are essentially the same as those of the static case. Thus, good approximations for the phase velocity, propagation constant and characteristic impedance can be obtained from static or quasi-static solutions [16].

2.5 Theoretical Design of a Rectangular Patch

The rectangular patch is by far the most widely used configuration, and thus central to this thesis. Consider the rectangular patch with probe feed using design theory of the Transmission-Line Model. An understanding of fringing field affects and a simplified formulation of them are described above. A design procedure given here will lead to practical designs of rectangular microstrip antennas in antenna engineering. Initially, the relative permittivity ε_r, the operating frequency f_o (in Hz), and the height of the substrate d are chosen. For an efficient radiator, a practical width that leads to good radiation efficiency is given by [4] as:

$$W = \frac{c}{2 f_o} \sqrt{\frac{2}{\varepsilon_r + 1}} \quad \text{(Eq.2.1)}$$

Next, determine the effective dielectric constant of the microstrip antenna from [4] by:

$$\varepsilon_{eff} = \frac{\varepsilon_r + 1}{2} + \frac{\varepsilon_r - 1}{2} \frac{1}{\sqrt{1 + 12 d/W}} \quad \text{(Eq.2.2)}$$

As noted previously, the effective permittivity calculation yields $\varepsilon_{eff} < \varepsilon_r$, where the effective relative permittivity accounts for the fact that the electric field lines are partly in the substrate dielectric and partly in the air due to fringing effects. If this inhomogeneous medium (air and the dielectric) is replaced with a homogeneous one having an effective relative permittivity of $\varepsilon_r = \varepsilon_{eff}$ as shown in Figure 2.8, then all

properties of the line or patch remain unchanged for the situation given in Figure 2.9 [17].

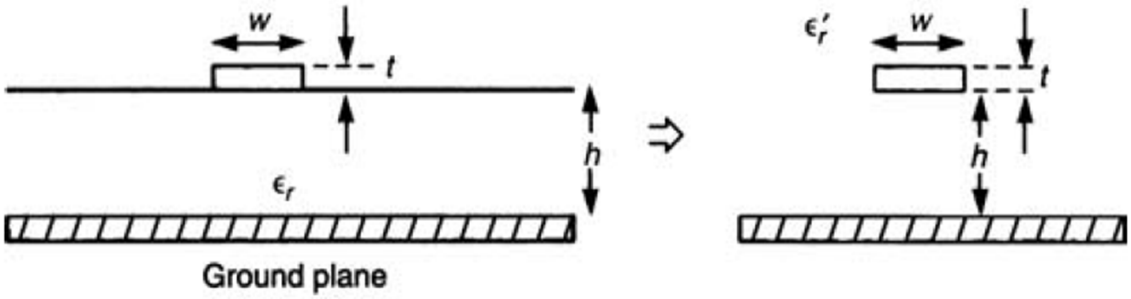

Figure 2.8 A microstrip line [17]

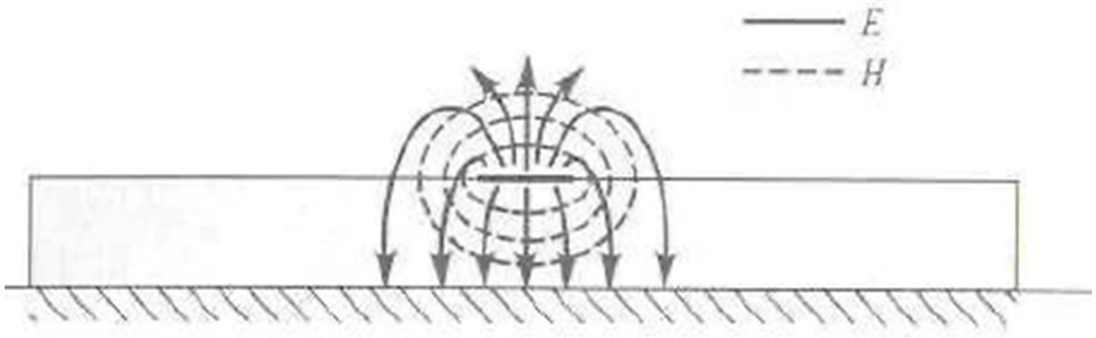

Figure 2.9 Electric and magnetic fields lines [16].

We have seen in Section 2.4 that because of the fringing effects the microstrip antenna appears (electrically) longer than its physical dimensions. For the principle E-plane (*zy* plane in this case), this is demonstrated in Figure 2.10 where the dimensions of the patch along its length have been extended on each end by a distance *ΔL*. This *ΔL* is a function of the effective dielectric constant ε_{eff} and width-to-height ratio (*W/L*) [4]. From [4], the effective length is calculated to be:

$$\Delta L = h(0.412)\frac{(\varepsilon_{eff}+0.3)(W/h+0.264)}{(\varepsilon_{eff}-0.258)(W/h+0.8)}. \qquad \text{(Eq.2.3)}$$

Since the length of the patch has been extended by ΔL on each side, the effective length of the patch is found to be:

$$L_{eff} = \frac{c}{2f_o\sqrt{\varepsilon_{eff}}} - 2\Delta L. \qquad \text{(Eq.2.4)}$$

where c is the speed of light.

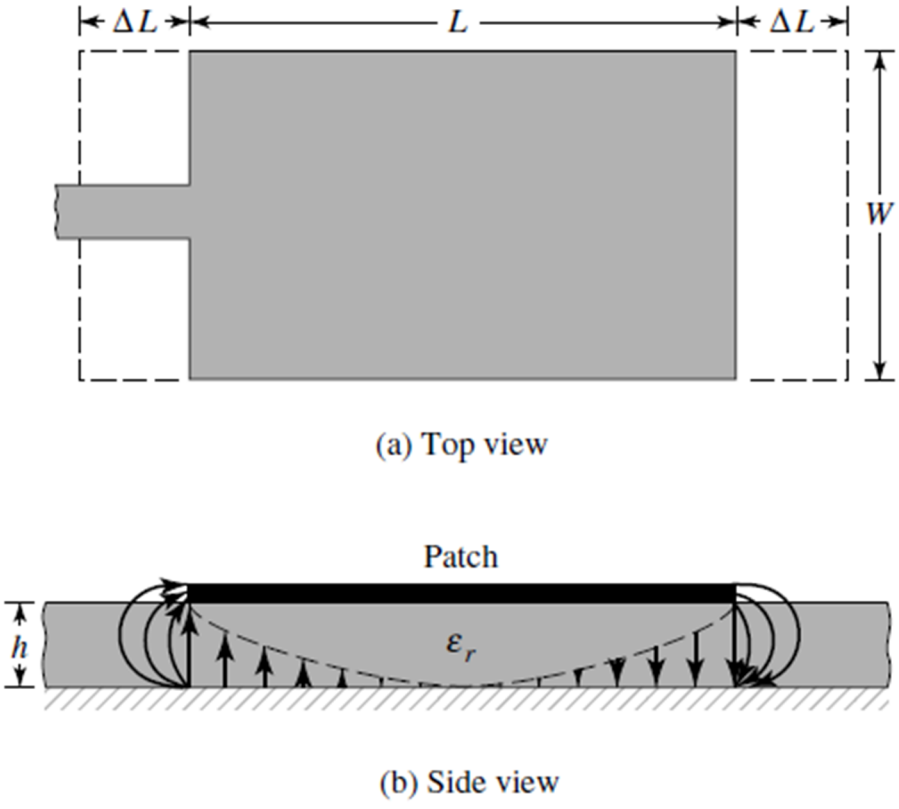

Figure 2.10 Physical and effective lengths of rectangular microstrip patch [4]

Note that, depending on the substrate of choice, in order to make the design more precise other factors need to be included such as the loss tangent (δ), and the surface conductivity (σ) of the material.

2.6 Basics of Electromagnetic Band Gap Structures

Examples of periodic structures exist throughout nature. When microwave elements are engineered in periodic arrays, the interactions of these engineered elements with electromagnetic waves bring about new phenomena. In particular, characteristics such as frequency stop bands, pass bands, and band gaps have been identified [11]. According to [11], "*generally speaking, electromagnetic band gap (EBG) structures are defined as artificial periodic (or sometimes non-periodic) objects that prevent/assist the propagation of electromagnetic waves in a specified band of frequency for all incident angles and all polarization states*". However, in practice, it is almost impossible to construct such a complete band-gap structure. Therefore, partial band-gaps are achieved frequently [18].

Periodic structures such as EBGs can also be engineered as an artificial ground plane. The beneficial features of the novel artificial ground plane in antenna engineering compared with the traditional perfect electric conductor (PEC) ground plane with wire antenna designs are illustrated in Table 2.1. In the top row of Table 2.1 we see an electric current perpendicular to a PEC ground plane, where its image current has the same direction in order to satisfy the boundary conditions. Thus, this antenna has good radiation efficiency. However, the antenna height is relatively large because of the vertical placement of the current. To realize a low-profile design that is always desired in modern wireless communication systems, one may put a wire antenna horizontally close to the ground plane as shown in the second row of Table 2.1. However, the problem with this structure is the poor radiation efficiency because the image current from the PEC ground plane, which has an opposite flowing direction, cancels the radiation from the

original current. Row 3 of Table 2.1 represents a novel artificial ground plane, as will be discussed throughout this chapter, which is capable of providing a constructive image current even with a low-profile configuration, resulting in good radiation efficiency. It overcomes the difficulty of the PEC ground plane to realize both low-profile and high-efficiency design goals. Therefore, the artificial ground plane has a great potential for antenna applications [19].

Table 2.1 Comparison of Conventional PEC and Artificial Ground Planes in Antenna Designs [19].

Options	Efficiency	Low Profile
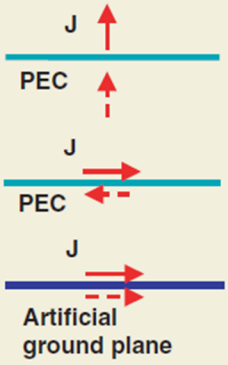	  	  

Before delving further into EBG or periodic structures a quick understanding of wavenumber is needed to continue. A constant $k = \omega\sqrt{\mu\varepsilon}$ is defined and called the angular wavenumber, or propagation constant of the medium with units of *rad/m*. The wavenumber is a property of a wave, its spatial frequency that is proportional to the reciprocal of the wavelength.

EBG structures can be realized from periodic arrangements of dielectric materials and metallic conductors. One way EBGs can be categorized is as a two-dimensional

planar surface. Two examples of a 2-D EBG surface are illustrated in Figure 2.11. One is a mushroom-like surface and the other a uni-planar (Jerusalem Cross) design without vertical vias. The 2-D EBG surfaces have advantages of low profile, light weight, and low fabrication cost and are widely considered in antenna engineering [11]. These 2-D EBG surfaces, especially mushroom-like EBGs, will be the reference focus of this thesis.

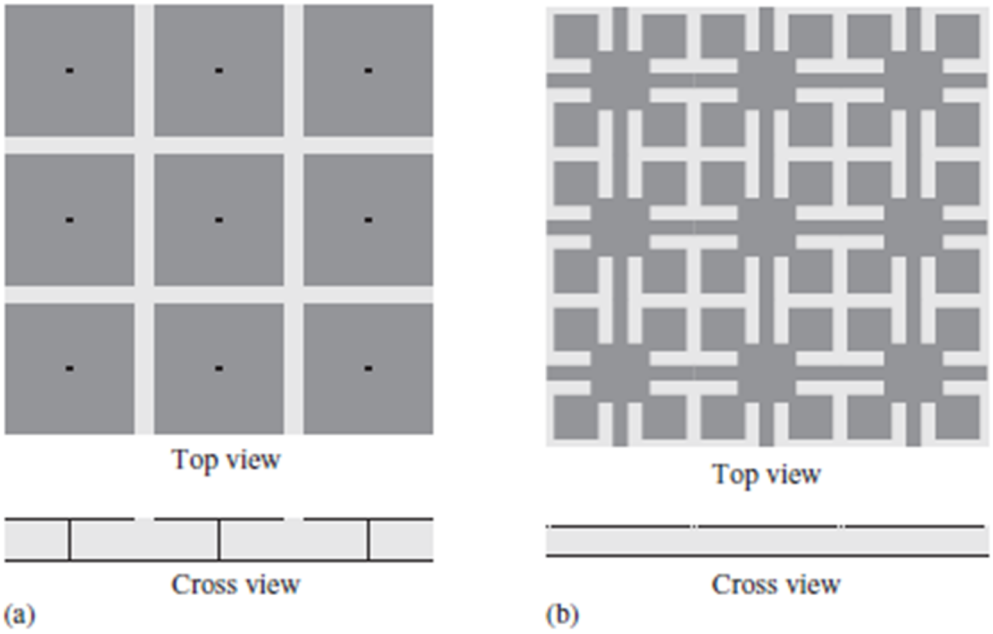

Figure 2.11 Two-dimensional EBG surfaces: (a) a mushroom-like surface and (b) a uni-planar surface, in courtesy of [11].

Planar EBG surfaces have shown distinctive electromagnetic properties with respect to incident electromagnetic waves, such as:

(1) When the incident wave is a surface wave ($k_x^2 + k_y^2 \le k_0^2$, k_z is purely imaginary), the EBG structures show a frequency band gap through which the surface wave cannot propagate for any incident angles and polarization states. A typical dispersion diagram is shown in Figure 2.12 [11].

(2) When the incident wave is a plane wave ($k_x^2 + k_y^2 \le k_0^2$, k_z has a real value), the reflection phase of the EBG structures varies with frequency, as shown in Figure 2.13. At a certain frequency the reflection phase is zero degrees, which resembles a perfect magnetic conductor that does not exist in nature [11].

In the above equations, k_x and k_y are the wavenumbers in the horizontal directions, k_z is the wavenumber in the vertical direction, and k_0 is the free space wavenumber.

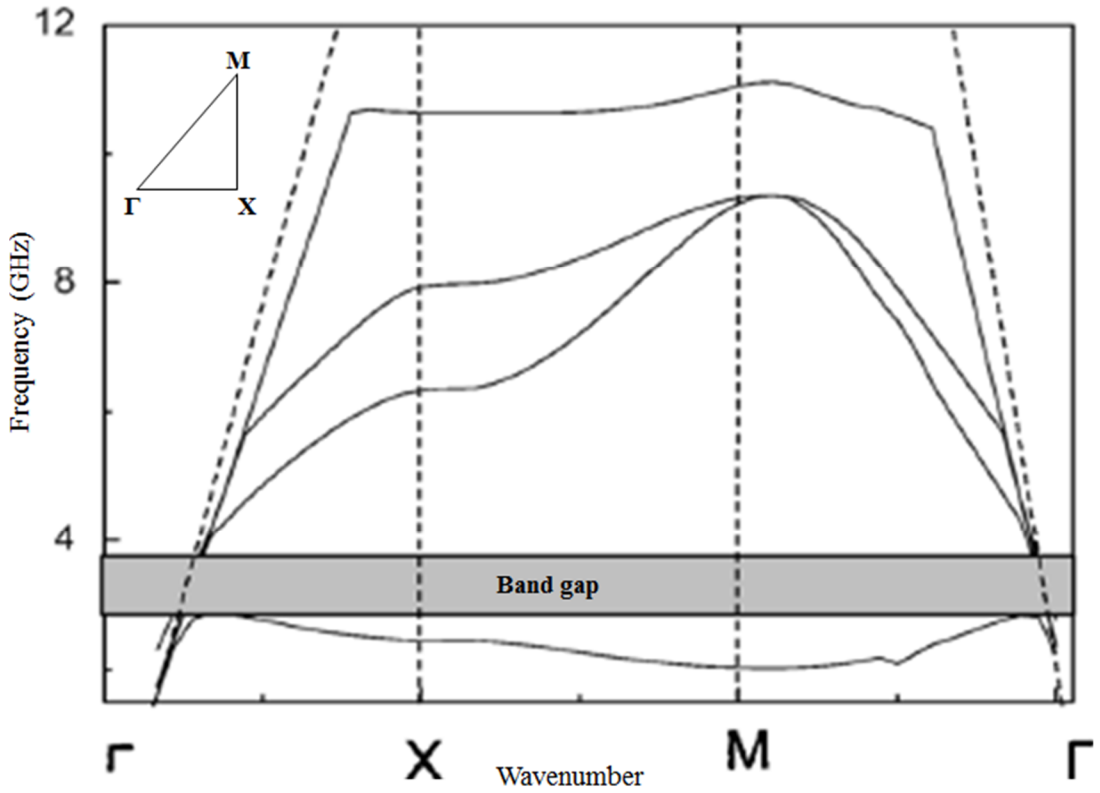

Figure 2.12 Dispersion diagram of conventional EBG structure [20].

The order and symbols (Γ X M Γ) of Figure 2.12 indicate the bombardment direction of traveling waves at the cell by varying the mode of the wave as well as its phase. From Γ to X the phase is 0˚-180˚, from X to M the phase is 180˚ to 360˚ and from M to Γ the phase is from 360˚ to 540˚.

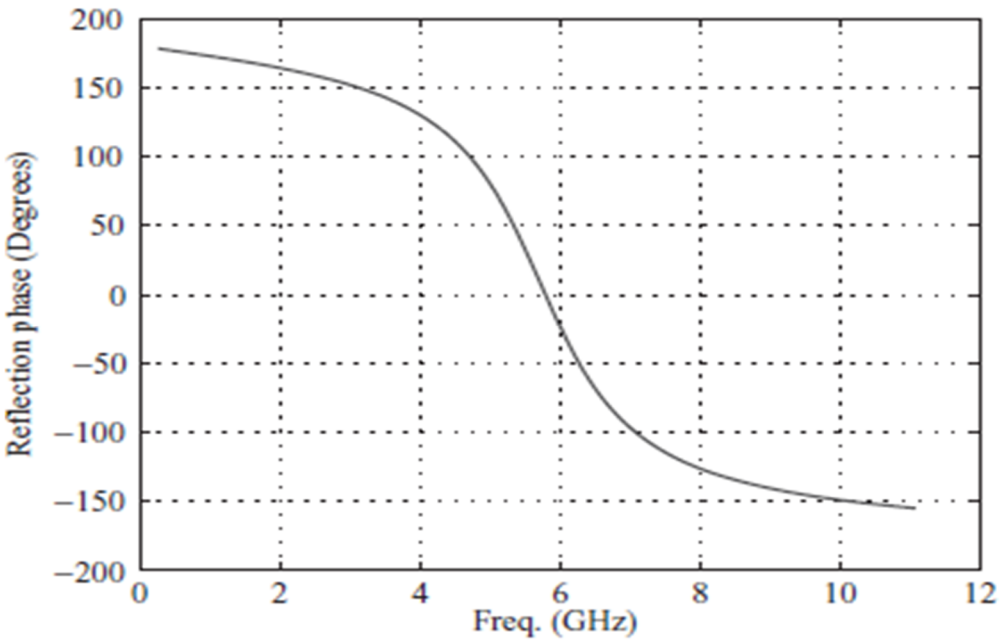

Figure 2.13 A planar EBG surface exhibits an in-phase reflection coefficient for plane wave incidence [11].

There are three categories in which to analyze the unique features of EBG or periodic structures: (1) lumped element model, (2) periodic transmission line method, and (3) full wave numerical methods. The lumped element model is the simplest one that describes the EBG structure as an *LC* resonant circuit [11], as shown in Figure 2.14.

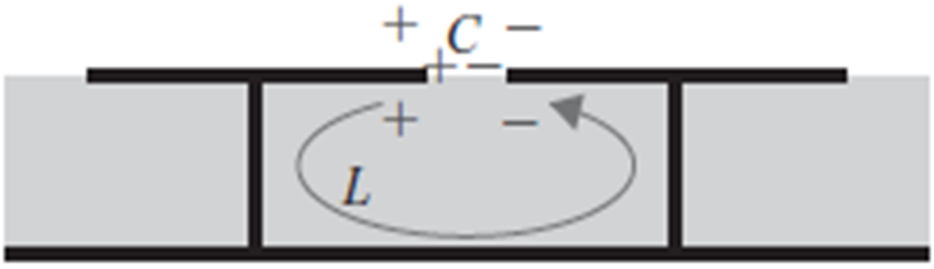

Figure 2.14 Lumped *LC* model for EBG analysis [11].

The values of the inductance *L* and the capacitance *C* are determined by the EBG geometry and its resonance behavior which is used to explain the band gap features of the

EBG structure. Given that this model is simple to understand, however, the results are not very accurate because of the simplified approximation of *L* and *C*. *LC* circuits are used either for generating signals at a particular frequency, or picking out a signal at a particular frequency from a more complex signal. Filtering in this respect is to design an ideally controlled set(s) of distinct waves to produce a desired behavior.

As mentioned above, the behavior of these EBG structures with microstrip (patch) can be described as an *LC* filter array like that of Figure 2.15. As is seen in this figure the high-impedance surface is built as a thin two-dimensional lattice of plates attached to a ground plane by metal-plated vias. The plates provide capacitance and inductance, and it has high electromagnetic impedance near its *LC* resonance frequency [21].

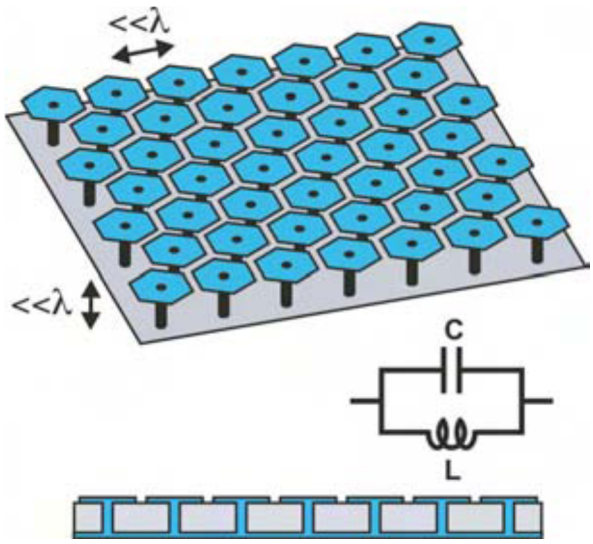

Figure 2.15 A high-impedance surface is built as a thin two-dimensional lattice of plates attached to a ground plane by metal-plated vias. [22].

The inductance *L* results from the current flowing through the vias, and the capacitance *C* is due to the gap effect between the adjacent patches, as presented in Figure 2.16. The capacitance in a high-impedance surface is due to the proximity of the

neighboring plates defined by the periodic boundary condition (PBC). The inductance comes from the current loops that are formed between the plates and the ground planes through the vias. The impedance of the surface can be modeled as a parallel resonant *LC* circuit, as shown in the picture to the right [22]. Take careful note that this particular EBG cell includes via, where in later chapters we will find that vias may not be present.

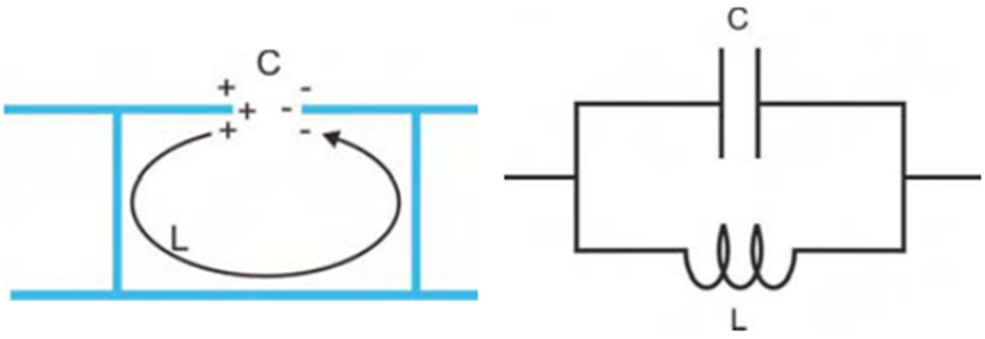

Figure 2.16 The capacitance and inductance demonstrated from the excitation of a high-impedance surface, as the picture on the left indicates. The impedance of the surface can be modeled as a parallel resonant LC circuit, as shown in the picture to the right [22].

For an EBG structure with patch width W, gap width g, substrate thickness h and dielectric constant with relative permittivity ε_r, the values of the inductor L and the capacitor C are determined by the following formulas [23]:

$$L = \mu_0 h$$
$$C = \frac{W\varepsilon_0\left(1+\varepsilon_r\right)}{\pi}\cosh^{-1}\left(\frac{2W+g}{g}\right). \qquad \text{(Eq.2.1)}$$

When L and C are connected together, an electric current can alternate between them at the circuit's resonant frequency. Note that, if a circuit is driven at the resonant frequency, then we say that the circuit is in resonance. This is because the frequency of

the forcing function is the same as the natural frequency of the circuit. Thus they are matched. The resonant frequency for an LC circuit is determined from:

$$\omega_0 = \frac{1}{\sqrt{LC}}. \qquad \text{(Eq.2.2)}$$

The periodic transmission line method is another technique used to analyze EBG structures [11]. Figure 2.17 displays a transmission line model of EBG structures, where Z_p is the impedance for each periodic element and X_C is the coupling capacitor. Upon analyzing the cascaded transmission line, the dispersion curve like that of Figure 2.12 can be obtained, thus providing more information than the lumped element method. The problem with this method is how to accurately obtain Z_P and X_C values for the EBG structures.

Key to understanding the behavior of a single cell element is knowing its inductance and capacitance. From understanding a single element's behavior the antenna systems designer is able to better understand the inductive and capacitive nature that arises from a periodic array of cells.

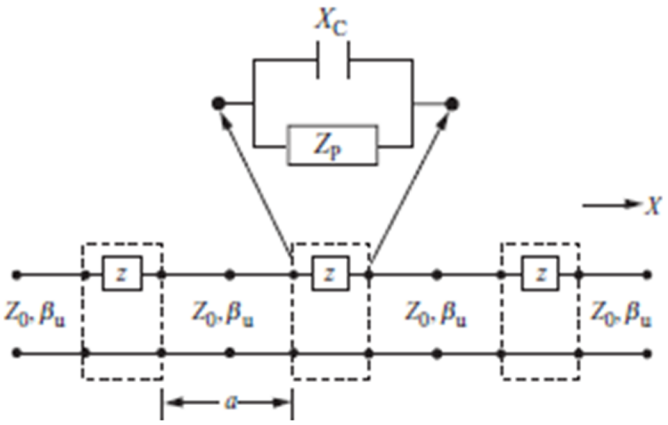

Figure 2.17 Periodic transmission line method for EBG analysis [11].

Because of the fast development in computational electromagnetics over the past years, various numerical methods have been applied in the full wave simulations of EBG and periodic structures. Both the frequency domain methods, such as the Method of Moments (MoM) and Finite Element Method (FEM), and the time domain methods like Finite- Difference Time-Domain (FDTD) have been utilized by different research groups to characterize EBG structures [11]. Analysis reported in this thesis has been using MoM from CAD called FEKO [24].

The main goal of using EBG or periodic structures integrated with microstrip antennas is to achieve better gain and efficiency, lower side-lobes and back-lobes levels, and better isolations among array elements by suppressing surface wave modes. This will be reported in Chapters 3 and 5.

2.7 Conclusion

In conclusion to Chapter 2, microstrip "patch" antennas were introduced. This included basic information regarding what they are, characteristics of them, examples of their geometries, and listing of different feeding methods for them. Furthermore, the theoretical designs of microstip patches were given. This included an understanding of electromagnetic behavior with respect to surface waves, and included mathematical equations unique for this design. Finally, some basic information on periodic structures, namely EBGs was given.

3 WEARABLE ANTENNAS AND THEIR APPLICATIONS

Wearable antennas are becoming more attractive in antenna engineering as is covered in Sections 3.1, and 3.2. The former introduces wearable antennas, and the latter presents emerging applications. Sections 3.3 and 3.4 review surface waves and wave modes, respectively, so as to have a physical understanding of how they negatively affect an antenna's performance. Once there behavior is understood, Sections 3.5, and 3.6 demonstrate how to use periodic structures to load the antennas to control and improve their radiation characteristics, mainly by suppressing surface waves. Section 3.7 includes a discussion of wearable antennas for space suit application. Finally, Section 3.8 concludes the chapter.

3.1 Wearable Antennas

The first public research report on wearable antennas dates back to 1999, in which a dual-band planar antenna was designed for wearable and ubiquitous equipment [25]. Since then research on wearable antennas has received growing interest among university and industry researchers.

Studies presented at international conferences [26-28] showed that fabrics are suitable for microstrip antenna substrates. The conductive electro-textiles or e-textiles are used as antenna patch and ground plane while non-conductive textiles constitute the antenna substrate. Once this was realized, the development of textile antennas for body

wearable applications and investigations of their performance under bent conditions became a new engineering feat. However, even though this type of antenna could be easily worn on body and integrated into clothing, there was still a balance of an integrated system, between the antenna and other electrical components, as well as the interaction between the antenna and the human body, which still needs to be studied.

Textile antenna requirements are application specific. However, [29, 30] came to the conclusion that desired antenna characteristics with most applications are:

(1) Light weight
(2) Low fabrication cost
(3) Low maintenance cost
(4) No setup requirement
(5) Flexible and stable to withstand bending and stretching
(6) Robust to withstand damage from obstacles
(7) Hidden and water proof to avoid wet weather conditions
(8) Capable of providing shielding from the adverse effects of the human body

Further elaborating on (5), the human body consists of a superposition of bends in arbitrary directions, where textiles satisfy these dynamic poses, a property called *Drapability* [31]. In order to preserve textile properties such as flexibility and comfort, the antennas should be fully integratable into the garments. Finally, the electromagnetic properties of e-textiles play important roles in antenna design and performance, and so the textile antennas should be able to withstand these bending strains while maintaining

their radiation specifications. Since bending of textile antennas and their analysis is outside the scope of this thesis, for further inquiry please refer to [32-34].

According to [29], important factors that can influence the wearable antenna performance are:

- ***Human body interaction with the antenna.*** The human body is an irregularly shaped object with frequency dependent permittivity and conductivity. The behavior of the electromagnetic field inside the body and the scattering field depends mainly on the body's physiological parameters, geometry, frequency and polarization of the incident field. Due to high permittivity of body tissues [35] the antenna resonant frequency will change and detune to a lower one. Another important parameter is the antenna gain that directly affects the power transmitted in a maximum radiation direction. The human body is electromagnetically lossy and some part of the radiating power from the antenna will be absorbed by it, thus resulting in a lower gain.

- ***Variations in dimensions.*** Due to stretching and compression, which are common for fabric, the antenna structure can easily deform and affect its performance characteristics. As a result it will be difficult to mass produce an antenna with the same radiation characteristics even using the same materials.

- ***Water absorption.*** Fabric antennas made of textile material contain voids that can easily absorb water and moisture, thus this can change the resonant frequency and bandwidth of an antenna.

With the above analysis in mind it is worthwhile to mention feeding methods for e-textiles. The feeding method has an important role in the overall characteristics of the devices specially the impedance bandwidth of the antenna [36]. As the reader can imagine soldering on fabric would be difficult, resulting in burning, and/or de-tuning of the resonant frequency of the antenna due to extra conducting sediments left from the solder, as Figure 3.1 indicates. To mitigate this problem [37] explored the first aperture coupled patch antenna for integration into wearable textile systems. In this feed method the feeding transmission line was totally isolated from the antenna, thus allowing optimal selection of antenna substrate and feed substrate material. This paper found that this feeding method was more convenient and comfortable for the user with a resulting potential product of a highly efficient and fully flexible wearable antenna that is integratable into garments.

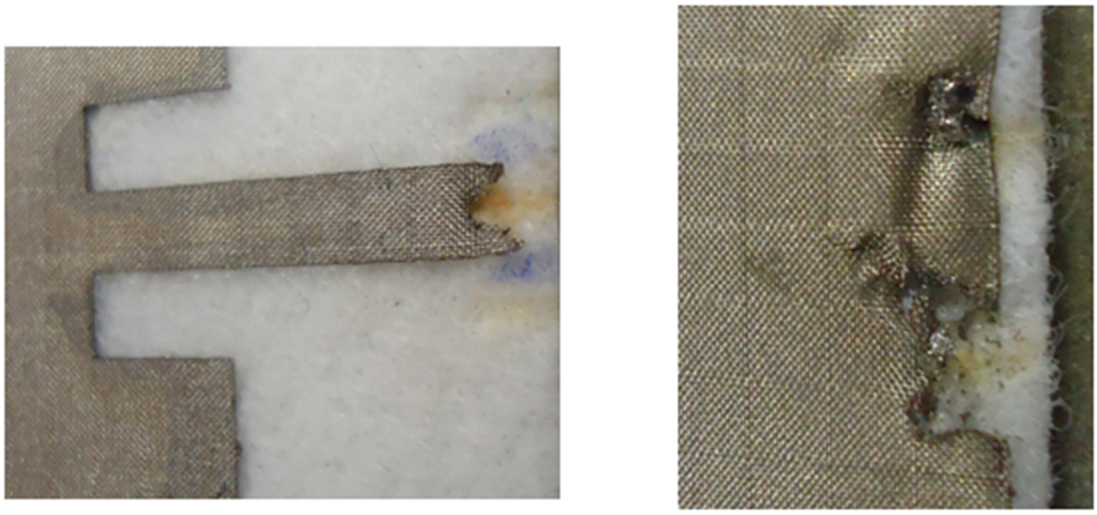

Figure 3.1 (a) E-textile inset feed antenna burned on the feed line, and (b) shows that the ground plane also burned.

In the next section, a general overview of wearable antenna applications is briefly covered, while Section 3.7 takes a more in-depth, application specific focus on wearable antenna arrays integrated with space suit.

3.2 Applications of Wearable Antenna Systems

The evolution of textile antennas has led to of a vast number of potential applications and other supporting systems benefiting flexible antennas. The earliest demand for wearable antennas was set by the military for concealing the identity of soldiers carrying a radio in the battlefield [29], as Figure 3.2 indicates. This allowed no visual signature, as well as all-weather operation. Besides military applications, textile antennas are becoming a part of the health sector for detection of early cancer using imaging methods [29]. Other interesting applications of wearable textile systems include:

- Assistance to emergency services such as police, paramedics and fire fighters
- Navigation support in the car or while walking
- Pulse rate monitoring in sports
- Space applications

More specifically, wearable antenna systems are of interest for monitoring the performance of the body during exercise, monitoring functions such as heart rate and blood pressure for medical diagnosis (i.e. life signs), security systems, transport fare payment, tracking systems for prisoner management, detecting systems for child protection, hospital patient health management, and for general network connections [30, 38].

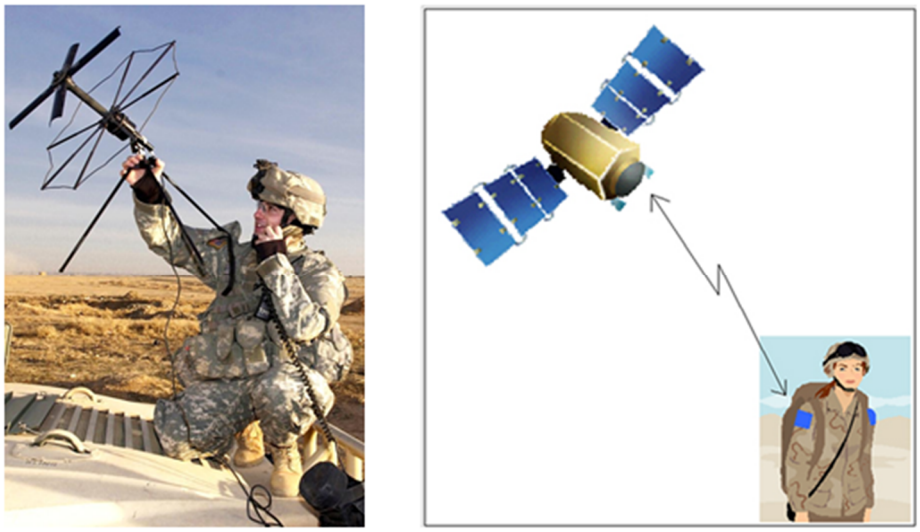

Figure 3.2 (a) Standard Antenna, (b) Textile Antenna.

The development of wearable electronic systems for applications has been rapid [33]. It is projected that a variety of consumer electronics will be built into the garments of future clothing. Actually, wearable electronic systems, sometimes referred to as electro-textiles or e-textiles, have been around for a period of time; however, they are mainly used as electromagnetic shielding materials [39]. Typical wearable systems, as shown in Figure 3.3, consists of Central Processing Unit (CPU), Liquid Crystal Display (LCD) display, wireless communication links, positioning system, and batteries [11]. Furthermore, with the development of the fourth generation of mobile communications (4G), wearable antennas, especially textile antennas, are receiving more and more attention [31, 40-42]. Ultimately, this wide range of unobtrusive wearable and ubiquitous computing devices integrated into daily clothing will create a so called Body Area Network (BAN).

This thesis is only concerned with the specific application of textile antennas integrated with space suit, elaborated upon in Section 3.7. For more inquiry on other applications of textile antennas please review [26, 38, 42, 43]. The next section gives details of what surface waves are, and what problems they cause to microstrip antennas.

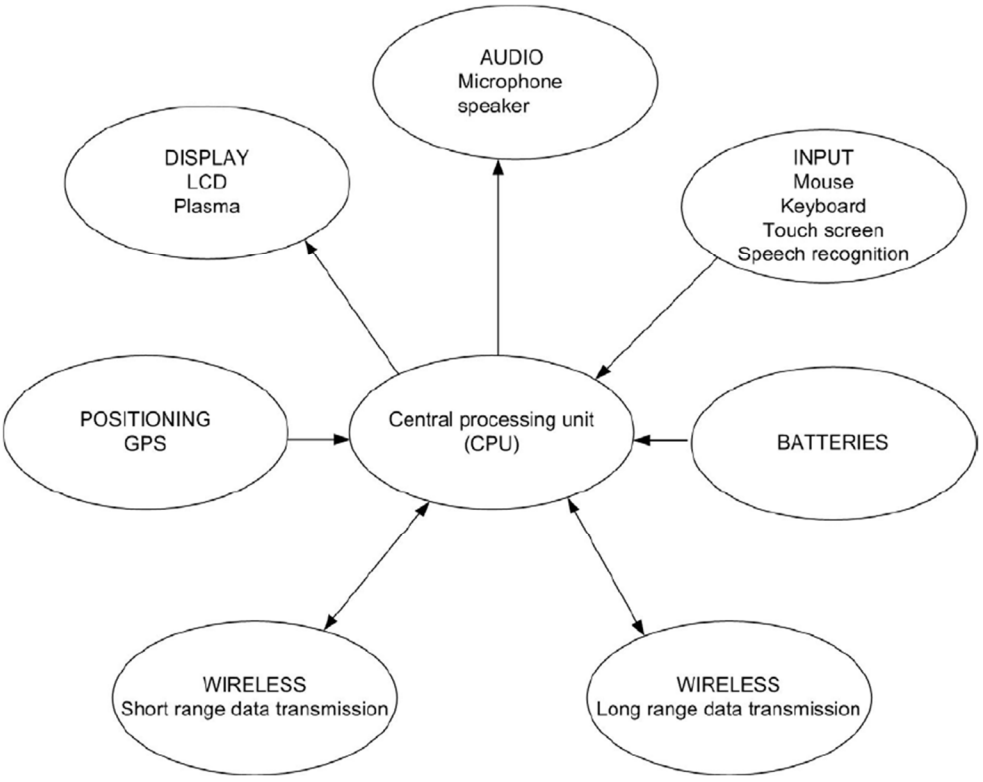

Figure 3.3 Block diagram of a typical body worn wearable system [29].

3.3 A Review of Surface Waves

Losses in a microstrip antenna occur in three ways: from conductor loss, dielectric loss, and surface wave excitation [17]. This thesis will elaborate on surface wave excitation. But before delving any further into surface waves, a quick elaboration on antenna radiation lobes is in order.

Various parts of a radiation pattern are referred to as lobes, which may be sub classified into *major* or *main*, *minor*, *side*, and *back lobes*. A *radiation lobe* is a "portion of the radiation pattern bounded by regions of relatively weak radiation intensity" [4]. Figure 3.4 demonstrates a symmetrical three-dimensional polar pattern with a number of radiation lobes. Some are of greater radiation intensity than others, but all are classified as lobes. Figure 3.5 illustrates a linear two-dimensional pattern [one plane of Figure 3.4] where the same pattern characteristics are indicated [4]. The half power beamwidth is the angular separation between the half power points on the antenna radiation pattern, where the gain is one half the maximum value.

Surface waves at microwave frequencies are ordinary surface currents, and they are only very weakly bound to the surface [22]. Surface waves can be controlled, by using periodic structures as shown in Sections 3.5 and 3.6.

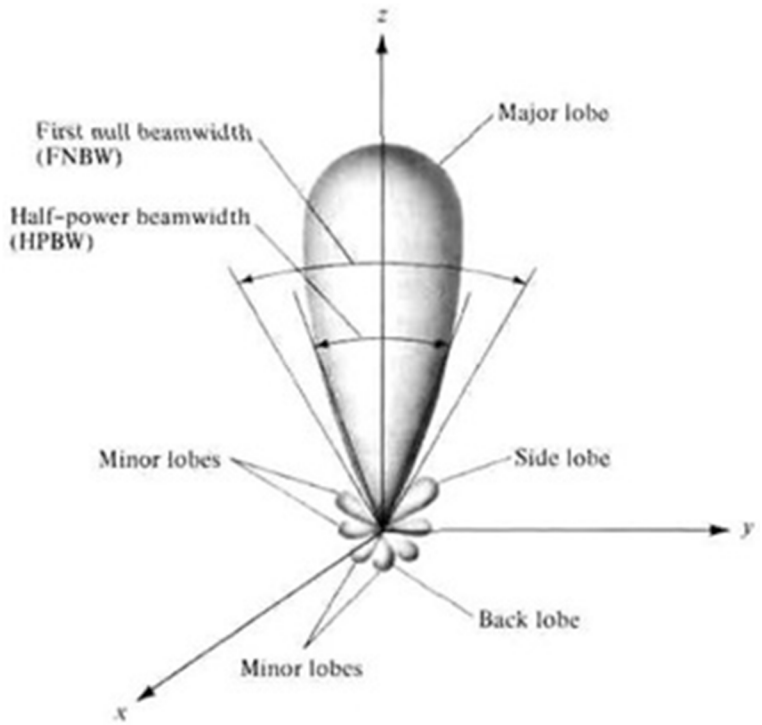

Figure 3.4 Radiation lobes and beamwidths of an antenna pattern [4].

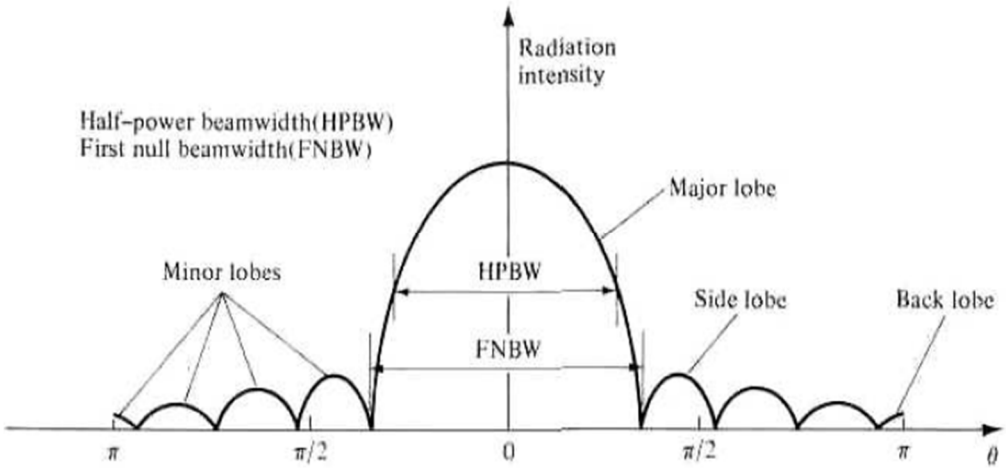

Figure 3.5 Linear plot of power pattern and its associated lobes and beamwidths [4]

Surface waves, as displayed in Figure 3.6, are a classification of ground waves [44] that naturally presents itself from applying an excitation to the patch antenna or other microstrip radiators. A surface wave comes into existence because not all the energy intended to radiate is radiated ideally broadside to the patch radiator, where some of that energy is radiated as side lobes and some as back lobes. These side and back lobes are generated initially from surface waves that are a portion of the total energy traveling relatively perpendicular to the broadside radiation pattern and are guided by the substrate and the ground plane. When a surface wave meets an object (cavity) and the dimensions of the object do not exceed its wavelength, the wave tends to curve or bend around the object [44]. Furthermore, the smaller the object, the more pronounced the diffractive action will be [44]. Surface waves at microwave frequencies are ordinary surface currents, and they are only very weakly bound to the surface [22].

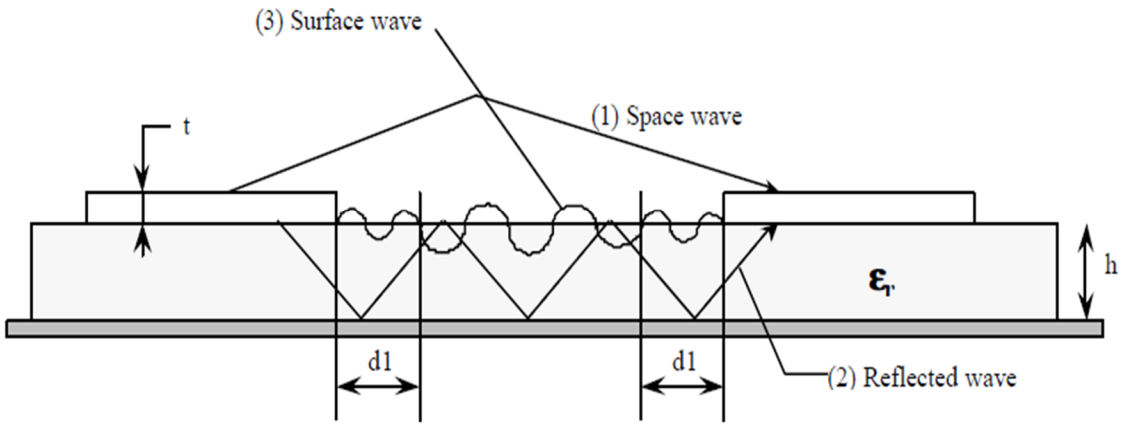

Figure 3.6 Waves excited in microstrip structure [45].

The surface wave phenomenon will prevent optimal antenna system gain, because the fraction of the energy that is not radiated into the main lobe is wasted energy. Gain in the horizontal directions (side lobes) as well as gain in the inverted direction (back lobe) results in less radiated energy than the gain in the zenith direction (main lobe). This radiation from side and back lobes is undesirable in many cases, and so it must be suppressed. Furthermore, this phenomenon of surface waves will create mutual coupling between multiple elements (array) printed on the same substrate.

Two dominating side effects of surface waves are the parasitic cross coupling and cavity effect [46, 47]. It is further mentioned from [47] that the performance of planner antenna arrays can be severely limited by the parasitic cross-coupling of the antennas via surface waves. It was found from [46] that the parasitic loading effect of EBG structures leads to a multi-resonance antenna resulting in a larger bandwidth. On the other hand, the cavity effect is due to reflecting energy from EBG towards the antenna and results in a larger Q value and thereby decreasing the bandwidth. We will elaborate on the Q factor next.

The Q factor (quality factor, antenna Q or radiation Q) is commonly used to get an estimate of the bandwidth of an antenna. The Q factor of the antenna is defined as the quotient of the power stored in the reactive field to the radiated power [48, 49] given as:

$$Q = \frac{2\omega \ \max(W_m, W_E)}{P}, \qquad \text{(Eq.3.1)}$$

where ω is the angular frequency, W_M the stored magnetic energy, W_E the stored electric energy, and P the dissipated power. At the resonance frequency, ω_o, there are equal amounts of stored electric and magnetic energy, *i.e.*, $W_E = W_M$ [50].

The goal is to get better isolations among objects with cavities as well as turning once wasted energy into usable energy by suppressing surface wave modes. A quick review of wave modes relevant to this thesis will be given in the next section. Following is a demonstration of how periodic structures accomplish the goal of surface wave suppression and parasitic phenomena, thus ultimately increasing the gain of the antenna system, as covered in Section 3.6, and Chapter 5.

3.4 Wave Modes

By applying a texture to a metal surface the surface impedance can be altered and thereby change its surface wave properties. The physical behavior of surface waves on a surface is found in many electromagnetics textbooks [21]. The derivation proceeds by making these assumptions: 1) the surface has impedance Z_s, and 2) there exists a wave that decays exponentially away from a surface with attenuation constant α, as shown in Figure 3.7. By applying Maxwell's equations the relationship between the surface

impedance and the surface wave properties of Transvers Magnetic (TM) and Transvers Electric (TE) waves can be determined. It can be shown that TM waves occur on an inductive surface, where the surface impedance is given by the expression

$$Z_s = \frac{j\alpha}{\omega\varepsilon} \quad \text{(Eq.3.2)}$$

Conversely, TE waves can occur on a capacitive surface with the following impedance:

$$Z_s = \frac{-j\omega\mu}{\alpha} \quad \text{(Eq.3.3)}$$

In the above expressions, ε and μ are, respectively, the permittivity and permeability of the space surrounding the surface (which may be vacuum) and ω is the angular frequency of the wave.

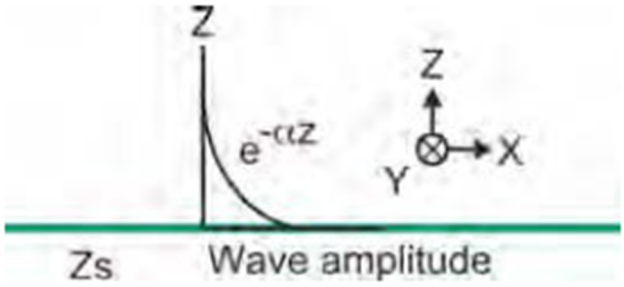

Figure 3.7 A surface wave is a wave that is bound to a surface and decays into the surrounding space [21].

Ordinary metals are slightly inductive, due to the skin effect, so they naturally support TM waves. At microwave frequencies, they are simply the ordinary surface currents, and they are only very weakly bound to the surface. A diagram of TM surface waves is shown in Figure 3.8(a). In a TM surface wave, shown here on a flat metal

surface, the electric field arcs out of the surface, and the magnetic field is transverse to the surface.

While bare metals do not support TE surface waves, dielectric-coated metals can support TE waves above a cutoff frequency that depends on the thickness and dielectric constant of the layer. Furthermore, electromagnetic bandgap structures such as Frequency-Selective Surfaces (FSS) can also support TE waves if the effective surface impedance is capacitive. The parallel resonant *LC* circuit illustrated in Figure 2.14-Figure 2.16, supports TE waves for high frequencies due to its capacitive structure, as shown in Figure 3.8(b), whereas at low frequencies this *LC* circuit is inductive and supports TM waves. Near the *LC* resonant frequency of this circuit, the surface impedance is very high, and in this region, the waves are not bound to the surface; instead, they radiate readily into the surrounding space as leaky waves.

The ultimate behavior an antenna designer wants to control for high impedance surface (EBG) structures is depicted in Figure 3.9. This particular figure indicates the support of a forward traveling transverse electric field wave below a resonant frequency (Perfect Electric Conductor), as well as supports a forward traveling transverse magnetic field wave above the resonant frequency (Perfect Magnetic Conductor).

The effective surface impedance model can determine many of the properties of the high-impedance surface, including the shape and polarization of the surface wave bands. This model does not predict the bandgap, but it does predict a region of radiative interaction [21].

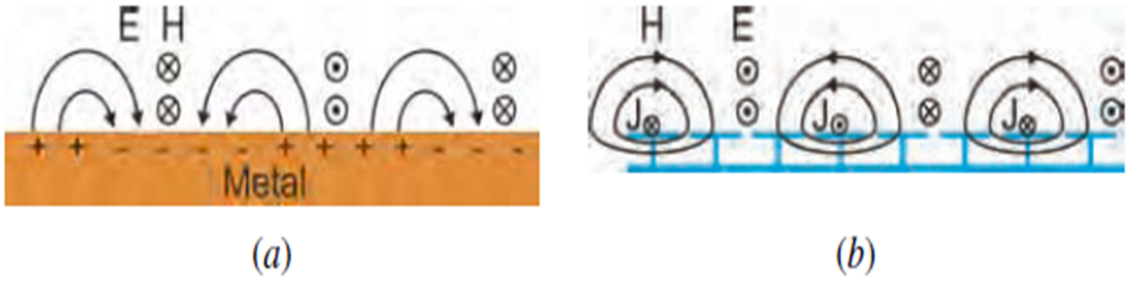

Figure 3.8 (a) TM surface wave on flat metal surface, and (b) fields on high-impedance surface [21].

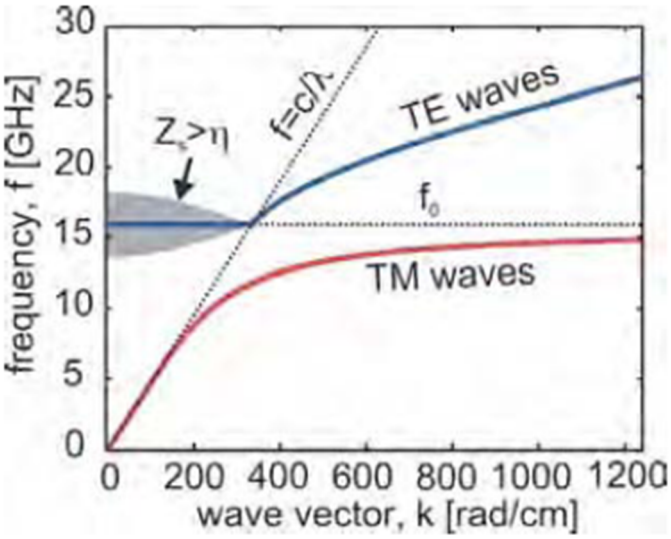

Figure 3.9 Example of band gap feature [21].

Now that we have covered; 1) information on wearable antennas, and 2) some needed knowledge with respect to relevant electromagnetic interactions. In Section 3.5 it demonstrates that by using periodic structures to improve an antenna systems performance, mainly its gain, by suppressing surface waves.

3.5 Controlling Electromagnetic Wave Phenomena using Periodic Structures

Electromagnetic Band Gap (EBG) structured antennas are a class of antennas which use periodic structures to enhance or increase the over-all performance of the

antenna. EBG antennas can be structures which are composed of a cavity and an EBG material (as was described previously). The EBG or other engineered electromagnetic surface textures can be used to alter the properties of metal or e-fabric surfaces to perform a variety of functions. These functions, depending on the design of the substrate, will change the behavior, and enhance the properties of the antenna accordingly. For example, the surface wave band gap has been utilized to enhance antenna gain, decrease back radiation, and reduce mutual coupling of microstrip antennas and arrays [11].

Several periodic cell shapes exist, such as; Jerusalem Cross, square, and rectangular geometries. Also, periodic shapes have been studied relative to their behavioral planar affects while 1) embedded on the same plane as the antenna, and 2) embedded on a different plane as the antenna.

Shown in Figure 3.10 is a periodic structure embedded on the same plane as the antenna with cross section. The cells arranged in this form are sometimes referred to as Frequency Selective Surfaces (FSS). In this uniplanar orientation, the behavior of the periodic cells with or without vias is understood through a dispersion characteristic graph, as Figure 3.11 and Figure 3.12 demonstrates.

Figure 3.11 displays a bandgap feature that a mushroom EBG cell produced, whereas Figure 3.12 shows no band gap feature. This particular type of graph allows the antenna systems engineer to know the designed bandgap, thus understanding its stopband capability as well as the resonance of the periodic structures.

It is worthwhile to mention that FSSs are sometimes referred to as EBGs. They are both considered periodic structures in this thesis.

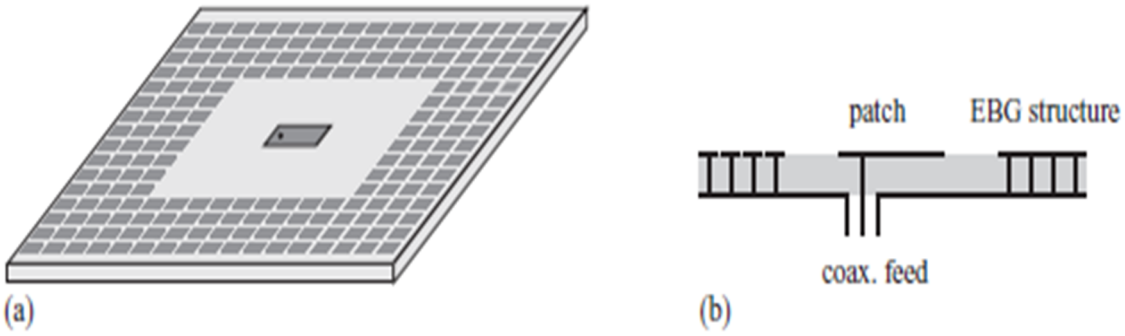

Figure 3.10 Patch antenna surrounded by a mushroom-like EBG structure: (a) geometry and (b) cross section [11].

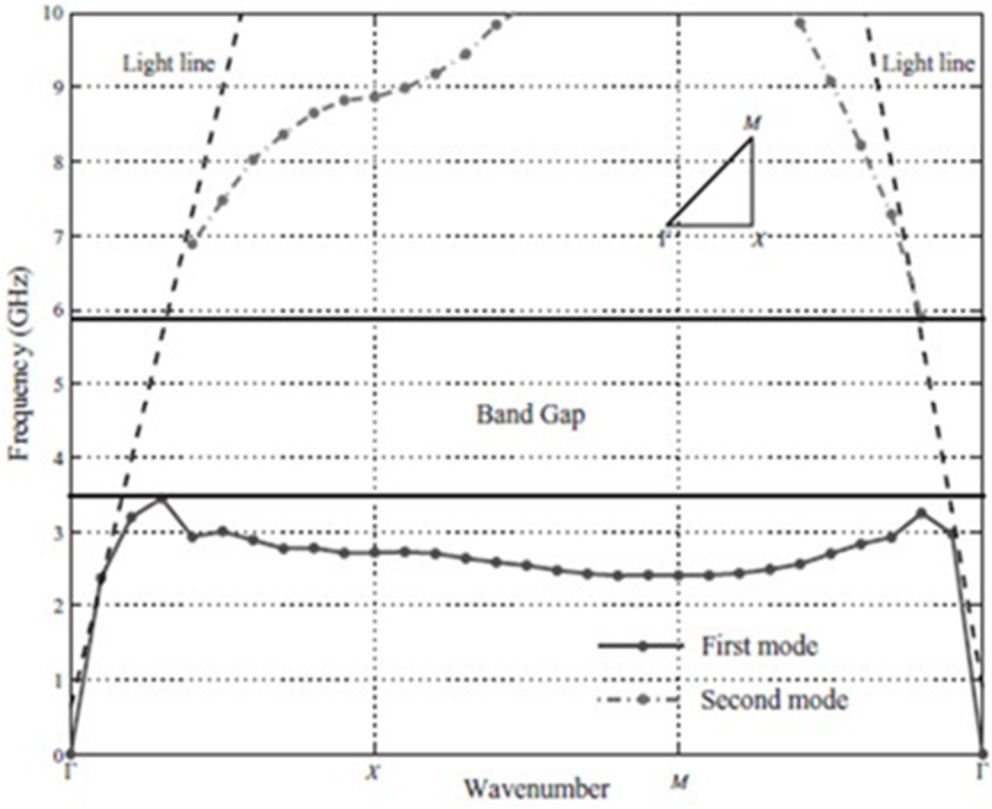

Figure 3.11 Dispersion diagram of an artificial ground plane: a mushroom-like EBG structure, with bandgap feature [11].

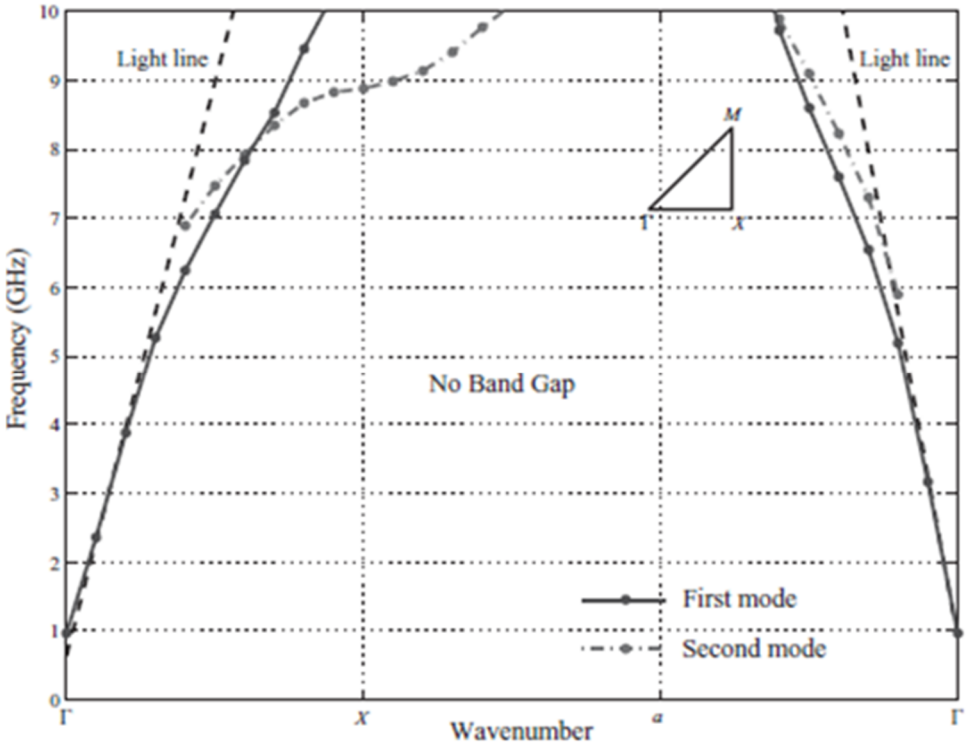

Figure 3.12 A grounded slab no bandgap with patch antenna [11].

Using mushroom like EBG cells, Figure 3.13 shows an example of when the FSS is embedded on a different plane than the antenna. From this, different planar orientation, the behavior of the periodic cells is understood through a reflection/transmission characteristics graph. Referring back to Figure 3.6, one can imagine a bouncing wave effect from reflected waves. Greater insight is found in Figure 3.14. In this figure it can be seen that it is essential for the reflection/transmission coefficients to have a matched resonant frequency to the incoming incident wave.

FSSs present a unique behaviour engineered to obtain a stopband for surface wave propagation along the interface, as well as incoming plane waves. A model for the problem of plane-wave scattering from an FSS as displayed in Figure 3.15 is given in terms of a quasi-static reactive *LC* impedance network that is placed in a TE or TM

vertical transmission line. This figure represents low-frequency equivalent transmission lines for FSS-based surface. Several authors have treated the periodic surface problem via equivalent *LC* circuits to characterize either the reflection or the dispersion properties of metamaterial surfaces [51, 52].

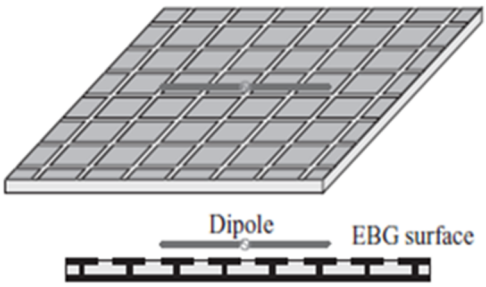

Figure 3.13 Models for the operational frequency band selection of an EBG ground plane. Low profile dipole antenna over a finite EBG ground plane [11].

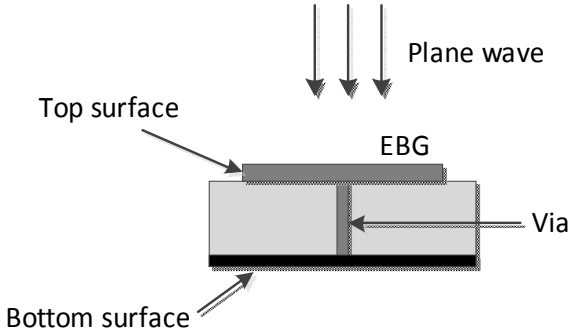

Figure 3.14 Operational frequency band selection of an EBG ground Plane wave normally incident upon the EBG surface.

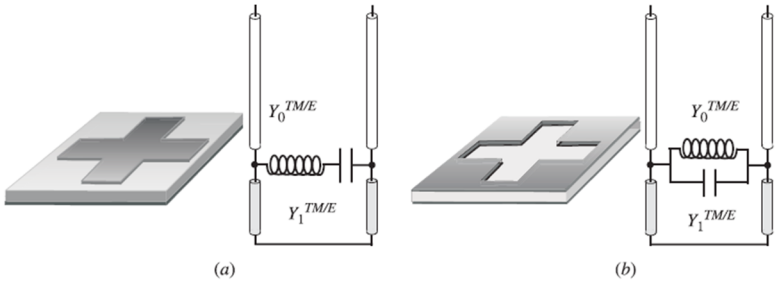

Figure 3.15 (a) Series *LC* circuit for patch-type FSS; (b) parallel *LC* circuit for aperture-type FSS [53].

Information has been covered regarding the use of EBGs or FSSs on how to suppress surface waves by means of applying stopband features. Section 3.6 will demonstrate how this engineered feature can improve the antennas performance, namely to increase gain, and decrease back and side lobe radiation.

3.6 Improving Antenna Performance by using Periodic Structures

The performance of antenna systems mounted on platforms (vehicles, ships, aircraft, satellite, space explorers, etc.) is limited and/or degraded by the electromagnetic interaction between the antenna and the platform. In some applications the desired radiation pattern for an antenna is omnidirectional, as seen on the left side of Figure 3.16. The right side of Figure 3.16 demonstrates the radiation pattern of the antenna from the electromagnetic interaction between the antenna and the platform. To reduce the interference, and to obtain a more "ideal" radiation pattern, EBG surfaces may be used. EBG surfaces can be engineered to mitigate or alter the electromagnetic interaction between an antenna and the platform [54]. This happens by using periodic structures to isolate the excitation fields of the antenna from the platform.

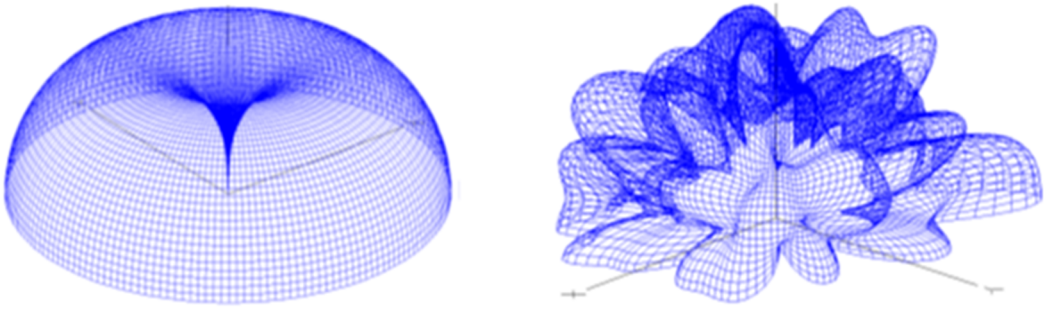

Figure 3.16 Radiation pattern of omnidirectional antenna as seen on the left and on the right is the radiation pattern of omnidirectional antenna on platform [54].

Among the variety of EBG structures which have been developed in recent years, an interesting role is played by FSSs printed on grounded stratified dielectric media. This type of structure creates a particular class of so-called artificial surfaces, whose applications are intended to create Artificial Magnetic Conductors (AMCs) [55, 56]. Imagine a situation as shown in Figure 3.17 where surface waves excited from the dipole amount ultimately to wasted energy. As we have described previously, FSSs (periodic structures) embedded on the same plane as the antenna can suppress or stop the surface waves as Figure 3.18 shows. A similar reaction happens between a microstrip antenna and FSSs (periodic structures).

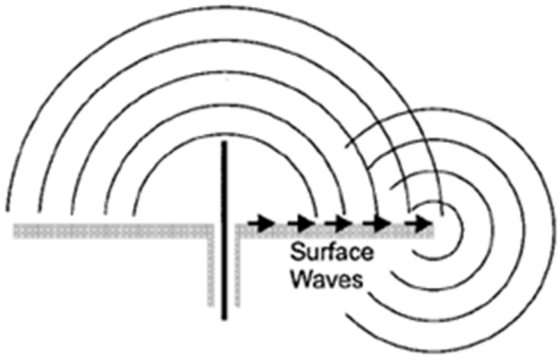

Figure 3.17 Antenna on a flat metal ground plane generates propagating surface currents, which cause multipath interference and backward radiation [22].

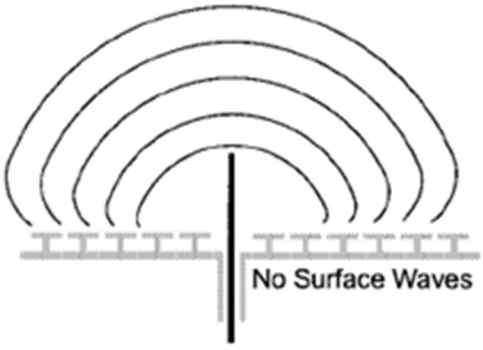

Figure 3.18 Surface waves are suppressed on a high-impedance ground plane [22].

In microstrip antennas, it was found from [46] that EBG structures surrounding a patch element (uni-planar orientation) suppress surface waves achieve better side lobe and back lobe levels resulting in increased radiation efficiency. As covered in previous sections, surface waves travel within the substrate and they are scattered at bends and surface discontinuities, such as the truncation of the dielectric and ground plane, thus degrading the antenna pattern and polarization characteristics [4]. The uni-planer EBG antenna system utilizes once wasted energy and transforms it into usable energy in the form of increased gain. This configuration also decreases or eliminates the electromagnetic interaction between the antenna and platform.

Furthermore, antennas with EBGs have been shown to decrease the size of the overall antenna [11]. Figure 3.19(a) shows an example of a common dipole antenna with its small radiator and longer profile compared to Figure 3.19(b) which has a lower profile design but requires a larger planner area for the radiator. To further illustrate this point, Figure 3.20 shows a top view and cross view of a horizontal dipole near a patch-loaded grounded slab.

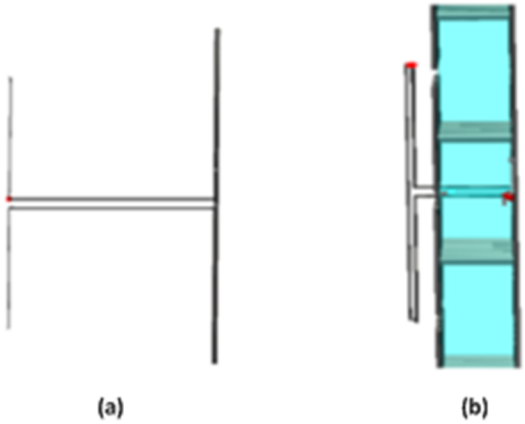

Figure 3.19 Illustration of profile reduction that can be achieved with an EBG surface [54].

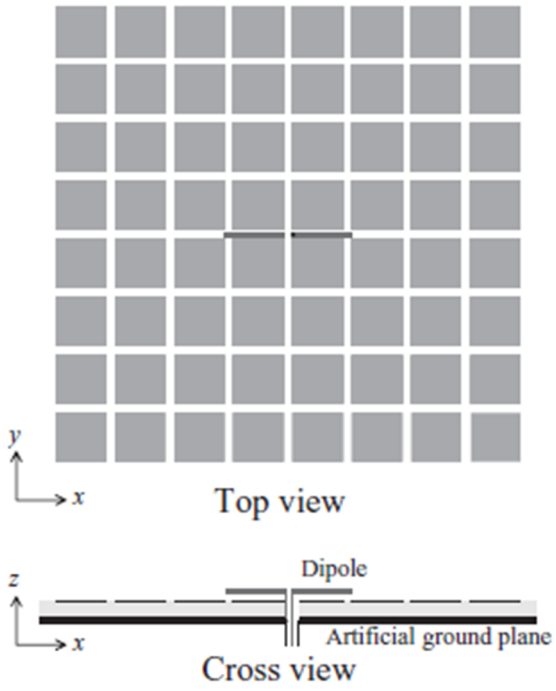

Figure 3.20 Geometry of a horizontal dipole near a patch-loaded grounded slab [11].

Another method of improving antenna performance is to positively utilize the side effect characteristics of EBG structures in microstrip patch antennas. The two dominating side effects of surface waves are the parasitic cross coupling and cavity effect [46, 47]. It is further noted in [47] that the performance of planner antenna arrays can be severely limited by the parasitic cross-coupling of the antennas via surface waves. According to [46] the design parameters of EBG structures can be managed so that the parasitic effect of EBG structure can be the dominating effect and consequently results in larger bandwidth. Furthermore, it was found [46] that an optimal design for EBG unit cell parameters with a specific number of rows can reduce surface waves optimally to achieve a larger bandwidth.

This thesis has provided a description of wearable antennas, EBG (periodic structured) antennas, and their interactions with electromagnetic waves. The EBG or periodic structure was shown to enhance the antenna's system performance. Section 3.7 condenses this information accumulated throughout the previous material into application specific wearable periodic antennas integrated with space suit, as this is the primary interest of this thesis.

3.7 Wearable Periodic Structured Loaded Antenna Arrays for Space Suit Application

Wearable antennas have received much interest due to the integration of personal communications into wearable electronics as covered in Sections 3.1 and 3.2. The wearable antennas are the most essential component to be chosen in order to obtain an optimized design of a wearable system since they are the point of transmission and reception of information. While designing these antennas, the electromagnetic interaction among the antenna, wearable unit and the human operator are important factors to consider. EBG technology has been proposed as a potential design solution [57, 58].

One such example of a wearable EBG antenna comes from [57], where a two-layer wearable EBG antenna was designed and fabricated, as shown in Figure 3.21. The authors used conventional felt fabric with a dielectric constant of 1.1, and a 6 X 6 EBG cell array. In the middle layer 36 EBG cells were glued in place and the main patch antenna was placed on top of the EBG substrate. The two layers were then sewn together and a coaxial SMA connector was used to feed the antenna.

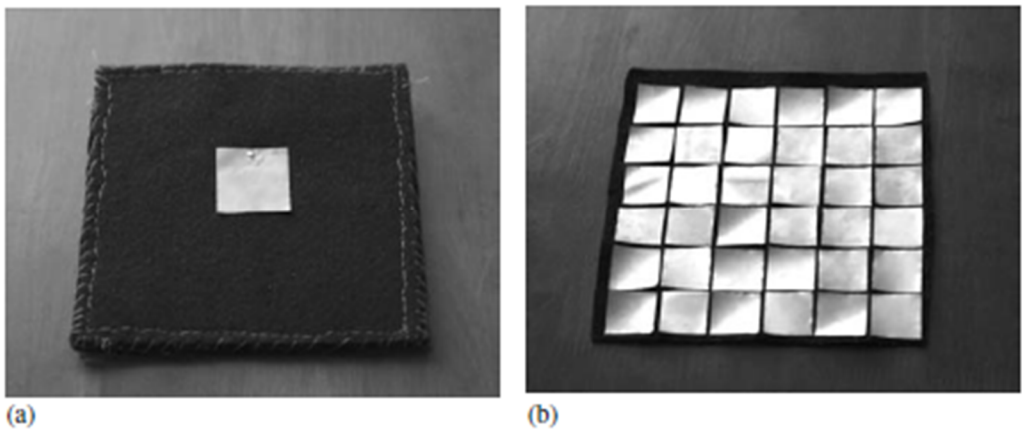

Figure 3.21 Photographs of a wearable EBG a patch antenna: (a) patch antenna on the top layer and (b) EBG surface in the middle layer [57].

Complete situational awareness for space applications involves many similar aspects being discussed for commercial applications, however there are some unique space suit aspects that also need to be considered. Voice over Internet Protocol (VoIP) coupled with standard and high-definition video of the astronaut and surroundings constitute a vital communications link between the astronaut and mission operation systems. Additionally, biotelemetry data, tracking and navigation, and mobile computing are expected to see use in the next generation of suits, as are integration of information about handheld tools and the status of onboard supply inventories [40].

In body-centric applications, the dynamics of the wearer can detune and otherwise alter the radiation properties of the antennas used. Additionally, in a body-worn antenna implementation, one needs to be not only concerned with the peak gain offered by the antennas chosen, but also how this coverage is distributed around the body. Operationally, it is important to maintain good antenna gain over most of the body to help avoid problems with excellent gain over some directions while having very deep nulls in

other directions, and the associated channel equalization problems that are incurred as the wearer moves or turns [40].

Wearable antennas have attracted more and more attention in recent years due to the fact that they can be seamlessly integrated into clothing [27, 31, 43, 59, 60] which is a desired feature for hands free applications. This is important from a space explorer's point of view in that they can continue about their exploring without the need to physically grip communication equipment. Furthermore, wearable antennas can use all the space on clothing that can be utilized to improve quality of signals in wireless communications. This feature alleviates the problem in wireless communication of multi-path fading. This is where the signal strength drops as the mobile terminal moves over a distance comparable to wavelength.

An effective way to overcome multipath fading is by strategically placing antennas into an array throughout the clothing, as depicted in Figure 3.22. Common knowledge tells us the antenna element spacing requires at least half a wavelength separation to avoid coupling. It was found from [40] that three antennas placed carefully throughout the Extra Vehicular Activity (EVA) suit provided significant contribution to radiation at the desired beamforming angle, as is shown in Figure 3.23. The antennas that were used in this experiment were complementary-8 antennas designed for use in the 2.45 GHz Industrial, Scientific, and Medical (ISM) band.

Strategically placing these antenna elements throughout the spacesuit allows for a space explorer to be independent of their orientation relative to the basestation. Furthermore, we have seen that wearable antennas on a space suit will give a more hands

free operations so that more concentration and time can be spent exploring. Figure 3.24 demonstrates space explorers and the base station.

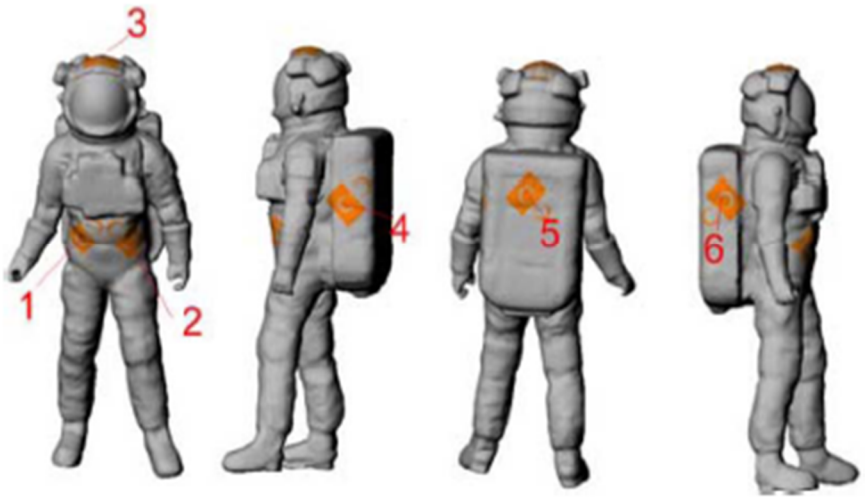

Figure 3.22 Six e-textile antennas positioned around an EVA suit [40]

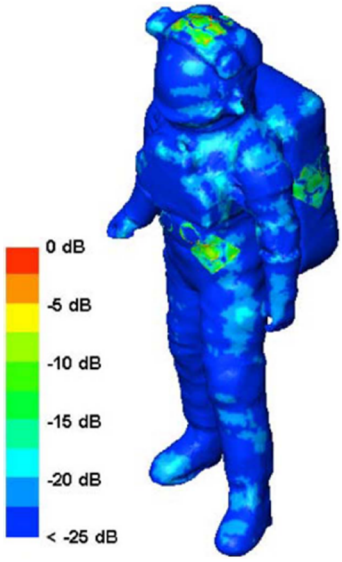

Figure 3.23 Illumination of the three antennas that provided a significant contribution to radiation at the desired beamforming angle by an incident Left Hand Circular Polarized (LHCP) plane wave [40].

Figure 3.24 Example of space explorers and the base station [61]

Once the placement of antennas throughout the spacesuit as an array is found optimal, then loading antennas with periodic structures will allow for an increased gain as was demonstrated earlier, thus allowing the transmitted signal from the space explorer to travel further, and with more certainty of reaching base station.

3.8 Conclusion

Wearable antennas are suitable for several applications. These applications can range from medical, firefighter suits, civilian, and spacesuits, etc. The Spacesuit application is of interest here and Section 3.7 looked at antenna placement on a spacesuit as well as electromagnetic interaction of antenna with the platform. Also, surface waves were covered in the chapter and a demonstration of how surface waves can be reduced by loading the antenna with periodic structures. This positive affect included a decrease in back lobe radiation, which in-turn gave an increase in gain.

4 MANUFACTURING, FABRICATION, AND APPLICATION

This Chapter covers the complete industrial process of manufacturing and fabricating of textile patch antennas, followed by performance, measurements and integration into spacesuit application. First, Section 4.1 gives several different fabric material examples. Laboratory experimental analysis was able to verify certain metric signatures from the material that were then used as initial conditions for the antenna systems design. Antennas were designed by CAD and verified for their resonant property. The experiments were done at UNDs Electrical Engineering Department, Applied Electromagnetic Laboratory.

Section 4.2 covers how textile materials are manufactured into antennas and ground planes using laser cutting. This was done at the Technology Department, Machine Shop. Section 4.3 describes the fabrication of textile antennas, where the antenna and ground planes were glued to a substrate fabric material, and then a probe feed was soldered to the antenna system. As described in section 4.4, testing of the fabricated antennas was done at North Dakota State University's (NDSU) anechoic chamber. These measurements were for planar as well as for bent antennas. Section 4.5 describes testing of the textile antenna system integrated on the space suit for placement as well as with interaction with the space suit platform. This was done at the Space Suit Laboratory, Space Studies Department. Finally, Section 4.6 concludes this chapter with a summary.

4.1 Material Selection

Conductive textile materials for the patch and ground plane were weighed against 1) cost, 2) low surface resistivity (<0.05 Ω/sq.), 3) flexibility that allows for incorporation into space suit exterior and movement with the wearer, 4) inelasticity, as stretching may change electrical properties of the material, 5) durability to withstand exposure to a harsh extraterrestrial environment(s), as well as multiple episodes of packing and unpacking, as well as compact storage in transport, and finally, 6) homogeneity throughout the material for even current distribution and secure adhesion to the substrate [62].

Several materials [62] were chosen for initial testing and prototype construction. These included pure copper polyester taffeta and nickel-copper polyester ripstop, both from Less EMF Inc., as well as copper-nickel-silver-plated nylon ripstop, with and without hot-melt adhesive, from Shieldex Trading USA. Material specs are given in Table 4.1.

Table 4.1 Conducting fabric material data [62].

Material	Thickness (mm)	Nominal Surface Resistivity (Ω)	Measured Surface Resistivity (Ω)
Pure copper taffeta	0.08	0.05	0.052
Nickel-copper polyester ripstop	0.08	0.03	0.035
Nora Dell-CR (nickel-copper-silver-plated nylon ripstop)	0.13	<0.009	0.020
Armor (nickel-copper-silver nylon with hot melt	0.20	<0.03	0.030

Furthermore, the relative permittivity (ε_r) of the substrate material was tested at 2.45 GHz. The results of this are given in Table 4.2. Values from this table were found using an Agilent E5071C ENA Series 300 kHz – 20 GHz network analyzer, and were done at the Applied Electromagnetics Laboratory. As can be seen from this table the relative permittivity of the substrate (~1.2) is near that of air.

Table 4.2 Substrate material data [62]

Material	**Single-layer thickness (mm)**	**ε_r (at 2.45 GHz)**
Pellon® Peltex® 72F, double-sided fusible ultra firm stabilizer	1.51	1.19
Nomex® felt	4.09	1.23
Creatology™ stiffened felt, 100 % eco-felt	1.38	1.12
Pellon® Peltex® 70 ultra firm stabilizer	1.84	1.15

4.2 Manufacturing Process

Manufacturing of e-textiles was done at UND's Technology Department's machine shop. The method used to cut the conducting fabric with a laser (Epilog laser, Mini/Helix-Model 8000, 75 Watts, 24x18):, as is illustrated in Figure 4.1 and Figure 4.2. The conducting fabric was experimented with two separate back plates; 1) a metal back plate, and 2) a granite back plate. These back plates allow the fabric sheet to be laid out flat so that irregularities (bending, crumpling, etc.) can be mitigated. Furthermore, before the cut was made the conducting fabric was dampened down with water, some with

distilled and others with tap water. It was found that the granite back plate reduced reflection burn stains on the conducting fabric. These burns were present with the metal back plate. Addition of water showed no visual side effect but the EM properties were not checked. The main goal was to run a laser cutting test on the conducting fabric in order to find the optimal aesthetic appearance of the material for the antenna as well as the periodic cells.

Figure 4.1 Laser machine at the Technology Department.

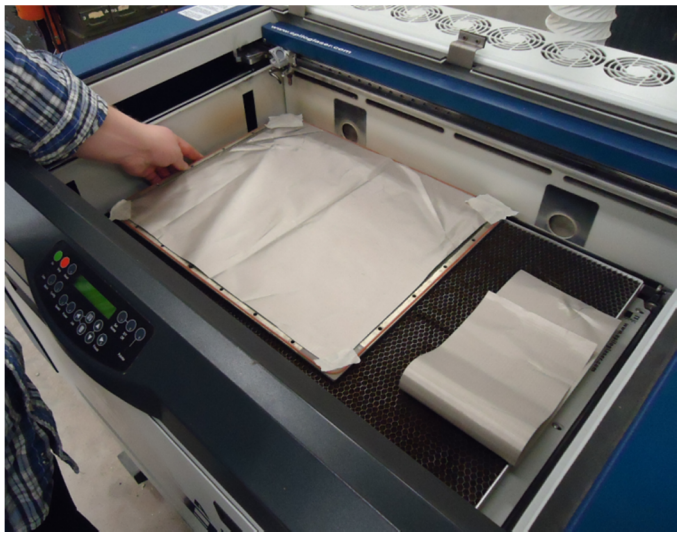

Figure 4.2 Placing e-textile in laser machine for cutting trials. This image shows a metal backed plate.

A series of laser cutting experiments for speed, power and frequency were run in the Technology Department. These tests consisted of keeping two of the parameters constant and varying the third. Through laborious hours of testing the final optimal settings to cut the conducting fabric (nickel/copper ripstop) came to 75% speed, 23% power, and at a frequency of 5000 Hz. Figure 4.3 shows an optimally cut C-mirror cell (more details in Chapter 5).

Another method of cutting the fabric that was explored by Matt Anderson in the Technology Department is called the cookie-cutter method as illustrated in Figure 4.4. A comparison of cutting results between these two types of cutting methods is shown in Figure 4.5. Notice in this figure that the blade cut from the cookie cutter is much cleaner in respect to frayed edges then the laser cut. However, currently the laser cutter can manufacture more quantities of product then the cookie cutter.

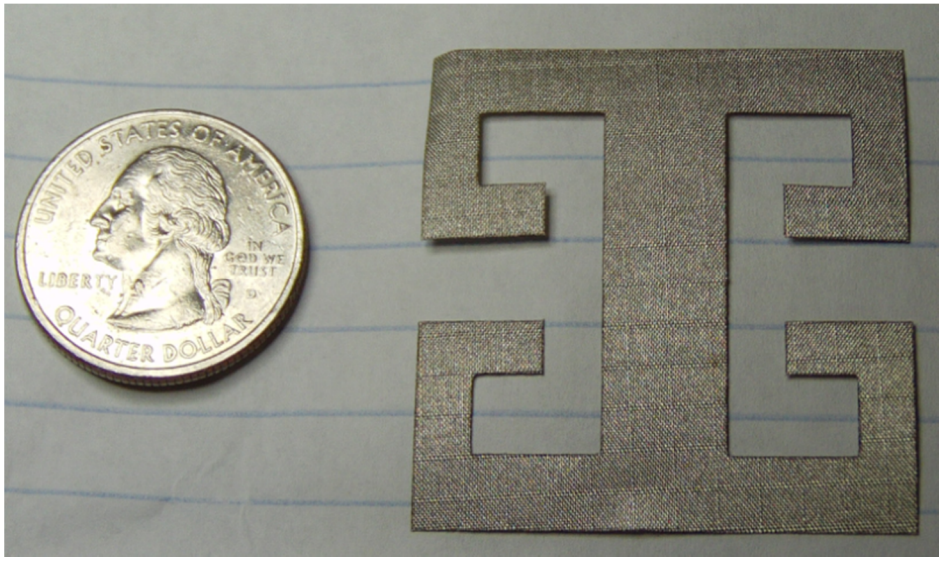

Figure 4.3 Optimal aesthetic cell that was cut by laser. Courtesy of Matt Anderson.

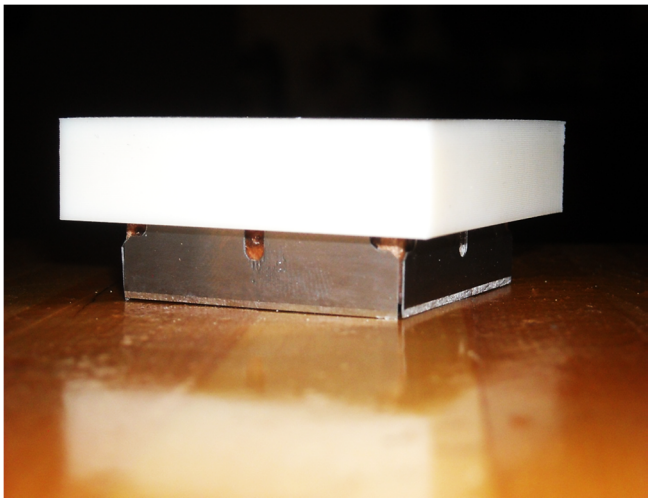

Figure 4.4 Cookie-cutter tool created by Matt Anderson in Technology Department.

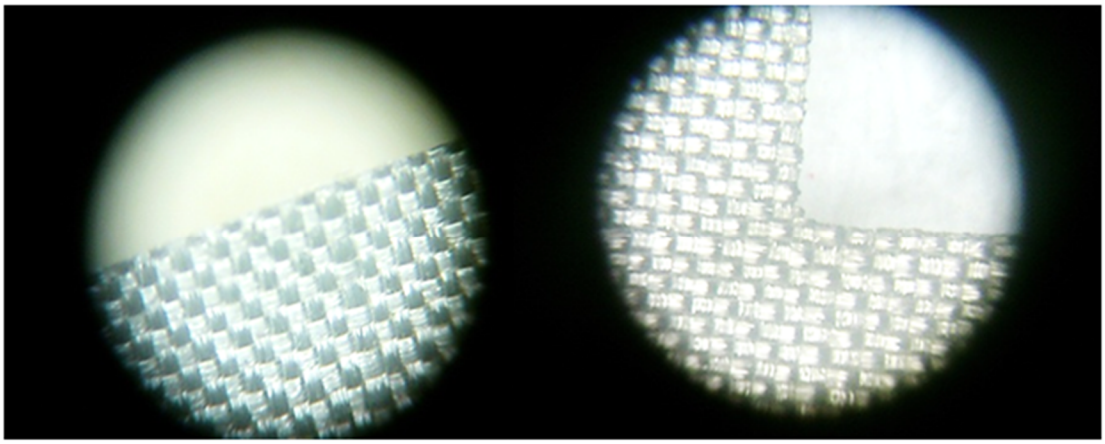

Figure 4.5 View of the cut fabric under a microscope. Courtesy of Matt Anderson.

4.3 Fabrication Process

Upon receiving the conducting textile material that was cut by the Technology Department, the fabrication process proceded. First, the conducting fabric (ground plane) was glued to substrate material, Figure 4.6. Next, the ground plane was substrate is cut with a scissors. Then the antennas are glued to the substrate on the opposite side of the

ground plane, Figure 4.7. Careful measurements of the precise placement of the antenna needed to be done in order to maintain antenna system accuracy.

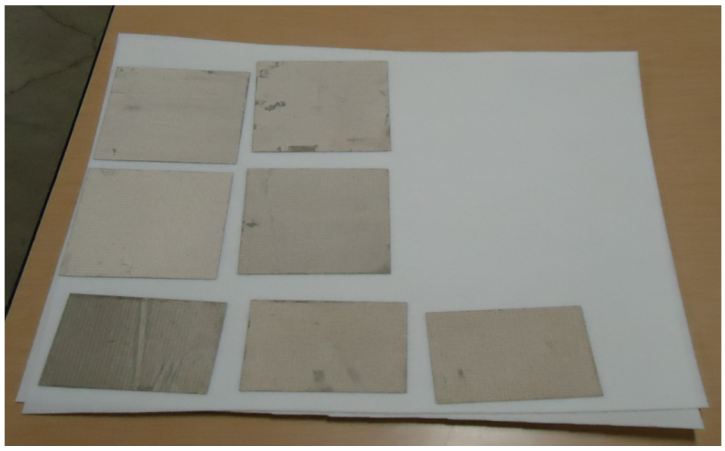

Figure 4.6 Cut ground plane glued on substrate material.

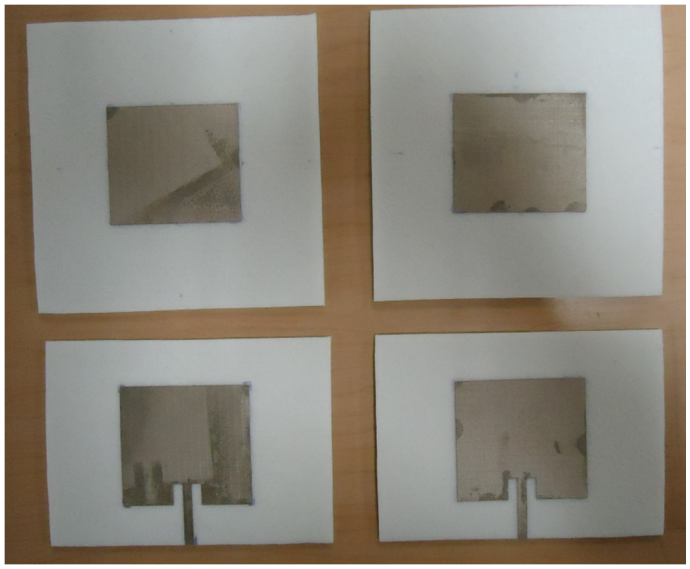

Figure 4.7 Antennas glued to substrate backed by a conducting ground plane.

4.4 E-Textile Antenna Testing in Anechoic Chamber

Once the antenna elements were fabricated, they were taken to NDSU for testing in an anechoic chamber, Figure 4.8. This chamber allowed a reduction of environmental

noise so the antenna's parameters could be accurately measured. Figure 4.8 demonstrates a horn antenna and the textile antenna placed some distance away. The horn antenna is the transmitter and the patch antenna is the receiver. Because of the reciprocity theorem mentioned in Section 2.2, the received power pattern of the antenna is identical to the transmitted power pattern. These measurements were done by Tessa Haagenson.

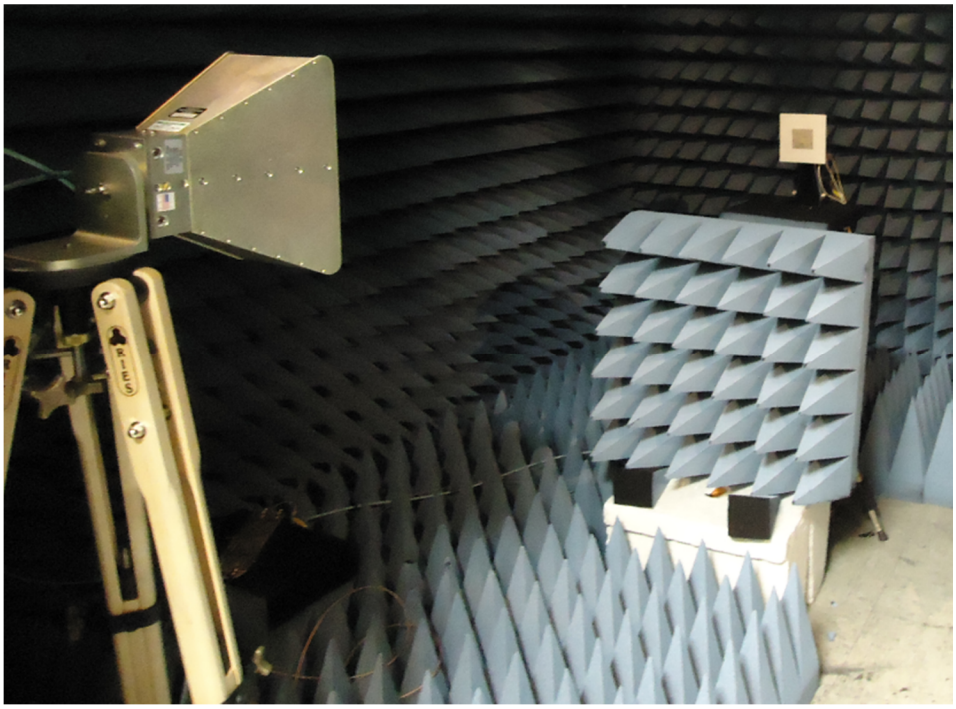

Figure 4.8 Horn and planar textile antenna in screening room at NDSU. Courtesy of Tessa Haagenson (EE), and NDSU.

As was mentioned earlier, textile antennas have the feature of conformability. Figure 4.9 and Figure 4.10 demonstrate textile antennas being conformed around a cylindrical object in different orientations. Figure 4.9 shows the textile antenna being bent in a manner that the left and right sides of the antenna system are curved. Figure 4.10 shows the textile antenna system being bent in a manner that the up and down sides

of the antenna system are curved. In both cases the antenna elements were bent around cylindrical pipes. Also, note the position of the feed cable to the antenna system.

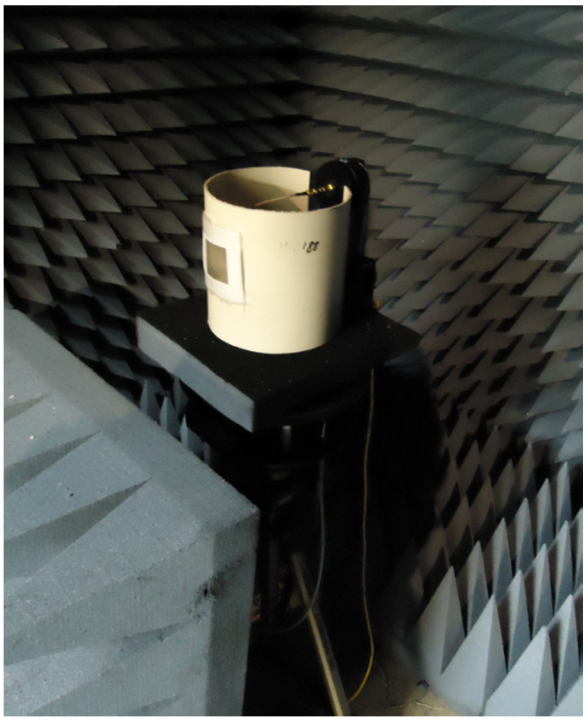

Figure 4.9 Textile antenna conformed around a cylindrical object. Courtesy of Tessa Haagenson.

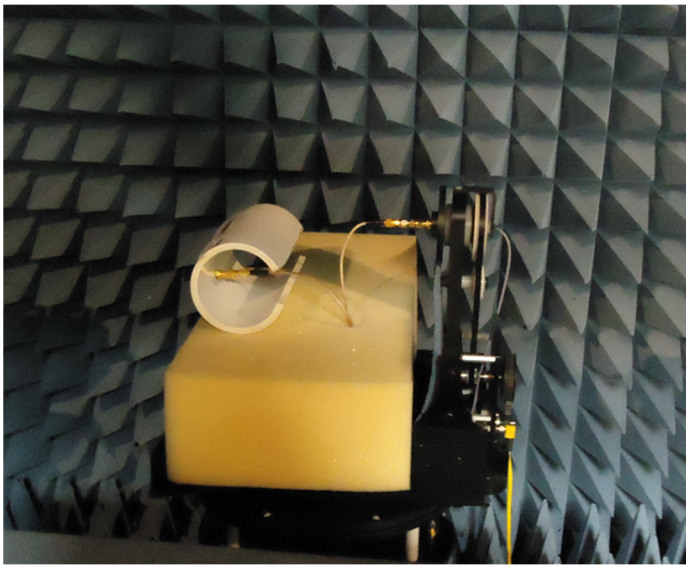

Figure 4.10 Textile antenna conformed around a cylindrical object. Courtesy of Tessa Haagenson.

4.5 Space Suit Application

Once the textile antennas were fabricated they were tested for placement around space suits as well as for electromagnetic interaction with the platform. The measurements were performed in the Spacesuit Laboratory, Space Studies Department, UND. Figure 4.11-Figure 4.14 demonstrate the multiple potential placements of the textile antenna around the space suit.

Figure 4.11 Textile antenna placed inside the space jacket.

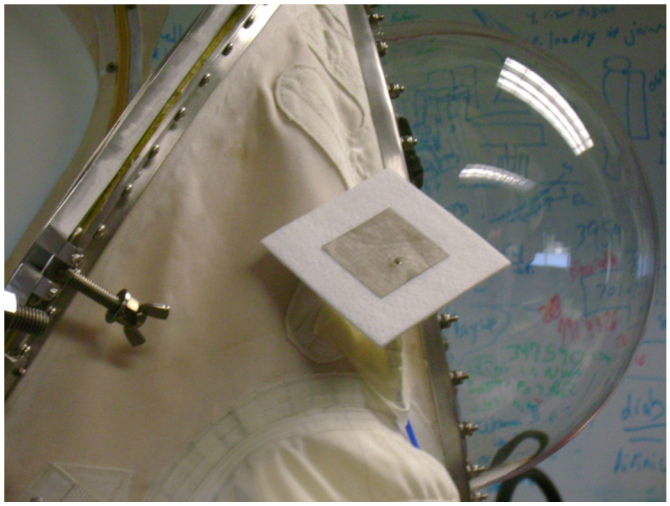

Figure 4.12 Textile antenna placed external near the suits head.

Figure 4.13 Textile antenna placed near shoulder of space suit.

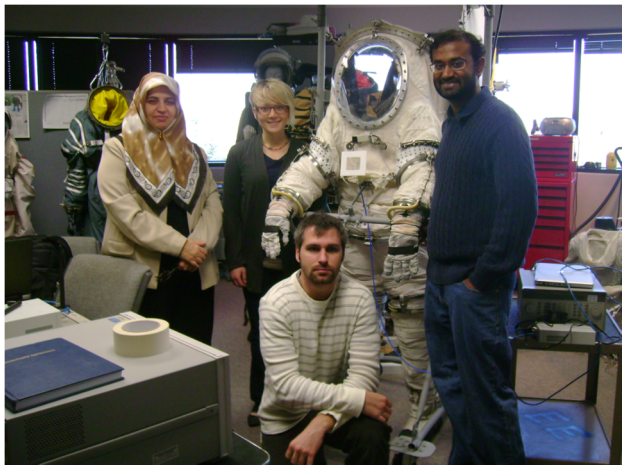

Figure 4.14 Textile antenna placed on the front of the body. Left to right: Dr. Sima Noghanian, Tessa Haagenson, Corey Bergsrud, and Arun Kumar.

4.6 Conclusion

It was demonstrated that wearable textile antennas can be created for space suit application at the University of North Dakota (UND). First UNDs EE Department's Applied Electromagnetic Laboratory tested fabric material for certain properties which gave the material properties that were used to design the antenna. Next the conducting textile material was cut using laser machining at the UND Technology Department. Note here that the Technology Department is currently exploring other methods of cutting the

fabric in order to increase production for example by using a stamping or cookie-cutter method. The Technology Department found optimal product appearance from using the laser cutter. A granite slab was used to back the textile material that was then damped down with water. The lasers optimal setting was: 75% speed, 23% power, and 5000 Hz frequency or a similar result came from 75% speed, 25% power, and 4500 Hz frequency. These measurements were done by Matt Anderson.

Once the manufacturing of the conducting material was complete, the fabrication process commenced. The textile conducting ground plane was glued to the substrate material, then cut out, and next the textile conducting patch was also glued to the substrate but on the reverse side of the ground plane. The antenna had to be carefully and accurate placed according to symmetry. Finally, probe feeds were inserted with the antenna system in order to supply an excitation. There were difficulties encountered with soldiering as Figure 3.1 indicates a burning effect on the fabric.

After fabrication of the textile antennas, laboratory measurement testing proceeded. Placement of textile antennas on the space suit was considered for minimizing the electromagnetic interactions of the antenna with the space suit platform. Note here that Tessa Haagenson (EE) and others are currently writing a paper [62] on the results of her findings. Also, Matt Anderson is currently writing a capstone project for his results on manufacturing the conducting fabric. This project had collaborations with UNDs: 1) EE Department, Applied Electromagnetic Laboratory, 2) Technology Department, Machine Shop, 3) Space Studies Department, Space Suit Laboratory, and 4) NDSUs Wireless Sensor Laboratory.

5 RESULTS

Chapter 5 covers simulation results of the antenna system that was journeyed. Section 5.1 describes a periodic cell, coined; C-Mirror. This includes dimensions of the cell, simulation results of reflection, and dispersion characteristics. The dispersion characteristics of the cell with via included a band gap feature near 1 GHz. Therefore, a 1 GHz antenna was designed in Section 5.2 using the material properties described in Chapter 4, as well as the initial conditions of the desired system.

Once the antenna was realized at 1 GHz then the C-mirror cells were integrated with the antenna on the same plane in Section 5.3. Several experimental trials commenced; including, different orientation, number of rows of cells, and spacing of the periodic array of cells with respect to the edge of the antenna to the center of the cell in terms of a free space wavelength. Upon finding an optimal outcome of the trials, Section 5.4 goes deeper into the analysis and of the cells to take a look at the surface current behavior. It can be seen that the embedding of parasitic cells evolved into its own *LC* network. The inductive nature occurs from the currents traveling through the cells as well as between the cells, and the capacitive nature arises between the stubs of the cell as well as between the cells defined by Periodic Boundary Conditions (PBC). Finally, Section 5.5 summarizes Chapter 5.

5.1 Building and Simulating the Periodic Cell

Experimentation done for this thesis mainly consisted of simulations using FEKO [24, 63]. These simulations provide an understanding of the electromagnetic behaviors of interacting traveling waves with periodic structures, namely FSSs, through simulation. Firstly, a free standing periodic cell with no via named C-Mirror, as shown in Figure 5.1, was created. The Periodic Boundary Conditions (PBC) of interfacing cells was set as 2 mm, as suggested from [57]. The cell was excited with a plane wave having magnitude of 1 V/m, and then tested for its reflection and transmission characteristics, Figure 5.2. As this graph indicates; f_o ≈2.45 GHz is where the reflection coefficient was '1' and transmission coefficient was '0'. Ideally, the entire wave is reflected and none is transmitted, literally suppressing the wave.

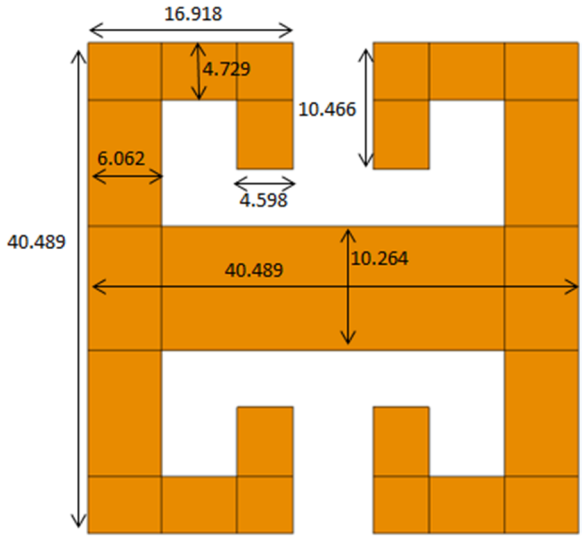

Figure 5.1 C-mirror Cell, units in mm.

This High Impedance Surface (HIS), as it is otherwise called, with the realization of the reflection coefficient has been tried in the situation of a multi-planar periodic

loaded antenna like that of Figure 5.3. This particular multi-planar antenna system is designed to interact with reflected waves in order to utilize them for enhancement of the antenna system. However, this particular design could not be fully simulated due to limited memory with the student version of FEKO. Therefore, uni-planar periodic loaded antennas were studied.

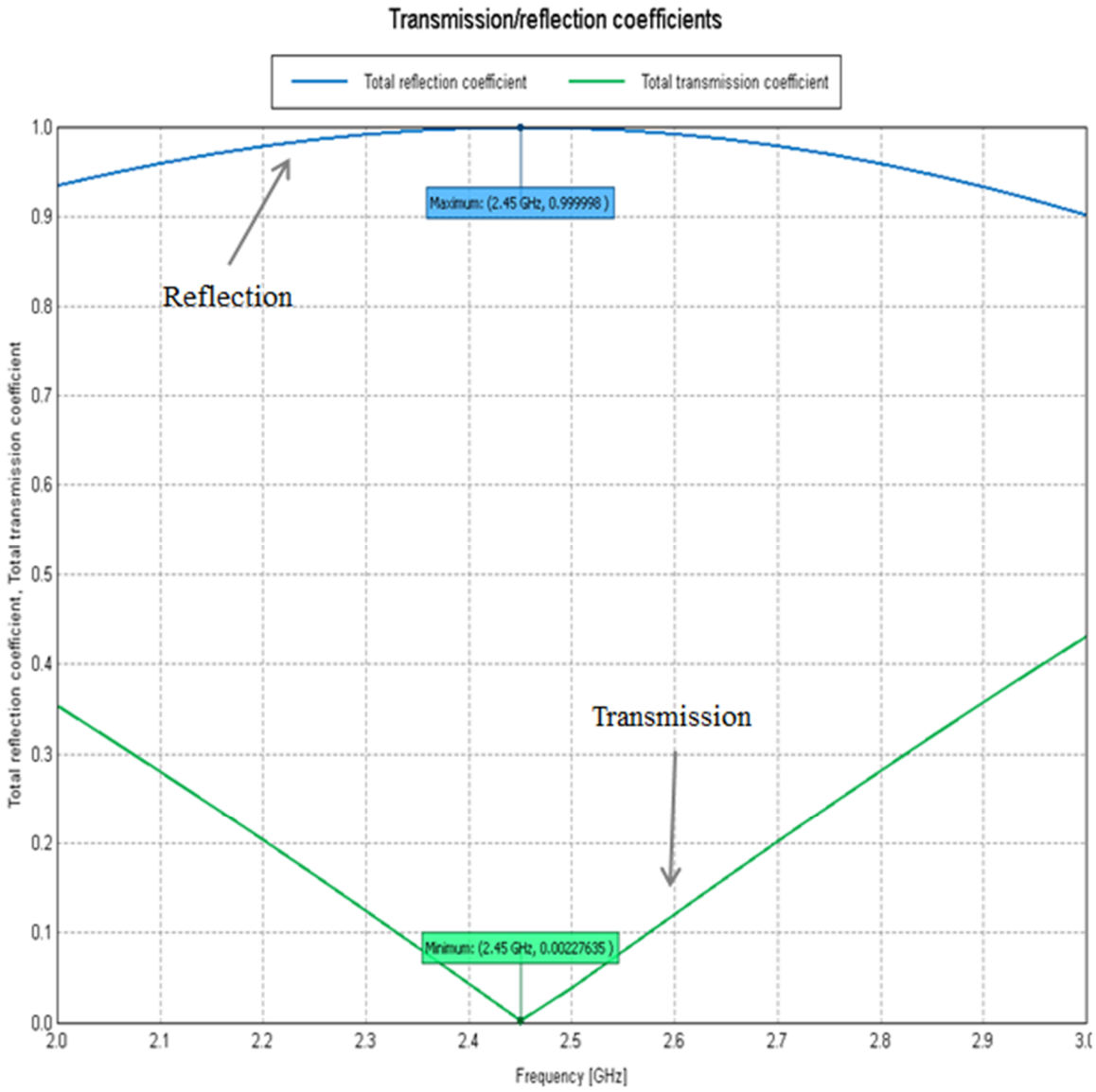

Figure 5.2 Reflection and Transmission Coefficients.

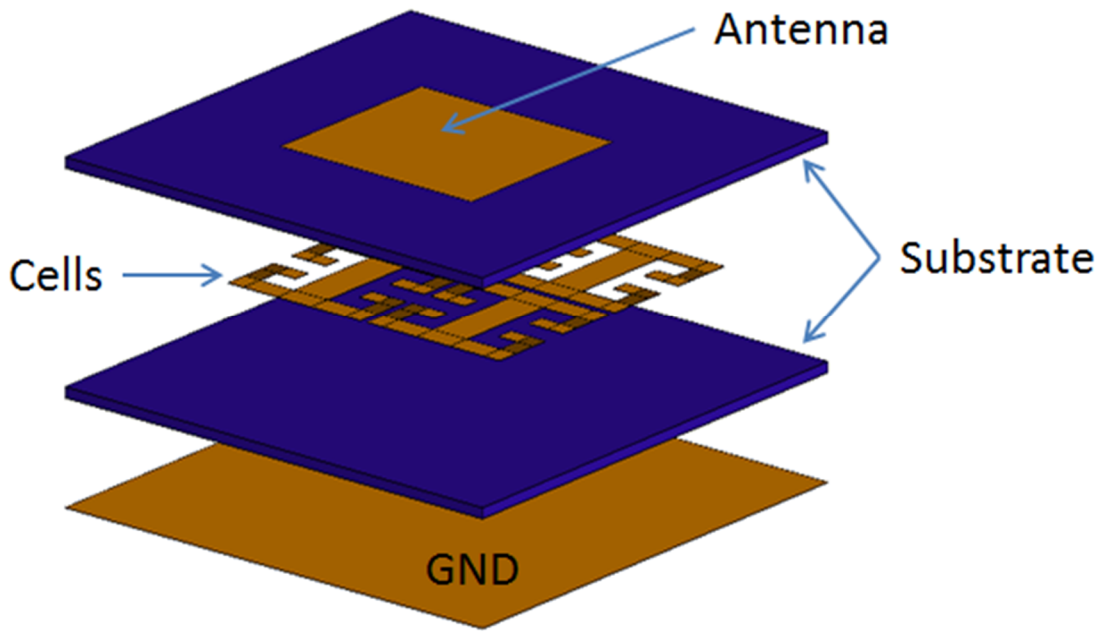

Figure 5.3 Multi-planar periodic loaded antenna.

This thesis will now journey with periodic cells loaded on the same plane as the antenna, a so called uni-planar antenna system. For this particular type of antenna system the cells dispersion characteristics needs to be found. Unfortunately, FEKO did not have this option available; however, simulations were done in CST Microwave Studio by Dr. Abas Sabouni.

The dispersion characteristics allow the designer to understand the bandgap feature of the specific cell by bombarding the cell with traveling EM surface waves at different angles and phases. Figure 5.4 shows the set-up frame in CST indicating bombardment of traveling waves with respect to direction and phase. These directional arrows with phase ranges in the figure indicate the direction of wave propagation with a respective phase sweep of the wave. These parameters are the Γ X M Γ from Figure 2.12.

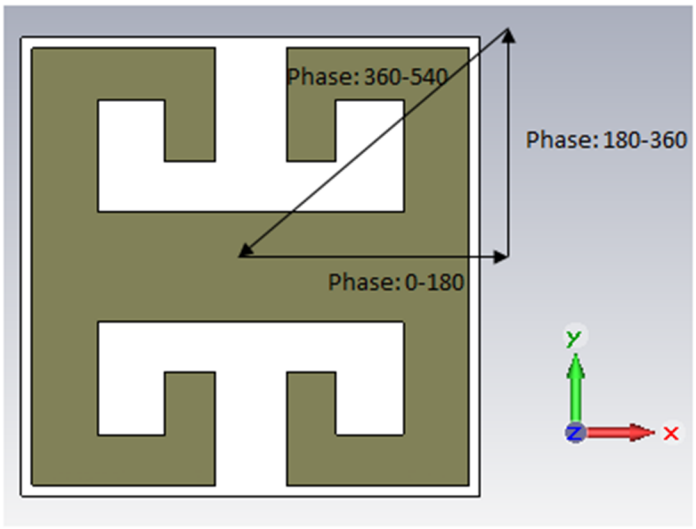

Figure 5.4 Set up for the bombardment of traveling EM wave. Courtesy of Abas Sabouni.

First C-mirror was simulated without via. The result of its dispersion characteristic is given in Figure 5.5. No band gap was found.

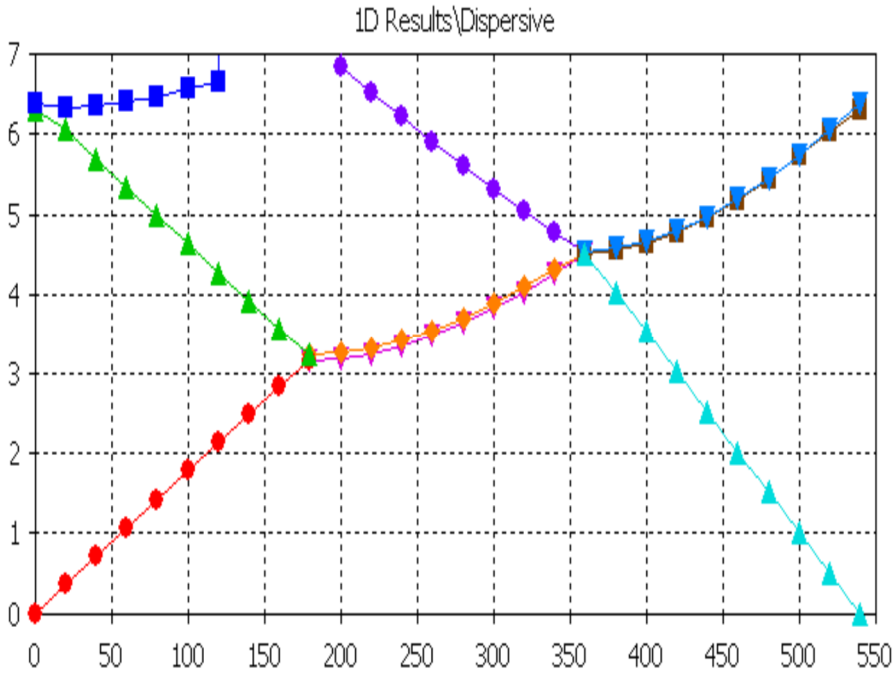

Figure 5.5 Dispersive characteristic of this C-Mirror Cell with no via and no bandgap feature. Courtesy of Abas Sabouni.

Next a via was inserted at the center of the cell, and on the stub of the cell as indicated in Figure 5.6 by black open circles. The results for each were similar and presented a bandgap feature ranging from a very low frequency up to about 1.5 GHz, as Figure 5.7 indicates.

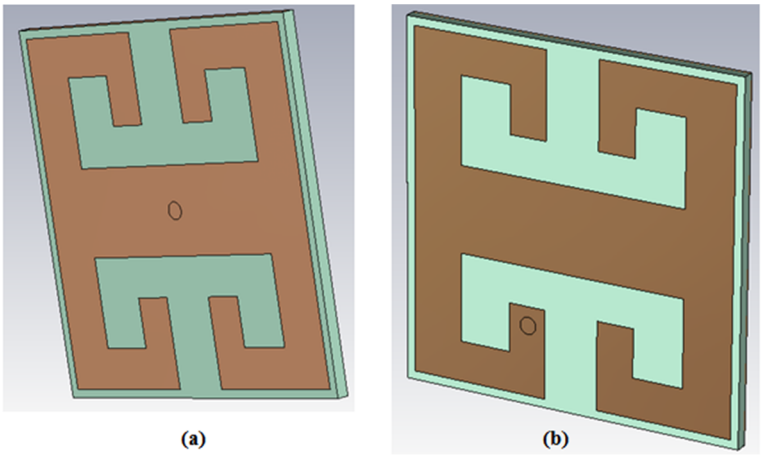

Figure 5.6 Via inserted at (a) the center of the cell, and (b) a stub of the cell, with via diameter of 2mm. Courtesy of Abas Sabouni.

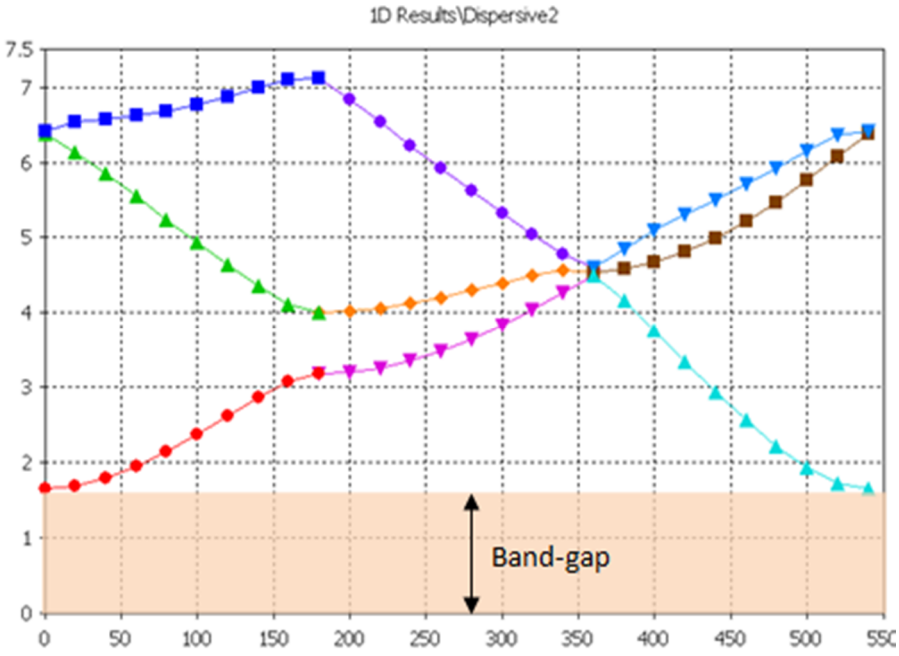

Figure 5.7 C-Mirror with via located in center and on stub showed band gap feature around 1 GHz. Courtesy of Abas Sabouni.

Because of the difficulty of actually inserting vias with fabrics for assembly, this was not a path taken. Therefore, relative to this thesis, periodic cells without vias were to be loaded uni-planar with the antenna as parasitic elements as Sections 5.3, and 5.4 will explore. Section 5.2 gives the details of antenna design at 1 GHz.

5.2 Antenna

A fabric microstip patch antenna with probe feed was designed with CAD FEKO, Figure 5.8, using these parameters of; 1) resonant frequency (f_o) of 1 GHz, 2) substrate height of 1.6 mm, and 3) relative permittivity (ε_r) of 1.2 F/m. Substrate height and relative permittivity were determined from the results of Chapter 4. Notice in this figure that there is a -2° pole, where this phenomenon occurs from beam steering the radiation pattern, however, this pole is suspected to be due to the simulation error and not the design of the antenna itself. Later consistencies with this argument will be given in subsequent sections to this chapter.

The antenna simulation results displayed a resonant frequency near 1 GHz as Figure 5.9 indicates. The return loss is slightly over 10 dB. Furthermore, this antenna displayed a gain of about 9.291 dBi, as shown in Figure 5.10. The half powered beam width is about 59.5°. Also, the E and H plane radiation patterns are shown in Figure 5.11 and Figure 5.12, respectively.

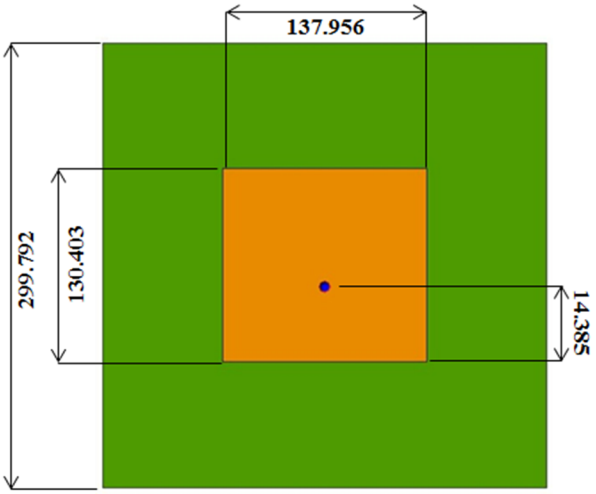

Figure 5.8 Microstrip patch antenna with probe feed designed with FEKO. Units in mm.

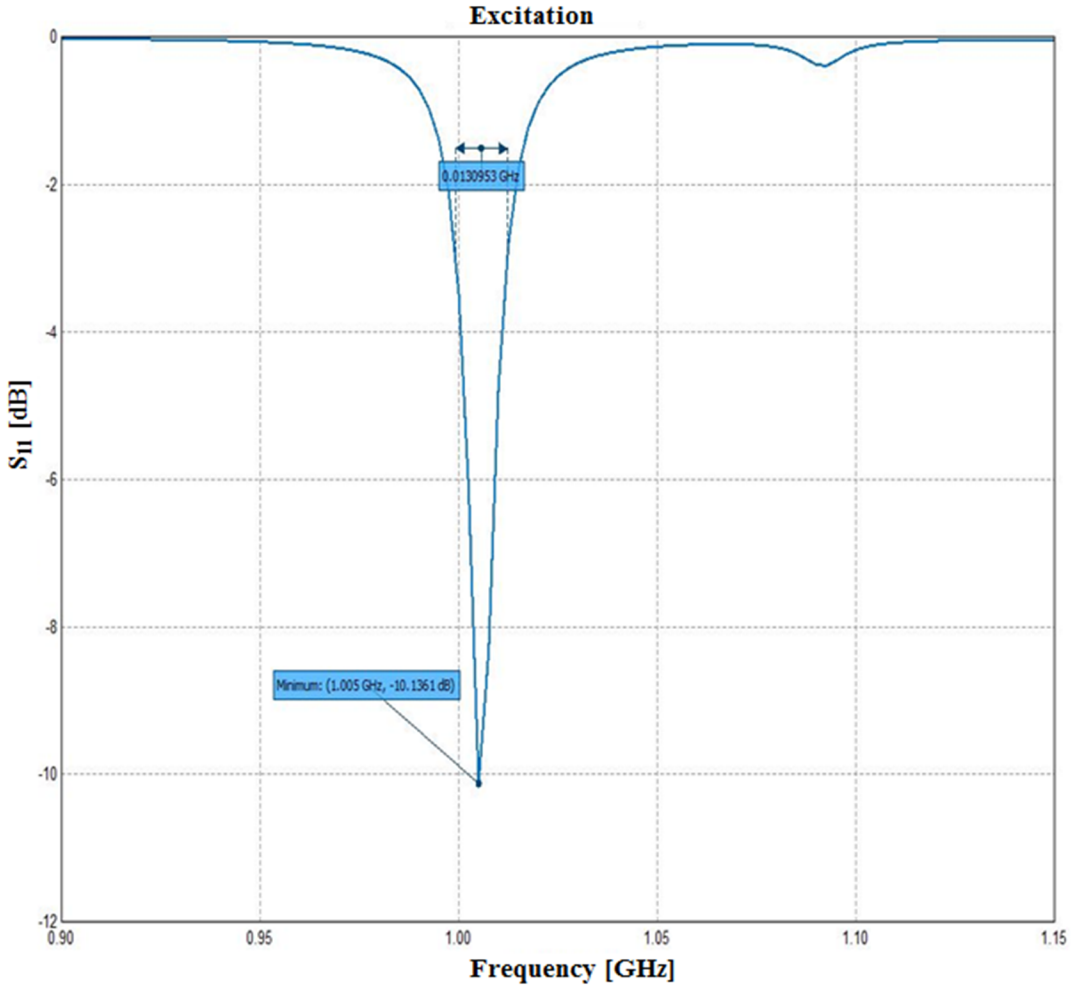

Figure 5.9 Patch antenna showing a resonant frequency of about 1 GHz.

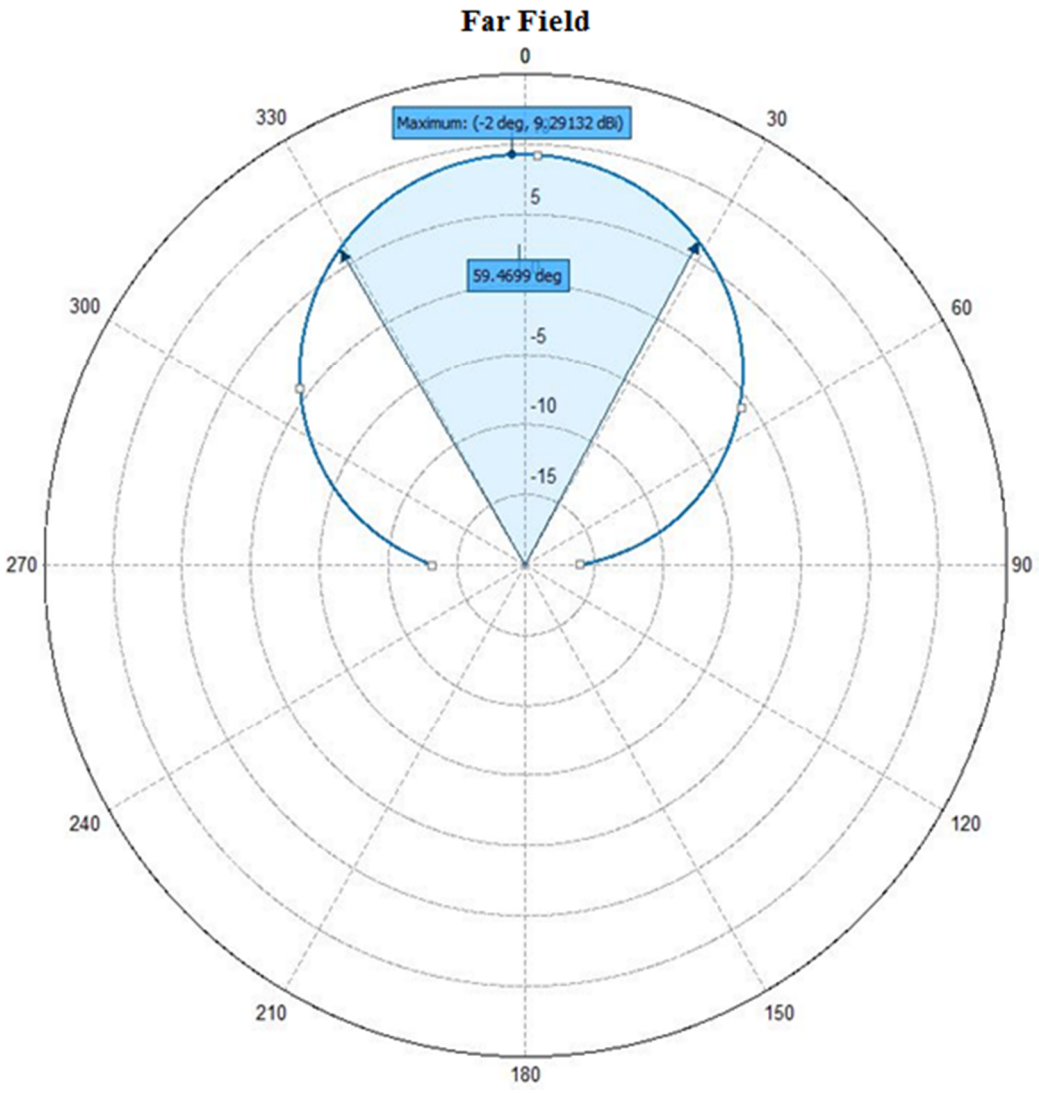

Figure 5.10 Gain and half-powered beam width of designed antenna at 1 GHz.

From the realized 1 GHz antenna a series of experimentations commenced with loading the antenna with periodic elements uni-planar to the antenna. Orientation of the cells with respect to the antenna, number of rows of cells, and distance of the cells from the antenna in terms of free space wavelength were of interest for analysis. No vias were used because of the assumed fabrication challenge. The next Section will now demonstrate this series of experimentations.

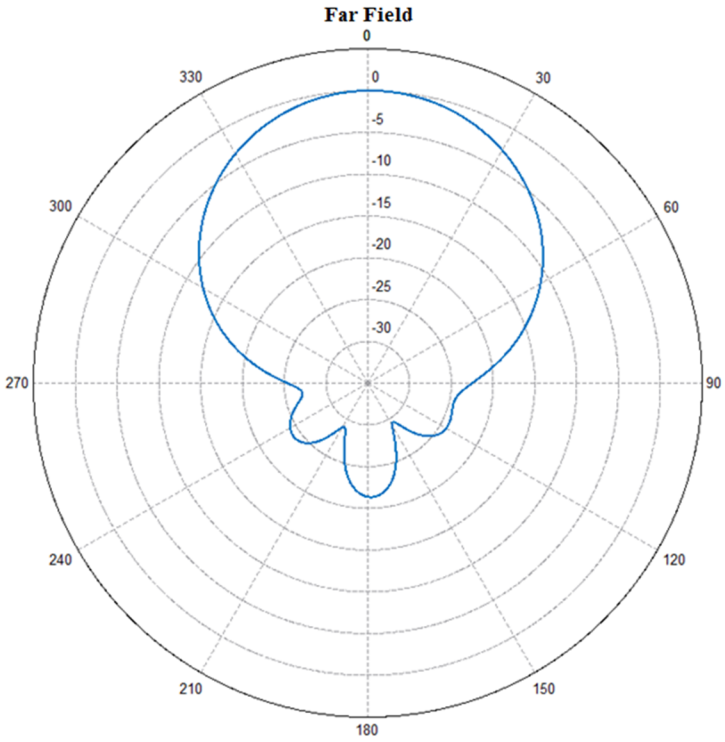

Figure 5.11 E-plane radiation pattern for 1 GHz antenna.

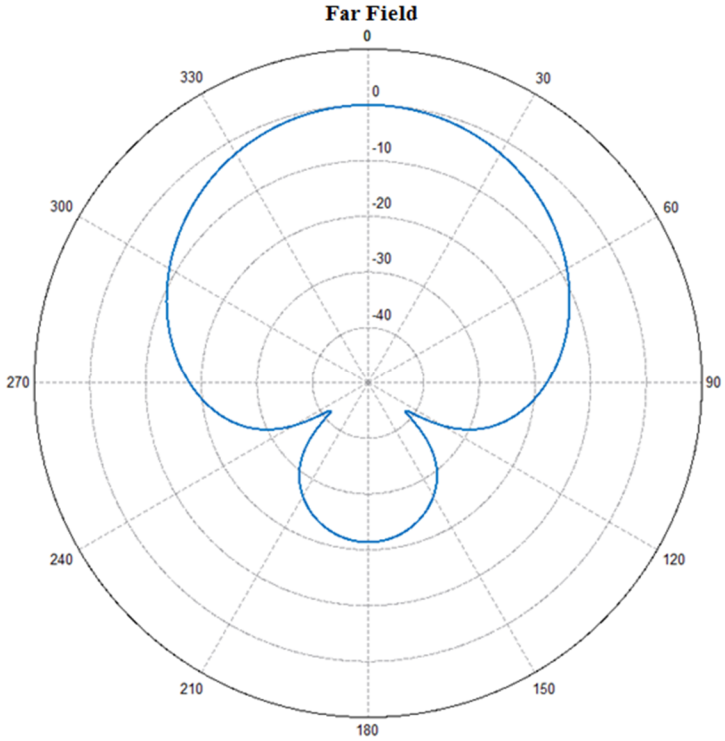

Figure 5.12 H-plane radiation pattern for 1 GHz antenna.

5.3 Simulation Results of Antenna Loaded with C-mirror

With respect to the antenna, there were three different orientation patterns: 1) cells with up and down (UD) orientation, 2) cells with left to right (LR) orientation, and 3) cells surrounding the antenna, as shown in Figure 5.13, Figure 5.14, and Figure 5.15, respectively. Note that for LR and UD orientation the number of cells in a row or a column, respectively, remained a constant five. UD and LR orientations were also evaluated on trialing various numbers of rows or columns with respect to 1 row, 2 rows, and 3 rows of periodic cells. Finally, the distance of UD and LR cell orientation was varied with respect to the edge of the antenna to some fraction of the free space wavelength $\left(\frac{\lambda_o}{10},\frac{\lambda_o}{12},\frac{\lambda_o}{15},\frac{\lambda_o}{17},\frac{\lambda_o}{20}\right)$ away with respect to the center of the cell. Note here that 'all the way around' configuration was not symmetrical in a wavelength sense for the complete loop. The main objective from these experimentations was to increase antenna gain.

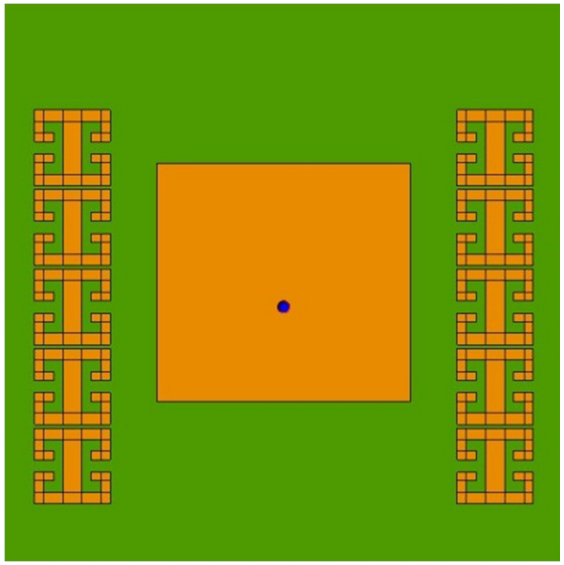

Figure 5.13 UD cell orientation.

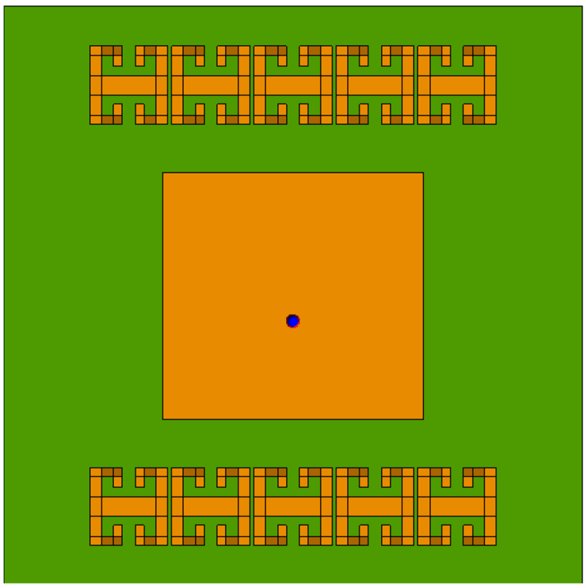

Figure 5.14 LR cell orientation.

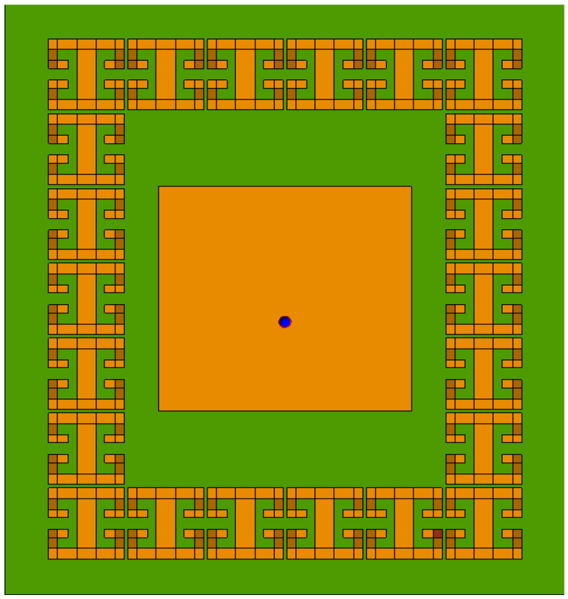

Figure 5.15 All the way around cell orientation.

The above experimentations showed the best increase in gain came from the UD orientation, with 2 rows, and $\lambda_o/12$ distance away from the edge of the antenna to the center of the cell, with the second row set by the PBC. Figure 5.16 shows the resonant frequency, bandwidth, and return loss for this uni-planar periodic loaded antenna, while

the results are given in Table 5.1. Notice from this figure and table that the extra rows resulted in little change in resonant frequency (f_o), bandwidth (BW), and return loss. Also, notice that by adding periodic cells to the antenna caused a shift in f_o to a higher frequency, a slight decrease in BW, and not as good a return loss.

Table 5.1 f_o, BW, and return loss results for $\lambda_o/12$.

Type	f_o (GHz)	BandWidth (MHz)	Return Loss (dB)
Antenna	1.0050	13.0953	10.1361
1 Row	1.0275	12.3186	8.4509
2 Rows	1.0275	12.3289	8.4213
3 Rows	1.0275	12.4188	8.5109

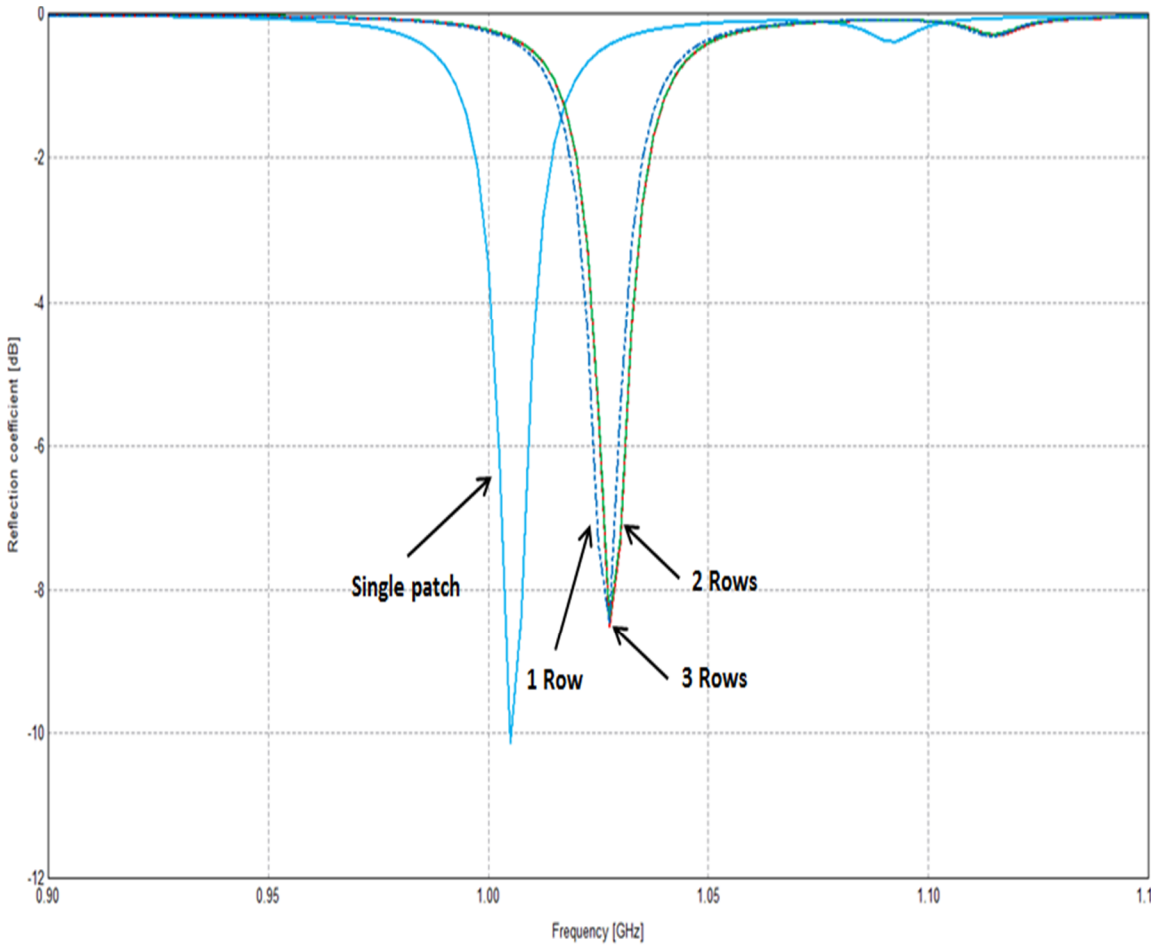

Figure 5.16 Simulation results for UD orientation, with (1-3) rows, and $\lambda_o/12$.

The E-plane, H-plane, and gain for UD orientation with $\lambda_o/12$ were simulated. Again, this arrangement is used because it showed the greatest gain increase. Figure 5.17 and Figure 5.18 demonstrate the E-plane and H-plane results for this situation. Notice here that by adding subsequent rows, the back lobe radiation decreased. The antenna with 3 rows showed the largest decrease in its back lobe. There is a limit on how many rows can be embedded with the antenna before negative affects arise. In this thesis up to 3 rows were considered due to software licensing memory as well as from what was seen in the gain, as will be elaborated below.

As the reader may predict, a decrease in back lobe radiation indicates an increase in gain, since there is more power radiated in the front lobe. Table 5.2 shows the results for the antenna without periodic cells, and the antenna loaded with 1, 2, and. 3 rows of cells for resonant frequency (f_o), gain, and half-powered beamwidth (HPBW). Also, the cross and co polarizations were compared where the cross polarization had negligible effects. Co polarization is the desirable component as the polarization is in the direction of the intended signal. The undesirable component is the cross polarization (X-pol). X-pol is the polarization orthogonal to the polarization being discussed. The X-pol has an opposite polarization than the Co-pol

Table 5.2 Results showing f_o, Gain, and HPBM, from the metamaterial antenna system: UD orientation, and $\lambda_o/12$.

Type	f_o **(GHz)**	**Gain (dB)**	**HPBW (degrees)**
Antenna	1.0075	9.29132	59.4699
1 Row	1.0275	9.34837	59.0652
2 Rows	1.0275	9.59714	59.1755
3 Rows	1.0275	9.56175	59.2112

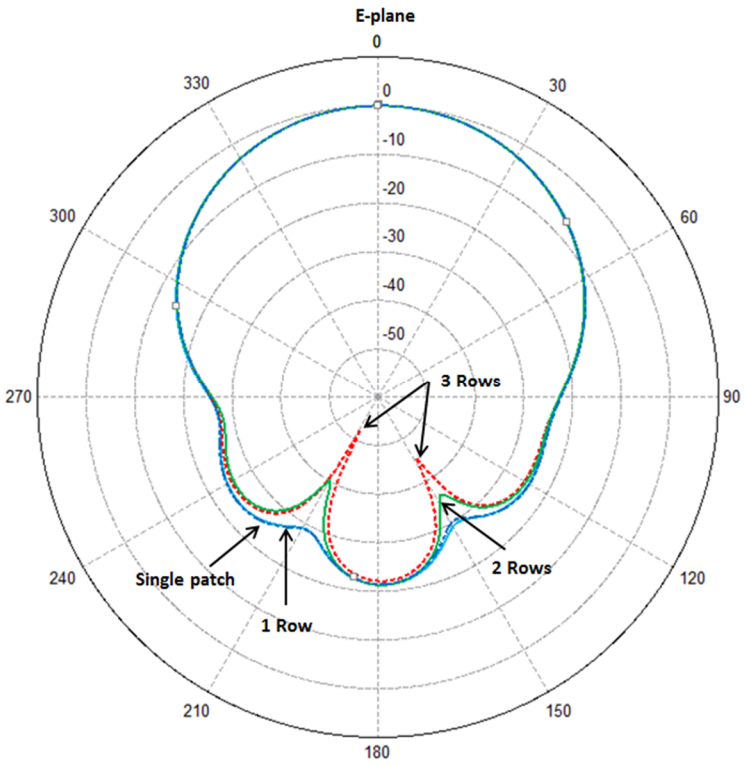

Figure 5.17 Back lobe radiation reduction in E-plane (co-pol).

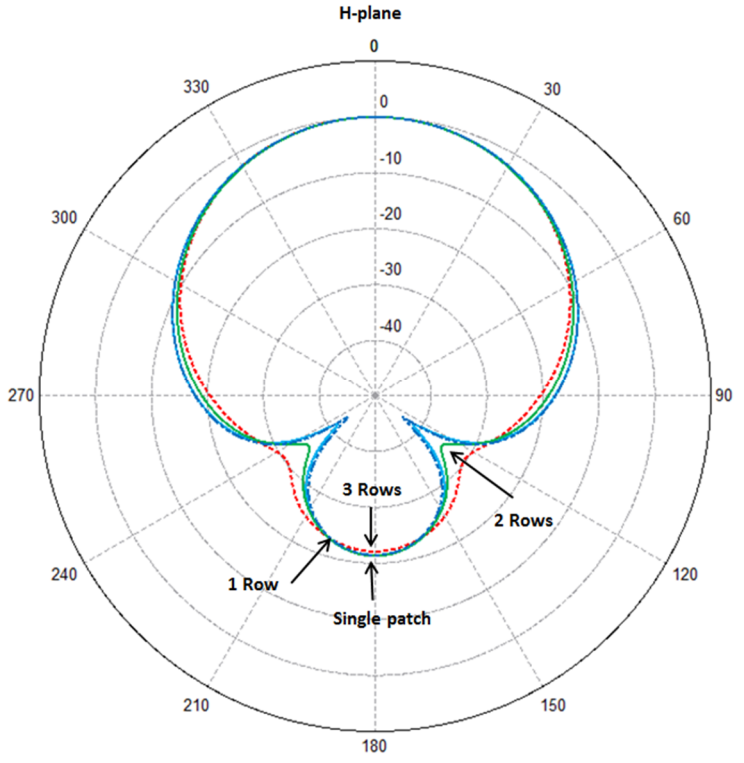

Figure 5.18 Back lobe radiation reduction in H-plane (co-pol).

It was mentioned above that several trials were run for orientation, whether it be UD, LR, or all the way around. Furthermore, trials were run by varying the free space wave length $\left(\frac{\lambda_o}{10},\frac{\lambda_o}{12},\frac{\lambda_o}{15},\frac{\lambda_o}{17},\frac{\lambda_o}{20}\right)$, and the number of rows up to 3 for UD and LR, and only up to 2 rows for all the way around. The results for UD orientation in regards to row resonant frequency, BW, return Loss (RL), gain, and Half Powered Beam Width (HPBW) are given in Table 5.3.

Table 5.3 UD orientation 1, 2, or 3 rows, resonant frequency, BW, RL, gain, and HPBW.

UD Orientation	**# of Rows**	f_o **(GHz)**	**BW (MHz)**	**RL (dB)**	**Gain (dBi)**	**HPBW (Degrees)**
λ_0/10	1	1.0275	12.041	8.179	9.362	59.062
	2	1.0275	12.221	8.304	9.569	59.133
	3	1.0275	12.447	8.636	9.594	59.236
λ_0/15	1	1.0275	12.227	8.405	9.356	59.038
	2	1.0275	12.383	8.482	9.585	59.129
	3	1.0275	12.374	8.581	9.571	59.175
λ_0/17	1	1.0283	12.061	8.284	9.553	59.110
	2	1.0283	12.093	8.391	9.541	65.718
	3	1.0265	11.1992	8.397	9.553	59.110
λ_0/20	1	1.0280	12.090	8.617	9.369	67.618
	2	1.0280	12.064	8.533	9.590	65.671
	3	1.0295	12.014	8.532	9.594	59.135

Note from this table that the resonant frequency hardly changed between analyses, as well as the BW maintained with some consistency. However, notice in the tables (RL) column from 1 row to 3 rows the RL improves. Furthermore, the LR orientation is laid out in a similar manner given in Table 5.4. Notice from this table the X indicates the trials could not be simulated due to memory limitations of the classroom license.

Table 5.4 LR orientation 1, 2, or 3 rows, resonant frequency, BW, RL, gain, and HPBW.

LR Orientation	# of Rows	f_o (GHz)	BW (MHz)	RL (dB)	Gain (dBi)	HPBW (Degrees)
λ_o/10	1	1.0284	12.114	8.619	9.351	67.699
	2	X	X	X	X	X
	3	X	X	X	X	X
λ_o/12	1	1.0275	12.363	8.597	9.345	59.887
	2	X	X	X	X	X
	3	X	X	X	X	X
λ_o/15	1	1.0275	12.020	7.894	9.302	58.948
	2	1.0250	12.205	8.611	9.503	56.113
	3	X	X	X	X	X
λ_o/17	1	1.028	12.090	8.617	9.302	58.948
	2	X	X	X	X	X
	3	X	X	X	X	X
λ_o/20	1	1.026	12.200	8.408		
	2	X	X	X	X	X
	2	X	X	X	X	X

Finally, all the way around orientation for 1 and 2 rows is given in Table 5.5. Table 5.5 gives the resonant frequency, BW, RL, gain and HPBW.

Table 5.5 All the way around orientation for f_o, BW, RL, gain, and HPBW by varying up to 3 rows.

Orientation	# of Rows	f_o (GHz)	BW (MHz)	RL (dB)	Gain (dB)	HPBW (Degrees)
	1	1.025	12.0382	7.92515	9.485	67.779
	2	1.025	12.3261	8.79578	9.479	60.190

Section 5.4 takes the analysis one step further by explaining the excited uni-planar antenna system in order to see how the surface currents behave when interacting with the periodic cells. Furthermore, it was noticed that for the UD orientation in-particular that

when aligning the probe feed on the antenna with the opening between the cell stubs seen a slight increase in gain as opposed to not aligning the antenna prove feed with the opening between the cell stubs.

5.4 Electric Current Behavior

Once the antenna is excited from an arbitrary applied excitation 12V source, surface currents evolve, as was covered previously. These surface currents take a specific pattern (paths) relative to the input parameters of the system. The current distribution pattern for a 1GHz patch antenna with probe feed is given in Figure 5.19. The surface current distribution for the uni-planar C-mirror loaded antenna was viewed, as shown in Figure 5.20-Figure 5.25. Note that the periodicity or repetitiveness of the cell was every 2 mm spacing (*i.e*. PBC). Figure 5.20, Figure 5.22, and Figure 5.24 represents a bird's eye view. Figure 5.21, Figure 5.23, and Figure 5.25 represents an expanded view.

Notice the behavior of the surface current as rows of cells were added. As the number of cells increased from 1 row to 3 rows, less current flowed through the outer layers of cells. The cells seem to adapt the surface current into a systematic pattern of flow and charge. This phenomenon within, and between the cells behaves as parasitic elements, and therefore this is a uni-planar parasitic loaded patch antenna. By following the arrows in these figures the reader can understand the current pattern that adapted due to the introducing of periodic parasitic elements. Notice from these current distributions (arrows) how an inductive and capacitive nature would derive from element to element.

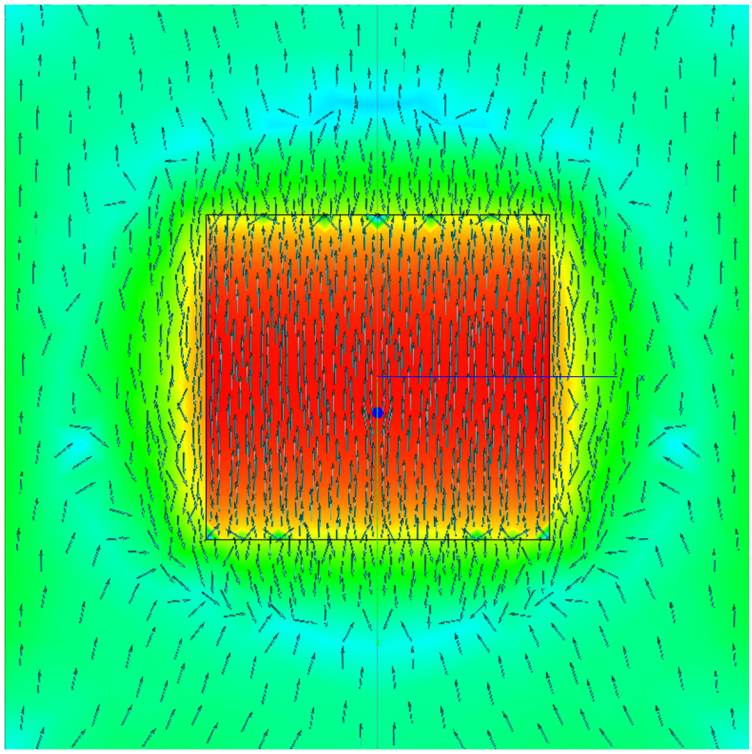

Figure 5.19 Current distribution pattern of a 1GHz patch antenna with probe feed.

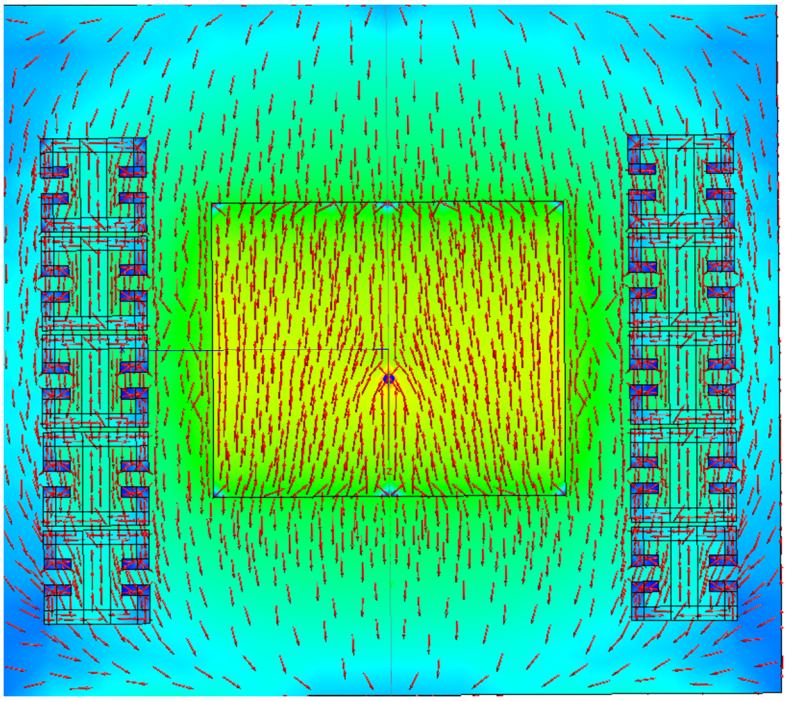

Figure 5.20 C-Mirror Antenna with 1 row.

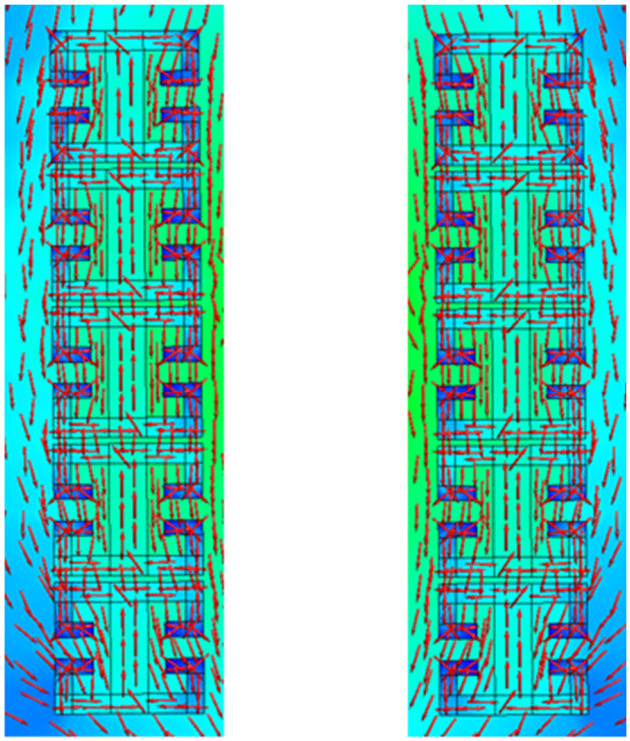

Figure 5.21 Zoomed in view of the cells from Figure 5.20.

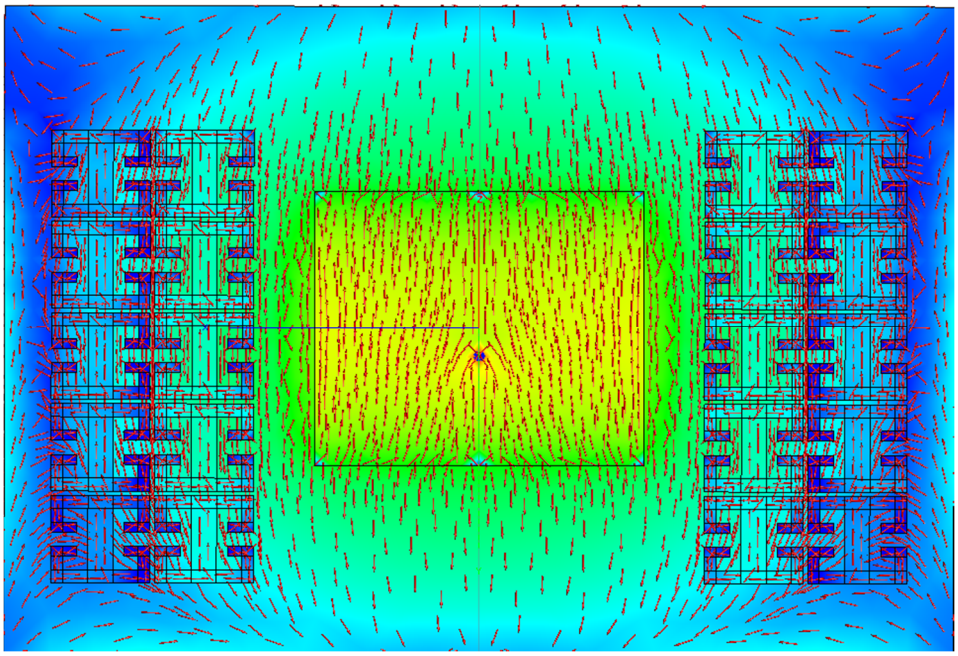

Figure 5.22 C-Mirror Antenna with 2 rows.

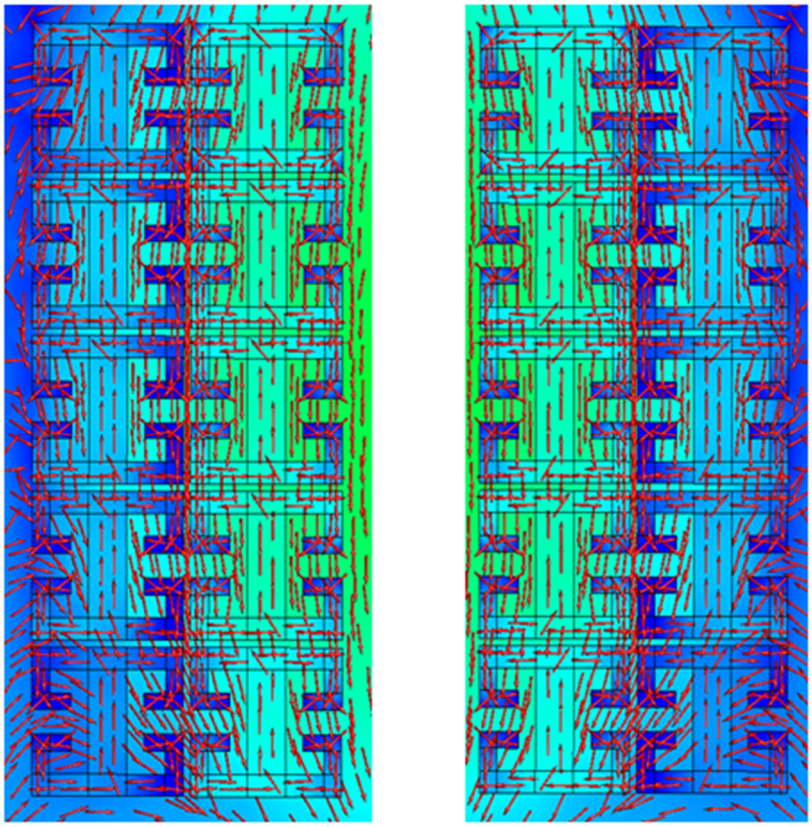

Figure 5.23 Zoomed in view of the cells from Figure 5.23.

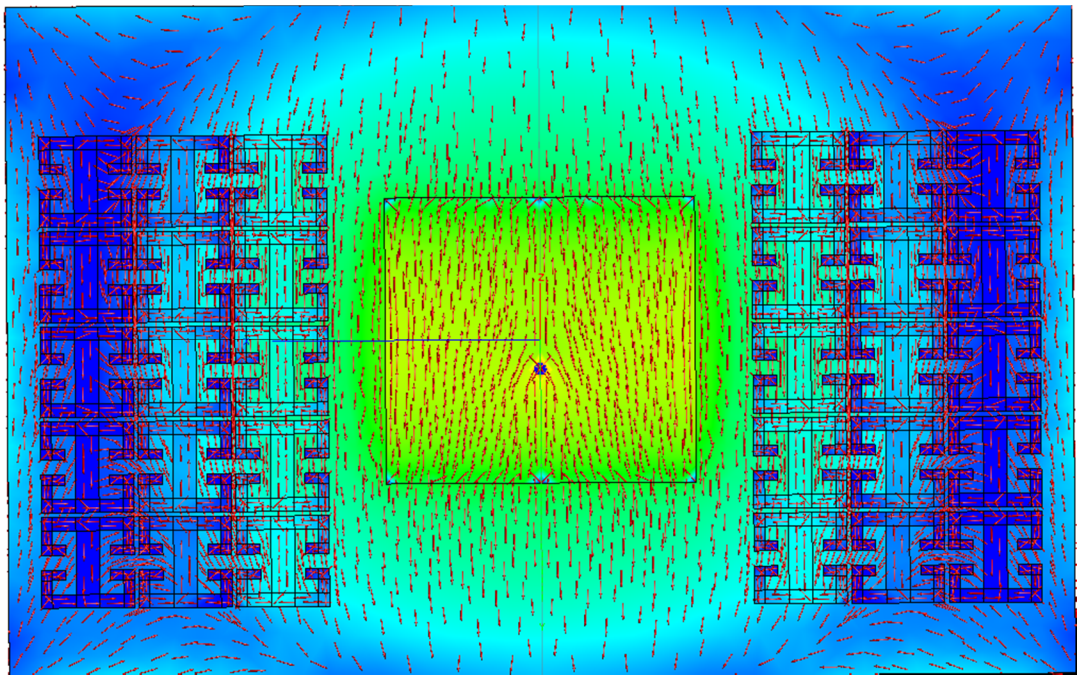

Figure 5.24 C-Mirror Antenna with 3 rows.

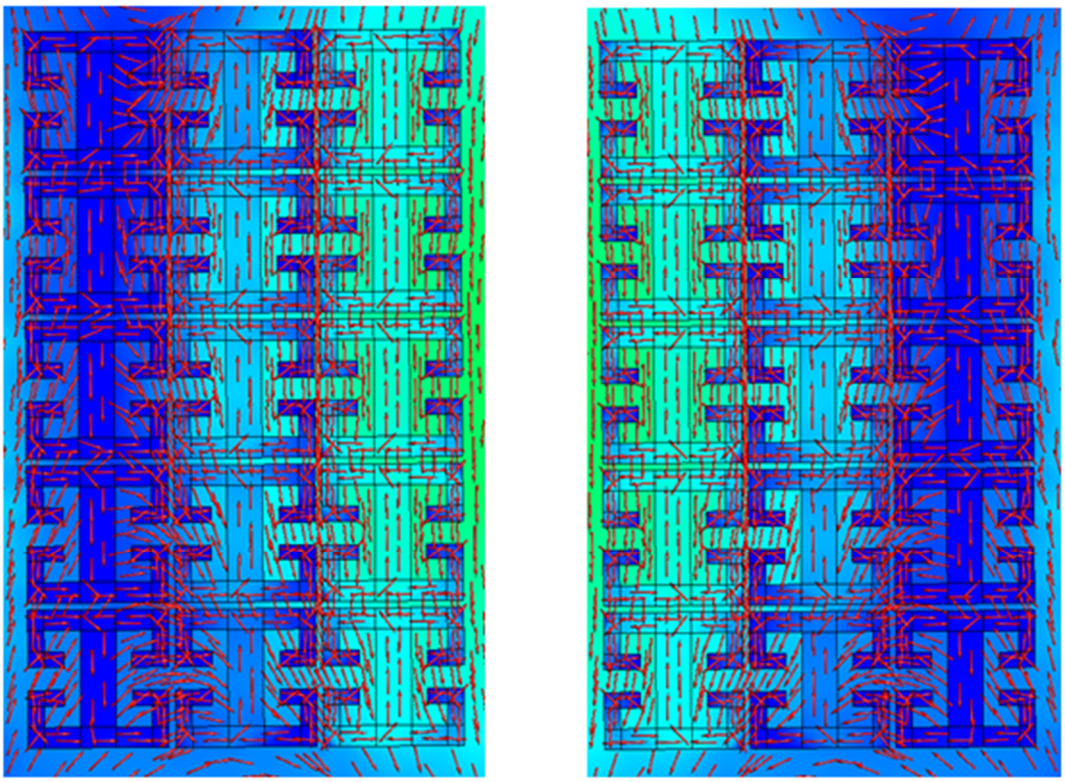

Figure 5.25 Zoomed in view of the cells from Figure 5.24.

5.5 Conclusion

In conclusion to this chapter, it was presented in Section 5.1 the building and simulating of C-mirror cell. This consisted of first looking at reflected waves which were for multi-layered applications. The C-Mirror cell was tested by calculation for dispersive characteristics, with and without via. Without via the simulated cell showed no band gap feature. Two simulation trials were run for the insertion of via in the cell 1) via in center of the cell, and 2) via on the cell stubs edge. Both trials showed a similar band gap feature. The bandgap exists from 0 to 1 GHz. In Section 5.2 a 1 GHz microstrip patch antenna was designed and simulated. Once the individual cell and the antennas behaviors were realized and matched, the antenna was then loaded with the C-mirror periodic cells in Section 5.3. Simulation parameters consisted of: 1) UD, LR, and all the way around orientations, 2) varying the number of cell rows; either, 1, 2, or 3 rows, and 3) varying the placement of the periodic cells according to $\left(\frac{\lambda_o}{10},\frac{\lambda_o}{12},\frac{\lambda_o}{15},\frac{\lambda_o}{17},\frac{\lambda_o}{20}\right)$ from the edge of the antenna to the center of the cell.

From simulations it was found that UD orientation, with 2 rows at $\lambda_o/12$ spacing obtained the best outcome with respect to the goal of this thesis work of increasing the antenna systems gain. This result showed a maximum gain increase of about 0.31 dB. This increase came from a decrease in back lobe radiation for the E and H-planes.

Since this uni-planar periodic loaded antenna system configuration had no vias inserted in the cells, the cells behaved as parasitic elements. These parasitic elements were more deeply understood from Section 5.4 by taking a look at surface wave currents

and their interacting behavior within the parasitic loaded antenna system. The C-Mirror parasitic element was seen to create a conducting current network. From the current simulations an inductive characteristic is displayed as the current flows through the cells, as well as a capacitive characteristic is displayed that occurs between the cells stubs, and between the cells.

6 FUTURE RESEARCH

6.1 Discussion

In earlier chapters of this thesis, I showed that there are many ways in which to design a periodic structure loaded antenna. A bottom-up approach was taken by first introducing microstrip antennas. This included basic characteristics, feeding methods, fringing field effects, and finally the theoretical design of a rectangular microstrip patch antenna. Once this was completed, the basics of EBGs were presented.

After a foundation was built I considered applications. Mainly, wearable antennas were of interest, where several examples are presented to the reader. A review of surface waves and wave modes was given. Surface waves are un-utilized energy that decreases the performance of the antenna system. However, this un-utilized energy can be utilized for antenna enhancements by loading the antenna with periodic structures that control the traveling EM wave to benefit positively the antenna system.

Ultimately, wearable e-textile antennas for integration with spacesuit application are of interest. It was demonstrated that placement of antenna array elements through the spacesuit is essential so the dependence on orientation is reduced or eliminated. Furthermore, wearable antennas present a hands free ability, which gives the space explorer the convenience of one less thing to do, so that they can concentrate more on the mission at hand. Also, increasing the gain by loading the antenna with periodic structures

was mentioned, so the space explorer can explorer further from the base station, and still maintain a continuous and confident communication link at all times.

The manufacturing, fabrication, and testing was explained. This included the material selection for relative permittivity and conductivity measurements. Then the design was sent to the Technology Departments Machine Shop for manufacturing. The assembly was done by EE students in the Applied Electro Magnetics Laboratory. Finally, the textile antennas were realized by testing them in an anechoic chamber at NDSUs Wireless Sensor Laboratory. The results from this are currently being documented in [62].

The results of this thesis covered simulation results of simulating of antenna properties. This included design of the C-mirror cell, and then testing of it for reflection as well as dispersive characteristics. The reflection coefficient was for applications of a multi-planar loaded antenna system and reasons were given as to why that route was not chosen to pursue. The cell was studied for bandgap with and without via. The dispersion graph showed no bandgap without via and a band gap up to 1.7 GHz with via. It was decided to use no via (due to fabrication difficulty) and use C-mirror as a parasitic element at 1 GHz. A 1 GHz antenna with appropriate specs for a textile antenna was designed and simulated. Once the 1 GHz antenna was realized, C-mirror periodic cells were loaded uni-planar to the antenna. Several calculations were done as to orientation, number of rows, and placement of the rows and/or columns with respect to the antenna.

Upon the calculations done the result concluded that the greatest increase in gain came from UD orientation, with 2 rows, and at $\lambda_o/12$ placement with respect to the

antennas edge. Once this was known a deeper look into the cells was approached. It was seen that the periodic cells created their own internal circuitry with current flowing through the cells as an inductor, while the spacing between the cells behaved as a capacitor. This phenomenon is called uni-planar parasitic loaded antennas.

6.2 Future Research

Clearly, this thesis presented many potential opportunities for parasitic loaded textile antennas that are confidently growing into uncountable application specific wearable e-textile electronic systems. To fulfill the full potential of a C-mirror parasitic loaded antenna system, in future research one has to first design the cells dispersive characteristic for more application reasonable frequencies of 2.45 GHz, 5.2 GHz, and 5.8 GHz. Next the antenna should be designed at these frequencies. Other possibilities include an aperture feed antenna which might be of interest for analysis to mitigate soldiering of components on a textile antenna. It might also be of interest to integrate a rectifier into the antenna system so that power can be supplied to the explorer as the base station sends power naturally with the signal already. Ultimately, the goal is to reduce the dependency on a battery, or to have it so that the batteries are being charged wirelessly from the base station.

Upon the aforementioned ideas, then C-mirror cells should be optimized to increase gain. This entails varying the Periodic Boundary Conditions (PBC) as well as modifying certain dimension of the C-Mirror. Furthermore, in terms of orientations, a multi-planar antenna system should be designed and tested, as well as a combination of

both uni and multi planar antenna system. These experimentations could be undertaken at UNDs EE Applied Electromagnetics Laboratory.

The C-mirror cells can be designed to be used in their stop band as an EBG structure or they can be controlled to rotate the main beam as parasitic elements. The use of multiple antennas on the space suit must be investigated. By adding beam forming to antenna arrays, one can increase the gain and signal to interference ratio and minimize the power consumption.

Also, in collaboration with the Technology Department, manufacturing, fabricating, and testing of textile antennas should be continued. Manufacturing of periodic structures with via and testing under bending conditions should be performed. Furthermore, applications of textile and wearable antennas on a space suit will continue by integrating these antennas into UND's space suit.

REFERENCES

[1] G. A. Deschamps, "Microstrip microwave antennas," in *Third USAF Symposium on Antennas*, 1953.

[2] J. Q. Howell, "Microstrip antennas," in *IEEE AP - S International Symposium Digest*, 1972, pp. 177-180.

[3] R. Munson, "Conformal microstrip antennas and microstrip phased arrays," *IEEE Transactions on Antennas and Propagation* vol. 22, pp. 74-78, Jan. 1974.

[4] C. A. Balanis, *Antenna Theory 3rd Edition*. Hoboken, New Jersey: John Wiley & Sons, Inc., 2005.

[5] R. Garg, P. Bhartia, I. Bahl, and A. Ittipiboon, *Microstrip Antenna Design Handbook*: Artech House, Inc., 2001.

[6] R. Bhalla, "Analysis of broadband and dual band microstrip patch antennas," Master of Science, University of Manitoba, Winnipeg, Canada, 2001.

[7] T. Huynh and K. F. Lee, "Single-layer single-patch wideband microstrip antenna," *Electronics Letters,* vol. 31, pp. 1310-1312, 1995.

[8] H. Legay and L. Shafai. (1994, 28 June - 2 July) New stacked microstrip antenna with large bandwidth and high gain. *IEE Proceedings - Microwaves, Antennas and Propogation*. 199-204.

[9] H. F. Pues and A. R. Van De Capelle, "An impedance-matching technique for increasing the bandwidth of microstrip antennas," *IEEE Transactions on Antennas and Propagation,* vol. 37, pp. 1345-1354, Nov. 1989.

[10] D. M. Pozar and D. H. Schaubert, *Microstrip Antennas, the Analysis and Design of Microstrip Antennas and Arrays*: IEEE Press, Piscataway, NJ, 1995.

[11] F. Yang and Y. Rahmat-Samii, *Electromagnetic Band Gap Structures in Antenna Engineering*. United States of America: Cambridge University Press, 2009.

[12] H. Gutton and G. Baissinot, "Flat aerial for ultra high frequencies," France Patent, 1955.

[13] D. M. Pozar, "Microstrip antennas," *Proceedings of the IEEE,* vol. 80, pp. 79-91, January 1992.

[14] R. A. Nelson. (2010). *Antennas: The Interface with Space*. Available: C:\Users\Corey\Desktop\Grad School_ Masters\Literature Review\Theis.Data\PDF\ATI Space, Satellite Technical Training Courses Tutorial on Antenna, Gain and B-1117254839\ATI Space, Satellite Technical Training Courses Tutorial on Antenna, Gain and Beamwidth.mht

[15] antenna-theory.com. (2011, 4/9/2012). *Rectangular Microstrip Antennas*. Available: http://www.antenna-theory.com/antennas/patches/antenna.php#introduction

[16] D. M. Pozar, *Microwave Engineering 3rd edition*: John Wiley & Sons, Inc., 2005.

[17] C. R. Paul, *Introduction to Electromagnetic Compatibility 2nd Edition*. Hoboken, New Jersey: John Wiley & Sons, Inc, 2006.
[18] Y. Rahmat-Samii and H. Mosallaei, "Electromagnetic band-gap structures: classification, characterization, and applications," 2001, pp. 560-564 vol. 2.
[19] Y. Rahmat-Samii and F. Yang, *Development of Complex Artificial Ground Planes in Antenna Engineering*: John Wiley & Sons, Inc., 2006.
[20] Z. Qiu-Rong, F. Yun-Qi, and Y. Nai-Chang, "A novel compact spiral electromagnetic band-gap (EBG) structure," *IEEE Transactions on Antennas and Propagation,* vol. 56, pp. 1656-1660, 2008.
[21] D. Sievenpiper, *Review of theory, fabrication, and applications of high-impedance ground planes*: John Wiley & Sons, Inc., 2006.
[22] D. Sievenpiper, "Review of Theory, Fabrication, and Applications of High-Impedance Ground Planes," in *Metamaterials*, ed: John Wiley & Sons, Inc., 2006, pp. 285-311.
[23] R. Cocciolo, F. R. Yang, K. P. Ma, and T. Itoh, "Aperture coupled patch antenna on UC-PBC substrate," *IEEE Transaction Microwave Theory Techniques,* vol. 47, pp. 2123-2130, Nov. 1999.
[24] FEKO. (4/9/2012). *Comprehensive electromagnetic simulation software*. Available: http://www.feko.info/
[25] P. Salonen, L. Sydanheimo, M. Keskilammi, and M. Kivikoski, "A small planar inverted-f antenna for wearable applications," in *The Third International Symposium on Wearable Computers*, 1999, pp. 95-100, San Francisco, CA.
[26] P. Salonen and H. Hurme, "Modeling of a fabric GPS antenna for smart clothing," in *Proc. IASTED International Conference Modeling and Simulation*, pp. 18-23, Palm Springs, CA, USA, 2003.
[27] P. Salonen and L. Hurme, "A novel fabric WLAN antenna for wearable applications," in *International Symposium on Antennas and Propagation and URSI North American Radio Science Meeting*, pp. 700-703 vol. 2, Columbus, OH, USA, 2003.
[28] M. Tanaka and J. H. Jang, "Wearable microstrip antenna," in *International Symposium on Antennas and Propagation and URSI North American Radio Science Meeting*, pp. 704-707 vol. 2, Columbus, OH, USA, 2003.
[29] S. Bashir, "Design and synthesis of non uniform high impedance surface based wearable antennas," Doctor of Philosophy, Loughborough University, 2009.
[30] M. A. R. Osman and M. K. B. Rahim, "Wearable Textile Antenna: Fabrics Investigation," *Journal of Communication and Computer,* vol. 7, pp. 75-80, 2010.
[31] I. Locher, M. Klemm, T. Kirstein, and G. Troster, "Design and characterization of purely textile patch antennas," *IEEE Transactions on Advanced Packaging,* vol. 29, pp. 777-788, Nov. 2006.
[32] Q. Bai and R. Langley, "Wearable EBG antenna bending and crumpling," in *Loughborough Antennas and Propagation Conference*, pp. 201-204, Loughborough, UK, 2009.
[33] P. Salonen and Y. Rahimat-Samii, "Textile antennas: Effects of antenna bending on input matching and impedance bandwidth," *IEEE Aerospace and Electronic Systems Magazine,* vol. 22, pp. 10-14, March 2007.

[34] S. Sankaralingam and B. Gupta, "Development of textile antennas for body wearable applications and investigations on their performance under bent conditions," *Progress In Electromagnetics Research,* vol. 22, pp. 53-71, 2010.
[35] F. C. Commission. (04/09/2012). *Body Tissue Dielectric Parameters*. Available: Http://www.fcc.gov/oet/rfsafety/dielectric.html.
[36] C. A. Balanis, *Modern Antenna Handbook* vol. 1 & 2: John Wiley & Sons, Inc, 2008.
[37] C. Hertleer, A. Tronquo, H. Rogier, L. Vallozzi, and L. Van Langenhove, "Aperture-coupled patch antenna for integration into wearable textile systems," *IEEE Antennas and Wireless Propagation Letters,* vol. 6, pp. 392-395, 2007.
[38] C. Hertleer, L. Van Langenhove, H. Rogier, and L. Vallozzi, A textile antenna for fire fighter garments [Online]. Available: http://www.proetex.org/publications.htm
[39] A. W. Guy, C.-K. Chou, J. A. McDougall, and C. Sorensen, "Measurement of shielding effectiveness of microwave-protective suits," *IEEE Transactions on Microwave Theory and Techniques,* vol. 35, pp. 984-994, 06 Jan. 1987.
[40] T. F. Kennedy, P. W. Fink, A. W. Chu, N. J. Champagne, G. Y. Lin, and M. A. Khayat, "Body-worn e-textile antennas: The good, the low-mass, and the conformal," *IEEE Transactions on Antennas and Propagation,* vol. 57, pp. 910-918, 2009.
[41] S. Zhu and R. Langley, "Dual-band wearable textile antenna on an EBG substrate," *IEEE Transactions on Antennas and Propagation,* vol. 57, pp. 926-935, 2009.
[42] C. Hertleer, H. Rogier, A. Tronquo, and L. Van Langenhove, "A textile antenna for off-body communication integrated into protective clothing for firefighters," *IEEE Transactions on Antennas and Propagation,* vol. 57, pp. 919-925, 2009.
[43] C. Hertleer, H. Rogier, L. Vallozzi, and F. Declercq, "A textile antenna based on high-performance fabrics," presented at the EuCAP2007, Edinburgh, 2007.
[44] NEETS, (2007, 29 Feb). *Surface Waves*, Available: http://electriciantraining.tpub.com/14182/css/14182_76.htm
[45] N. I. Dodov and P. Z. Petkov, "The surface waves impact on the coupling effect in microstrip antennas," *Microwave Review,* vol. 8, pp. 6-7, Dec. 2002.
[46] M. Fallah, F. Kashani, and S. Mohseni, "Side effect characterization of EBG structures in microstrip patch antenna," in *Progress in Electromagnetics Research Symposium Proceedings*, Cambridge, USA, 2010, pp. 323-326.
[47] I. Ederra, R. Gonzalo, B. Alderman, P. G. Huggard, B. P. de Hon, M. C. van Beurden, A. Murk, L. Marchand, and P. de Maagt, "Sub-millimeter-wave imaging array at 500 GHz based on 3-D electromagnetic-bandgap material," *IEEE Transactions on Microwave Theory and Techniques,* vol. 56, pp. 2556-2565, 2008.
[48] L. J. Chu, "Physical limitations of omni-directional antennas," *Journal of Applied Physics,* vol. 19, pp. 1163-1175, 1948.
[49] R. F. Harrington, *Time Harmonic Electromagnetic Fields*. New York: McGraw-Hill, 1961.
[50] M. Gustafsson and S. Nordebo, "Bandwidth, Q factor, and resonance models of antennas," *Progress In Electromagnetics Research,* vol. 62, pp. 1-20, 2006.

[51] S. Savia and E. Parker, "Equivalent circuit model for superdense linear dipole FSS," in *IEE Proceedings Microwaves Antennas Propagation*, pp. 37-42, 2003.
[52] S. Tretyakov, *Analytical Modelling in Applied Electromagnetics*. New York: Artech House, 2003.
[53] S. Maci and A. Cucini, *FSS-Based EBG Surfaces*: John Wiley & Sons, Inc., 2006.
[54] S. R. Best and D. L. Hanna. (2008). *Electromagnetic Band Gap (EBG) Surfaces for Antenna Applications*. Available: http://www.mitre.org/news/events/exchange08/3728.pdf
[55] D. Sievenpiper, L. Zhang, R. F. J. Broas, N. G. Alexopolous, and E. Yablonovitch, "High-impedance electromagnetic surfaces with a forbidden frequency band," *IEEE Transactions on Microwave Theory and Techniques,* vol. 47, pp. 2059-2074, 1999.
[56] F.-R. Yang, K.-P. Ma, Y. Qian, and T. Itoh, "A novel TEM waveguide using uniplanar compact photonic-bandgap (UC-PBG) structure," *IEEE Transaction Microwave Theory Techniques,* vol. 47, pp. 2092-2098, 1999.
[57] P. Salonen, F. Yang, Y. Rahmat-Samii, and M. Kivikoski, "WEBGA-wearable electromagnetic band-gap antenna," in *2004 Digest IEEE Antennas and Propagation Society Symposium*, pp. 451-454 Vol. 1, Monterey, California, 2004.
[58] P. Salonen, M. Keskilammi, and L. Sydanheimo, "A low-cost 2.45 GHz photonic band-gap patch antenna for wearable systems," presented at the *Proc. 11th International Conference Antennas and Propagation ICAP*, Manchester, UK, 2001.
[59] P. Salonen, Y. Rahmat-Samii, H. Hurme, and M. Kivikoski, "Dual-band wearable textile antenna," in *Proc. Antennas and Propagation Society International Symposium*, 2004, pp. 463-466 Vol. 1.
[60] R. Langley and S. Zhu, "Dual band wearable antenna," in *Antennas and Propagation Conference*, pp. 14-17, Loughborough, UK, 2008.
[61] G. Entertainment. (04/09/2012). *As the new Mars Rover begins its Journey to the Red Planet, here are the other plans that didn't QUITE work out.* Available: http://www.dailymail.co.uk/sciencetech/article-2067754/As-new-Mars-Rover-begins-journey-Red-Planet-predictions-didnt-QUITE-work-out.html
[62] T. Haagenson and S. Noghanian, "Title," unpublished|.
[63] G. Gopinath, R. Sammeta, and C. J. Reddy, "A thin, low-profile antenna using a novel high impedance ground plane," *Microwave Journal,* July 2010.